Published for SISSA by Springer

Received: October 29, 2025
Revised: January 21, 2026
Accepted: March 23, 2026
Published: May 15, 2026

Measurement of the Higgs boson production in association with top quarks in multilepton final states in pp collisions at $\sqrt{s} = 13$ TeV with the ATLAS detector

The ATLAS collaboration

Full author list at the end of the paper

E-mail: atlas.publications@cern.ch

Abstract: A measurement of the associated production of a top-quark pair with the Higgs boson ($t\bar{t}H$) in multilepton final states is presented. The analysis is based on a data sample of proton-proton collisions at $\sqrt{s} = 13$ TeV recorded with the ATLAS detector at the CERN Large Hadron Collider and corresponding to an integrated luminosity of 140 fb^{-1}. Six final states defined by the number and flavour of reconstructed charged leptons are combined in a simultaneous likelihood fit to extract the $t\bar{t}H$ signal and constrain the most relevant backgrounds. The measured $t\bar{t}H$ cross-section normalised to Standard Model (SM) prediction is $\sigma_{t\bar{t}H}/\sigma^{\mathrm{SM}} = 0.63^{+0.20}_{-0.19}$. This result corresponds to an observed (expected) significance of 3.3σ (5.3σ). Additionally, two other fits are used to measure the $t\bar{t}H$ cross-section differentially in bins of the Higgs boson transverse momentum in the simplified template cross-section framework, and to extract the associated production cross-section of a single top-quark with the Higgs boson (tH) together with the $t\bar{t}H$ one. The CP structure of the top quark-Higgs boson Yukawa coupling is probed through an analysis of $t\bar{t}H$ and tH events. The results are compatible with the SM hypothesis, and values of the mixing angle between CP-even and CP-odd top-Higgs Yukawa couplings of $|\alpha| > 62°$ are excluded at 68% confidence level.

Keywords: Hadron-Hadron Scattering

ArXiv ePrint: 2510.23755

https://doi.org/10.1007/JHEP05(2026)183

JHEP05(2026)183

Contents

1 Introduction

Since the discovery of the Higgs boson with a mass of approximately 125 GeV by the ATLAS [1] and CMS [2] Collaborations in 2012, the measurement of its properties has been one of the primary goals of the physics programme at the Large Hadron Collider (LHC) [3]. So far no significant deviation from the Standard Model (SM) has been observed [4, 5]. The interaction between the Higgs boson and the top quark is of particular interest. The large mass of the top quark of approximately 173 GeV requires that it couples strongly to the Higgs boson in the SM. For this reason, the top quark could play a special role in the electroweak symmetry breaking. The measurement of the inclusive cross-section of the associated production of the

JHEP05(2026)183

Higgs boson with a top-quark pair ($t\bar{t}H$) allows a more direct determination of the top-quark Yukawa coupling, relying on fewer theoretical assumptions than the loop-induced gluon-gluon fusion process. The measurement of the Higgs boson production cross-section in association with a single top quark (tH) and the kinematic properties of tH and $t\bar{t}H$ events can also provide information about the CP nature of the coupling [6–9]. In the SM the Higgs boson is a scalar and its interactions are CP-even. The pure pseudoscalar hypothesis having CP-odd interactions with weak vector bosons and fermions has been excluded [10–13]. However, it remains experimentally allowed that the Higgs boson is a CP-mixed state, which arises in extended Higgs sectors, and would provide a new source of CP-violation beyond the SM, which is necessary to explain baryogenesis [6–9, 14].

The $t\bar{t}H$ process was observed with a partial dataset of the LHC Run 2 by both ATLAS [15] and CMS [16] using a combination of different channels. Measurements of $t\bar{t}H$ at $\sqrt{s} = 13$ TeV with the full Run-2 dataset, including CP interpretations, exist from ATLAS and CMS in the $H \to \gamma\gamma$ channel [17–20], the $H \to ZZ^* \to 4\ell$ channel [21, 22], the $H \to \tau^+\tau^-$ channel [23], and the $H \to b\bar{b}$ channel [24–26]. In multilepton final states (with several light or τ-leptons originating from both the decays of the Higgs boson and the top quarks), measurements of the inclusive $t\bar{t}H$ production cross-section have been performed at $\sqrt{s} = 13$ TeV by ATLAS [27] and CMS [28] using datasets corresponding to a luminosity of 36 fb^{-1} and 137 fb^{-1}, and reporting a signal strength[1] of $\mu_{t\bar{t}H} = 1.6^{+0.5}_{-0.4}$ and $\mu_{t\bar{t}H} = 0.92^{+0.26}_{-0.23}$ respectively. A search for CP violation in $t\bar{t}H$ and tH was also performed by CMS using the same dataset [29]. The tH process has been searched for by both ATLAS [18, 30] and CMS [26, 28] in the $H \to \gamma\gamma$, $H \to b\bar{b}$ and multilepton channels with the full Run-2 dataset. The measured signal strengths by ATLAS are $\mu_{tH} = 3^{+4}_{-3}$ in $H \to \gamma\gamma$, $\mu_{tH} = 8.1 \pm 3.3$ combining the $H \to b\bar{b}$ and multilepton channels, and $\mu_{tH} = 5.7^{+4.1}_{-4.0}$ by CMS in the multilepton channel. All those results are compatible with, but slightly above the SM prediction.

This paper describes measurements of the inclusive $t\bar{t}H$ production cross-section, and of the differential $t\bar{t}H$ production cross-section as a function of the Higgs boson transverse momentum (p_{T}^{H}), as well as an interpretation of the CP nature of the Higgs boson, using a dataset corresponding to an integrated luminosity of 140 fb^{-1} collected with the ATLAS detector at a centre-of-mass energy $\sqrt{s}$=13 TeV during the LHC Run 2 (2015–2018). A simultaneous measurement of the $t\bar{t}H$ and tH signal strengths is also presented. At the LHC, tH production occurs via three modes: $tHqb$ (t-channel), tWH, and s-channel. This analysis focuses on $tHqb$, which has a larger cross-section and is easier to distinguish from $t\bar{t}H$ than tWH. The s-channel has a very low cross-section and is neglected. Examples of Feynman diagrams for both $t\bar{t}H$ and $tHqb$ production are shown in figure 1.

In addition to the increased size of the analysed dataset, this measurement features significant improvements over the previous publication based on 36 fb^{-1} [27], benefitting from improved jet flavour tagging and lepton identification, a better understanding of the dominant backgrounds $t\bar{t}W$ and $t\bar{t}Z$ from dedicated measurements [31, 32], a new simulation and a new systematic uncertainty model; besides, an improved photon conversion rejection is used and the main backgrounds estimation relies on *in situ* normalisation.

[1]The signal strength is defined as the ratio of the measured cross-section to the SM cross-section. Uncertainties on both the measurement and the prediction are included.

JHEP05(2026)183

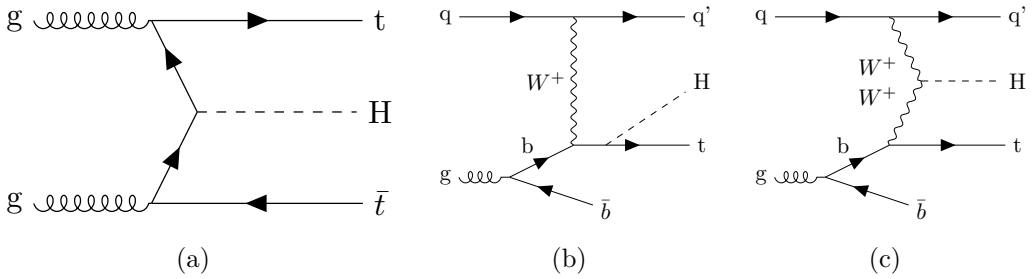

Figure 1. Representative Feynman diagrams for the signal processes considered in this analysis: (a) $t\bar{t}H$ production and (b,c) $tHqb$ production.

The differential p_{T}^{H} measurement is done in the simplified template cross-section (STXS) [33, 34] formalism. Since the leptons and missing transverse momentum in these final states can arise from either the Higgs boson or the top-quark decays, the Higgs system cannot be fully reconstructed unambiguously. To overcome this, a Graph Neural Network (GNN) is trained to estimate p_{T}^{H} using the full event information.

CP-violation in the top-Higgs interaction is searched for using the same region definitions and background estimates, but with a fit parameterised to accommodate for a possible admixture of CP-odd and CP-even Higgs states, affecting $t\bar{t}H$, $tHqb$, and tWH cross-sections and event kinematics. Indirect model-dependent constraints on the CP structure of the top-quark Yukawa coupling can be inferred from the measurements of electron electrical dipole moments, Higgs boson gluon-gluon fusion production and $H \to \gamma\gamma$ decays rates [35]. The top-Higgs interaction Lagrangian term can be extended beyond the SM as [36]:

$$\mathcal{L}_{t\bar{t}H} = -\kappa_t' y_t \phi \bar{\psi}_t (\cos\alpha + i\gamma_5 \sin\alpha)\psi_t$$

where y_t is the SM Yukawa coupling, modified by a coupling modifier κ_t'; α is the CP-mixing angle; ϕ is the Higgs field; ψ_t and $\bar{\psi}_t$ are top-quark spinor fields and γ_5 is a Dirac matrix. The term containing γ_5 corresponds to a pseudoscalar component. The above expression reduces to the SM case for $\kappa_t' = 1$ and $\alpha = 0$. Combining multilepton, $H \to ZZ^* \to 4\ell$, and $H \to \gamma\gamma$ final states, CMS [29] constrains the CP-mixing angle to $|\alpha| < 48°$ at the 68% confidence level. ATLAS results in the $H \to \gamma\gamma$ channel [17] excluded values of $|\alpha| > 43°$ at the 95% confidence level.

The measurements are performed by combining a total of six channels, categorised by their number of hadronically decaying τ-leptons (τ_{had}) and light leptons ($\ell = e$ or μ). Requirements on the τ_{had} and ℓ multiplicities ensure that all channels are statistically independent. These signatures are targeting $t\bar{t}H$ events in which one or both top quarks decay leptonically, and the Higgs boson decays to $H \to WW^*$, $H \to \tau^+\tau^-$ or $H \to ZZ^*$ with subsequent decays involving ℓ and τ_{had}. The event selection also accepts a large fraction of tH events. There are two zero-τ_{had} channels (two-lepton same-sign, $2\ell\mathrm{SS}0\tau_{\mathrm{had}}$, and three-lepton, $3\ell 0\tau_{\mathrm{had}}$), one single-$\tau_{\mathrm{had}}$ channel ($2\ell\mathrm{SS}1\tau_{\mathrm{had}}$), two two-$\tau_{\mathrm{had}}$ channels ($1\ell 2\tau_{\mathrm{had}}$ and $2\ell 2\tau_{\mathrm{had}}$) and one channel with no τ_{had} requirement (4ℓ). In the zero-τ_{had} channels the strategy builds upon the recent ATLAS $t\bar{t}W$ measurement [31] to make use of the improved understanding of the non-prompt lepton background and $t\bar{t}W$ modelling derived in that analysis.

JHEP05(2026)183

The paper is structured as follows. The ATLAS detector is presented in section 2. The recorded data and the Monte Carlo (MC) simulation samples used in the analysis are described in section 3. The definition of reconstructed objects is described in section 4. The event selection in each channel is given in section 5. The background estimation method and the systematic uncertainties are described in sections 6 and 7, respectively. The results are presented in section 8.

2 ATLAS detector

The ATLAS detector [37] at the LHC covers nearly the entire solid angle around the collision point.[2] It consists of an inner tracking detector surrounded by a thin superconducting solenoid, electromagnetic and hadronic calorimeters, and a muon spectrometer incorporating three large superconducting air-core toroidal magnets.

The inner-detector system (ID) is immersed in a 2 T axial magnetic field and provides charged-particle tracking in the range $|\eta| < 2.5$. The high-granularity silicon pixel detector covers the vertex region and typically provides four measurements per track, the first hit generally being in the insertable B-layer (IBL) installed before Run 2 [38, 39]. It is followed by the SemiConductor Tracker (SCT), which usually provides eight measurements per track. These silicon detectors are complemented by the transition radiation tracker (TRT), which enables radially extended track reconstruction up to $|\eta| = 2.0$. The TRT also provides electron identification information based on the fraction of hits (typically 30 in total) above a higher energy-deposit threshold corresponding to transition radiation.

The calorimeter system covers the pseudorapidity range $|\eta| < 4.9$. Within the region $|\eta| < 3.2$, electromagnetic calorimetry is provided by barrel and endcap high-granularity lead/liquid-argon (LAr) calorimeters, with an additional thin LAr presampler covering $|\eta| < 1.8$ to correct for energy loss in material upstream of the calorimeters. Hadronic calorimetry is provided by the steel/scintillator-tile calorimeter, segmented into three barrel structures within $|\eta| < 1.7$, and two copper/LAr hadronic endcap calorimeters. The solid angle coverage is completed with forward copper/LAr and tungsten/LAr calorimeter modules optimised for electromagnetic and hadronic energy measurements respectively.

The muon spectrometer (MS) comprises separate trigger and high-precision tracking chambers measuring the deflection of muons in a magnetic field generated by the superconducting air-core toroidal magnets. The field integral of the toroids ranges between 2.0 and 6.0 T m across most of the detector. Three layers of precision chambers, each consisting of layers of monitored drift tubes, cover the region $|\eta| < 2.7$, complemented by cathode-strip chambers in the forward region, where the background is highest. The muon trigger system covers the range $|\eta| < 2.4$ with resistive-plate chambers in the barrel, and thin-gap chambers in the endcap regions.

[2] ATLAS uses a right-handed coordinate system with its origin at the nominal interaction point (IP) in the centre of the detector and the z-axis along the beam pipe. The x-axis points from the IP to the centre of the LHC ring, and the y-axis points upwards. Polar coordinates (r, ϕ) are used in the transverse plane, ϕ being the azimuthal angle around the z-axis. The pseudorapidity is defined in terms of the polar angle θ as $\eta = -\ln\tan(\theta/2)$ and is equal to the rapidity $y = \frac{1}{2}\ln\left(\frac{E+p_z}{E-p_z}\right)$ in the relativistic limit. Angular distance is measured in units of $\Delta R \equiv \sqrt{(\Delta\eta)^2 + (\Delta\phi)^2}$.

JHEP05(2026)183

The luminosity is measured mainly by the LUCID-2 [40] detector that records Cherenkov light produced in the quartz windows of photomultipliers located close to the beampipe.

Events are selected by the first-level trigger system implemented in custom hardware, followed by selections made by algorithms implemented in software in the high-level trigger [41]. The first-level trigger accepts events from the 40 MHz bunch crossings at a rate below 100 kHz, which the high-level trigger further reduces in order to record complete events to disk at about 1.25 kHz.

A software suite [42] is used in data simulation, in the reconstruction and analysis of real and simulated data, in detector operations, and in the trigger and data acquisition systems of the experiment.

3 Data and simulated event samples

The data were collected by the ATLAS detector in pp collisions at the LHC with a centre-of-mass energy of $\sqrt{s} = 13$ TeV with a peak instantaneous luminosity of $\mathcal{L} = 2.1 \times 10^{34}$ cm^{-2}s^{-1}, and a mean number of pp interactions per bunch crossing of $\langle\mu\rangle = 34$. Data quality requirements are applied to ensure that all relevant components were in nominal operating conditions and that the LHC beams were in stable-collision mode [43]. The integrated luminosity of the resulting data sample corresponds to 140 fb^{-1} [44]. The uncertainty in the combined 2015–2018 integrated luminosity is 0.83% [44], obtained using the LUCID-2 detector [40] for the primary luminosity measurements with complementary measurements from the ID and calorimeters.

Events are selected based on a combination of single-lepton[3] and dilepton triggers [45, 46]. The use of a given trigger depends on the flavour and the transverse momenta (p_{T}) of the leptons in the event, and on the data-taking period. Single-lepton triggers have p_{T} thresholds between 20 GeV and 26 GeV while dilepton triggers have p_{T} thresholds as low as 12(8) GeV for the leading (subleading) lepton. The requirements imposed on the lepton p_{T} in the analysis are tighter than those applied in the trigger-object reconstruction and trigger decision, in order to be on the trigger efficiency plateau.

Simulated MC event samples are used to model the $t\bar{t}H$ and tH signals and to estimate the backgrounds from SM processes. A summary of the generators used for the simulation is shown in table 1, and further details are provided below for the most relevant samples in the analysis.

3.1 Signal MC event samples

The signal from $t\bar{t}H$ production was simulated using Powheg Box v2 [51–54]. The h_{damp} parameter, which controls the p_{T} of the first additional emission beyond the Born configuration and therefore regulates the high-p_{T} emission, was set to $3 \times (2m_t + m_H)/4 = 352.5$ GeV. The functional form of the renormalisation (μ_{r}) and factorisation (μ_{f}) scales was set to $\sqrt[3]{m_{\mathrm{T}}(t) \cdot m_{\mathrm{T}}(\bar{t}) \cdot m_{\mathrm{T}}(H)}$, where $m_{\mathrm{T}} = \sqrt{m^2 + p_{\mathrm{T}}^2}$ is the transverse mass of a generated particle, m is its mass, and p_{T} is its transverse momentum. For this sample, the NNPDF3.0nlo parton distribution function (PDF) set [55] was used. The Monte Carlo

[3] Unless otherwise stated, the term 'lepton' will be used to refer to light leptons (e or μ).

JHEP05(2026)183

Physics process	Event generator	Matrix element order	Parton shower	PDF set	Tune
$t\bar{t}H$	Powheg Box	NLO	Pythia 8	NNPDF3.0nlo	A14
$t\bar{t}H$ (CP interpretation)	MadGraph5_aMC@NLO	NLO	Pythia 8	NNPDF3.0nnlo	A14
$tHqb$	MadGraph5_aMC@NLO	NLO	Pythia 8	NNPDF3.0nnlo	A14
tHW	MadGraph5_aMC@NLO	NLO	Pythia 8	NNPDF3.0nnlo	A14
$t\bar{t}$	Powheg Box	NLO	Pythia 8	NNPDF3.0nlo	A14
$t\bar{t}W$	Sherpa 2.2.10	MEPS@NLO	Sherpa	NNPDF3.0nnlo	Sherpa default
$t\bar{t}W$ (EWK)	Sherpa 2.2.10	LO	Sherpa	NNPDF3.0nnlo	Sherpa default
$t\bar{t}Z/\gamma^*$	MadGraph5_aMC@NLO	NLO	Pythia 8	NNPDF3.0nlo	A14
$t\bar{t}Z/\gamma^*$ (rad. decay)	MadGraph5_aMC@NLO	LO	Pythia 8	NNPDF3.0lo	A14
$t\bar{t}t\bar{t}$	MadGraph5_aMC@NLO	NLO	Pythia 8	NNPDF3.1nlo	A14
$t\bar{t}t$	MadGraph5_aMC@NLO	LO	Pythia 8	NNPDF2.3lo [49]	A14
VV, $qqVV$, VVV	Sherpa 2.2.2(1)	MEPS@NLO	Sherpa	NNPDF3.0nnlo	Sherpa default
Single top (t-, Wt-, s-channel)	Powheg Box	NLO	Pythia 8	NNPDF3.0nlo	A14
$Z \to \ell^+\ell^-$	Sherpa 2.2.1	MEPS@NLO	Sherpa	NNPDF3.0nnlo	Sherpa default
$Z \to \ell^+\ell^-(\gamma \to e^+e^-)$	Powheg Box	NLO	Pythia 8	CTEQ6L1nlo [50]	A14
$Z \to \ell^+\ell^-(\gamma* \to e^+e^-)$	Powheg Box	NLO	Pythia 8	CTEQ6L1nlo	A14
$t\bar{t}WW$	MadGraph5_aMC@NLO	LO	Pythia 8	NNPDF2.3lo	A14
tZ, tWZ	MadGraph5_aMC@NLO	NLO	Pythia 8	NNPDF3.0nlo	A14

Table 1. The configurations used for event generation of signal and background processes. The matrix element order refers to the order in the strong coupling constant of the perturbative calculation. The '$t\bar{t}W$ (EWK)' sample also includes next-to-leading-order electroweak corrections. Tune refers to the underlying-event tune of the parton shower generator, being either A14 [47] or the default in Sherpa. All samples include leading-logarithm photon emission, either modelled by the parton shower generator or by Photos [48]. The mass of the top quark (m_t) and SM Higgs boson were set to 172.5 GeV and 125 GeV, respectively.

prediction was normalised to cross-sections calculated at next-to-leading order (NLO) in quantum chromodynamics (QCD) and electroweak (EWK) couplings [56–60].

The $tHqb$ (tHW) samples were produced with MadGraph5_aMC@NLO 2.6 (2.8) [61] in the four-flavour (five-flavour) scheme with the NNPDF3.0nnlo PDF. The same flavour scheme was used in the matrix element (ME) calculation and the PDF. The top-quark and W boson decays were handled by MadSpin [62] to account for spin correlations in the decay products. The overlap of the tHW process with $t\bar{t}H$ at NLO was removed by using a diagram removal technique [63, 64].

To study CP-violation in the top-Higgs interaction, signal samples for $t\bar{t}H$, $tHqb$ and tHW were also produced using MadGraph5_aMC@NLO 2.6 for different values of κ_t' and α, with all other parameters fixed to the SM predictions. Following the procedure described in ref. [24], the yields of $t\bar{t}H$ and tH signals in each analysis bin are parameterised as a function of the model parameters by smoothly interpolating between generated MC samples. This parameterisation makes use of two $t\bar{t}H$, ten $tHqb$ and ten tHW samples generated with different values of α (between 0° and 180°) and κ_t' (between 0.5 and 2), in addition to the samples corresponding to the SM case.

3.2 Background MC event samples

The production of $t\bar{t}$ events was modelled using the Powheg Box v2 generator at NLO with the NNPDF3.0nlo PDF set and the h_{damp} parameter set to $1.5\,m_{\text{top}}$ [65].

JHEP05(2026)183

The production of top-quark pairs in association with W bosons ($t\bar{t}W$) is one of the largest backgrounds in the analysis. Similarly to ref. [31], simulated event samples for this process were produced using Sherpa 2.2.10 [66] with the NNPDF3.0nnlo PDF set. The ME was calculated for up to one additional parton at NLO and up to two partons at leading order (LO) using Comix [67] and OpenLoops [68–70], and merged with the Sherpa parton shower [71] using the MEPS@NLO prescription [72] with a merging scale of 30 GeV. The μ_{r} and μ_{f} were chosen to be $\mu_{\mathrm{r}} = \mu_{\mathrm{f}} = H_{\mathrm{T}}/2$, where H_{T} is defined as the scalar sum of the transverse masses $\sqrt{p_{\mathrm{T}}^2 + m^2}$ of all final-state particles with transverse momentum p_{T} and invariant mass m. Higher-order corrections related to EWK contributions were also included to account for corrections of orders $\alpha^2\alpha_{\mathrm{s}}^2$ and α^3 [66, 73, 74]. Real emission contributions of the sub-leading EWK corrections at order $\alpha^3\alpha_{\mathrm{s}}$ [75] were also included. The combination of contributions from NLO QCD and NLO EWK effects taken from this Sherpa configuration closely follows the strategy described in ref. [76]. This $t\bar{t}W$ event sample is normalised to a total cross-section of $\sigma(t\bar{t}W) = 745.3$ fb which also includes corrections at next-to-next-to-leading order (NNLO) in QCD as computed in ref. [77].

The production of $t\bar{t}Z/\gamma^*$ events was simulated using the MadGraph5_aMC@NLO 2.8.1 generator at NLO in α_{s} with the NNPDF3.0nlo PDF set. The functional form of the renormalisation and factorisation scales (μ_{r}, μ_{f}) was set to the default scale $0.5 \times \sum_i \sqrt{m_i^2 + p_{\mathrm{T},i}^2}$, where the sum runs over all the particles generated from the matrix element calculation. Top quarks were decayed at LO using MadSpin [62, 78] to preserve all spin correlations.

A dedicated $t\bar{t}$ sample including rare $t \to Wb\gamma^*(\to \ell^+\ell^-)$ radiative decays, i.e. $t\bar{t} \to W^+bW^-\bar{b}\ell^+\ell^-$, was generated using a LO matrix element and requiring $m(\ell^+\ell^-) > 1$ GeV. In this sample the photon can be radiated from the top quark, the W boson, or the b-quark. The $t\bar{t}Z/\gamma^*$ and $t\bar{t} \to W^+bW^-\bar{b}\ell^+\ell^-$ samples were combined and together form the "$t\bar{t}Z/\gamma^*$" sample. The contribution from internal photon conversions ($\gamma^* \to \ell^+\ell^-$) with $m(\ell^+\ell^-) < 1$ GeV was modelled with QED multiphoton radiation via the parton shower in an inclusive $t\bar{t}$ sample. These three components were combined to estimate the total $t\bar{t}Z/\gamma^*$ production. Care was taken to avoid both double-counting of contributions and uncovered regions of phase space when combining the different simulated event samples. The LO cross-section for the $t\bar{t} \to W^+bW^-\bar{b}\ell^+\ell^-$ sample was scaled to match the higher-order cross-section used for $t\bar{t}$ production in the phase space they overlap, and was assigned a 50% normalisation uncertainty.

The production of SM $t\bar{t}t\bar{t}$ events was modelled using the MadGraph5_aMC@NLO v2.6.2 generator that provides matrix elements at NLO in QCD with the NNPDF3.1nlo PDF set. The functional form of the renormalisation and factorisation scales was set to $0.25 \times \sum_i \sqrt{m_i^2 + p_{\mathrm{T},i}^2}$, where the sum runs over all the particles generated from the matrix element calculation, following ref. [75]. Top quarks were decayed at LO using MadSpin to preserve all spin correlations. The production of $t\bar{t}t\bar{t}$ events is normalised to a cross-section of 13.37 fb computed at NLO in QCD including EWK corrections [75].

Samples of diboson final states (WW, WZ and ZZ, collectively referred to as VV) were simulated with the Sherpa 2.2.1 or 2.2.2 generator depending on the process, including

JHEP05(2026)183

off-shell effects and Higgs boson contributions, where appropriate. Fully leptonic final states and semileptonic final states, where one boson decays leptonically and the other hadronically, were generated using matrix elements at NLO accuracy in QCD for up to one additional parton and at LO accuracy for up to three additional parton emissions. Samples for the loop-induced processes $gg \to VV$ were generated using LO-accurate matrix elements for up to one additional parton emission for both the cases of fully leptonic and semileptonic final states. The matrix element calculations were matched and merged with the Sherpa parton shower based on Catani-Seymour dipole factorisation [67, 71] using the MEPS@NLO prescription [72, 79, 80]. The virtual QCD corrections were provided by the OpenLoops library. The NNPDF3.0nnlo set of PDFs was used, along with the dedicated set of tuned parton-shower parameters developed by the Sherpa authors.

Additional MC samples are used to model processes with smaller impact in the analysis (such as single top, VVV, $t\bar{t}t$, $t\bar{t}WW$, tZ, tW, tWZ or $Z \to \ell^+\ell^-$), whose generator and settings are shown in table 1.

All MC samples produced with Powheg Box and MadGraph5_aMC@NLO are interfaced with Pythia 8.2 [81] for parton shower, hadronisation, and underlying event, with parameters set according to the A14 tune [47]. For all MC samples except those produced with Sherpa, the decays of bottom and charm hadrons were performed by EvtGen [82].

To simulate the effects of additional pp collisions in the same, following or previous bunch crossings (pile-up), additional interactions were generated using the soft QCD processes provided by Pythia 8.186 [83] with the A3 tune [84] and the MSTW2008LO PDF set [85], and overlaid onto each simulated hard-scatter event. The MC samples were reweighted so that the pile-up distribution matches the one observed in the data. All MC samples were processed through an ATLAS detector simulation [86] based on Geant4 [87] or a fast simulation using a parameterisation of the calorimeter response and Geant4 for the other parts of the detector. All MC samples were reconstructed in the same manner as the data.

4 Object reconstruction and selection

Interaction vertices from the pp collisions are reconstructed from at least two tracks with p_{T} larger than 500 MeV that are consistent with originating from the beam collision region in the x-y plane. If more than one primary vertex candidate is found in the event, the candidate for which the associated tracks form the largest sum of squared p_{T} is selected as the hard-scatter primary vertex [88].

Electron candidates are reconstructed from energy clusters in the electromagnetic calorimeter matched to a track in the ID [89]. They are required to satisfy $p_{\mathrm{T}} > 10$ GeV and $|\eta_{\mathrm{cluster}}| < 2.47$, excluding the transition region between the endcap and barrel calorimeters ($1.37 < |\eta_{\mathrm{cluster}}| < 1.52$). "*Loose*" and "*Tight*" electron identification working points (WPs) are used, based on a likelihood discriminant employing calorimeter and tracking variables that provide separation between electrons and jets, and between electrons and photons.

Muon candidates are reconstructed by performing a combined fit of the track information from the ID and MS [90]. They are required to satisfy $p_{\mathrm{T}} > 10$ GeV and $|\eta| < 2.5$. "*Loose*" and "*Medium*" muon identification WPs are used. In the case of "*Loose*" identification, muon candidates in the region $|\eta| < 0.1$, where muon spectrometer coverage is reduced, are

JHEP05(2026)183

also reconstructed from ID tracks matched to isolated energy deposits in the calorimeters consistent with the passage of a minimum-ionising particle.

Electron (muon) candidates are matched to the primary vertex by requiring that the significance of their transverse impact parameter, d_0,[4] satisfies $|d_0/\sigma(d_0)| < 5\,(3)$, where $\sigma(d_0)$ is the measured uncertainty in d_0, and by requiring that their longitudinal impact parameter, z_0,[5] satisfies $|z_0 \sin\theta| < 0.5$ mm.

Trigger leptons must be matched to a reconstructed lepton. The matched lepton transverse momentum must be at least 1 GeV above the trigger threshold.

Electron and muon candidates arising from photon conversions, hadron decays, or mis-reconstruction, are collectively referred to as non-prompt leptons. To further suppress this source of background, lepton candidates are required to be isolated in the tracker and in the calorimeter. The track-based lepton isolation criterion is based on the quantity $I_R = \sum p_{\mathrm{T}}^{\mathrm{trk}}$, where the scalar sum includes all tracks (excluding the lepton candidate itself) compatible with the primary vertex, with $p_{\mathrm{T}}^{\mathrm{trk}} > 1$ GeV, and within a cone of size $\Delta R = R_{\mathrm{cut}}$ around the direction of the lepton. The value of R_{cut} is the smaller of 0.3 and 10 GeV$/p_{\mathrm{T}}^{\ell}$, where p_{T}^{ℓ} is the lepton p_{T}. All lepton candidates must satisfy $I_R/p_{\mathrm{T}}^{\ell} < 0.15$. They are also required to satisfy a calorimeter-based isolation criterion: the sum of the transverse energy within a cone of size $\Delta R = 0.2$ around the lepton, after subtracting contributions from pile-up and the energy deposit of the lepton itself, is required to be less than 20% (30%) of the electron (muon) p_{T}^{ℓ}.

The "*Loose*" electron and muon identification and the impact parameter and isolation criteria described above constitute the "loose" lepton (L) definition. It is used (together with the τ_{had} definition described later) to pre-select events and categorise them into the different channels, as described in section 5, ensuring that the channel event selections are mutually exclusive. The "*Tight*" electron and "*Medium*" muon identification WPs and additional lepton criteria, described below, are used to reject further non-prompt leptons and electrons with an incorrect charge assignment or coming from a photon conversion. In total five different lepton definitions are used in this analysis: loose inclusive (L, and L', further described below), medium inclusive (M), medium exclusive (M_{ex}), and tight (T). The various lepton definitions are summarised in table 2 and their use in the different channels is described in sections 5 and 6.

Non-prompt leptons from hadron decays that contain bottom- or charm-quarks (referred to as "heavy-flavour (HF) non-prompt leptons") are further rejected using a boosted decision tree (BDT) discriminant, referred to as the non-prompt-lepton BDT [27, 31], based on isolation and lifetime information about a track-jet that matches the selected lepton. Three WPs based on the non-prompt-lepton BDT are used: *Tight*, *VeryTight*, and *Tight-not-VeryTight*. The *Tight* WP allows prompt muons (barrel/endcap electrons) satisfying the calorimeter- and track-based isolation criteria to be selected with an efficiency that is about 60% (60%/70%) for $p_{\mathrm{T}} \sim 20$ GeV and reaches a plateau of 95% (95%/90%) for $p_{\mathrm{T}} \sim 40$ (40/65) GeV. The prompt-lepton efficiency of the *VeryTight* WP for muons (barrel/endcap electrons) that satisfy

[4]The transverse impact parameter, d_0, is defined in the x-y plane as the distance of closest approach of the track to the beamline.

[5]The longitudinal impact parameter, z_0, is defined as the distance in z between the primary vertex and the point on the track used to evaluate d_0.

JHEP05(2026)183

the calorimeter- and track-based isolation criteria is about 55% (55%/60%) for $p_{\mathrm{T}} \sim 20$ GeV and reaches a plateau of 90% (85%/83%) for $p_{\mathrm{T}} \sim 40$ (40/65) GeV. The corresponding rejection factor[6] for muons (electrons) from the decay of b-hadrons ranges from 33 to 50 (20 to 50) for the *Tight* WP, and from 50 to 100 (33 to 66) for the *VeryTight* WP, depending on p_{T} and η, after resolving ambiguities between overlapping reconstructed objects. The *Tight-not-VeryTight* WP selects leptons that pass the *Tight* WP but not the *VeryTight* one; it enhances the selection of non-prompt leptons and is part of the event selection for control regions (CRs) enriched in HF non-prompt-lepton background, as described in section 6.

In order to further suppress electrons with incorrect charge assignment, a BDT discriminant based on calorimeter and tracking quantities [91] is used. Rejection factors of 19 (40) in the barrel (endcap) region are obtained in $t\bar{t}$ events, for an efficiency of approximately 96% (81%).

Most electrons arising from material conversions, i.e. from photon conversions in the detector material, are rejected by the standard electron identification selection, but additional requirements are imposed to remove residual material-conversion candidates. These candidates have a reconstructed displaced vertex with radius $r > 20$ mm that includes the track associated with the electron.[7] The invariant mass of the associated track and the closest (in $\Delta\eta$) opposite-charge track reconstructed in the silicon detector, calculated at the conversion vertex, is required to be less than 100 MeV. Internal conversion candidates, which correspond to low-mass virtual photon conversions (see section 3), must fail the requirements for material conversions, and the di-track invariant mass, calculated here at the primary vertex, is also required to be less than 100 MeV. Material and internal conversion candidates thus reconstructed are vetoed except in the L definition (no veto applied), and in the electron selection of the CR enriched in conversions described in section 6 (the conversion candidate e^* passes the M selection except that the conversion veto is reversed).

A looser lepton definition, denoted L', which omits the non-prompt-lepton BDT requirement, while retaining the tighter identification, charge mis-assignment, and conversion vetos, is used to increase the acceptance of backgrounds in corresponding control regions.

The constituents for jet reconstruction are identified by combining measurements from both the ID and the calorimeter using a particle flow (PFlow) algorithm [92]. Jet candidates are reconstructed from these PFlow objects using the anti-k_t algorithm [93, 94] with a radius parameter of $R = 0.4$. They are calibrated using simulation with corrections obtained by using *in situ* techniques in data [95]. Jet candidates with $p_{\mathrm{T}} > 25$ GeV and within $|\eta| < 2.5$ are used to define the event selection. In order to reduce the effect of pile-up, each jet with $p_{\mathrm{T}} < 60$ GeV and $|\eta| < 2.4$ must satisfy the "*Tight*" WP of the jet-vertex tagger (JVT) [96] criteria used to identify jets that originate from the primary vertex. Forward jets with $p_{\mathrm{T}} > 25$ GeV and $2.5 < |\eta| < 4.5$ are not used in the event selection but in some kinematic variables. They must satisfy the "*Tight*" WP of the forward jet-vertex-tagger (fJVT) [97]. A set of quality criteria is also applied to reject events containing at least one jet arising from non-collision sources or detector noise [98].

[6]The rejection factor for a background is defined as the reciprocal of the efficiency evaluated for that background.

[7]The beampipe and IBL inner radii are 23.5 mm and 33 mm, respectively.

JHEP05(2026)183

	Electron					Muon				
Lepton definition	L	L'	M	M_{ex}	T	L	L'	M	M_{ex}	T
Identification	*Loose*	*Tight*				*Loose*	*Medium*			
Transverse impact parameter significance $\lvert d_0\rvert/\sigma_{d_0}$	< 5					< 3				
Longitudinal impact parameter z_0	$\lvert z_0 \sin\theta\rvert < 0.5$ mm									
Isolation	Yes					Yes				
Non-prompt lepton WP	—		*Tight*	*Tight-not-VeryTight*	*VeryTight*	—		*Tight*	*Tight-not-VeryTight*	*VeryTight*
Electron charge-misassignment veto	—	Yes				—				
Electron conversion candidate veto	—	Yes (except e^*)				—				

Table 2. Description of the loose inclusive (L and L'), medium inclusive (M), medium exclusive (M_{ex}), and tight (T) lepton definitions. The electron e^* is required to fulfil, in addition to the corresponding lepton definition requirements, those corresponding to an internal or material conversion candidate. The symbol '—' denotes that no requirement is applied for a given lepton definition.

Jets containing b-hadrons are identified (b-tagged) via the DL1r algorithm [99] that uses a deep-learning neural network based on the distinctive features of b-hadron decays, primarily the impact parameters of tracks and the displaced vertices reconstructed in the ID. Additional input to this network is provided by discriminating variables constructed by a recurrent neutral network (RNN) [99], which exploits the spatial and kinematic correlations between tracks originating from the same b-hadron. A multivariate b-tagging discriminant value is calculated for each jet. In this article, three different WPs corresponding to 85%, 77%, and 70% average expected efficiency to tag a b-quark jet are used, with light-jet[8] rejection factors of about 40 to 600, and charm-jet (c-jet) rejection factors of about 3 to 12, as determined for jets with $p_{\text{T}} > 20$ GeV and $|\eta| < 2.5$ in simulated $t\bar{t}$ events [100–102]. Only the 85% and 77% WPs are used for event selection, while the 70% WP is used for the overlap removal described below. The notations $b^{85\%}$, $b^{77\%}$, and $b^{70\%}$ are used to denote a b-tagged jet (b-jet) that passed the corresponding WP. Correction factors derived from dedicated calibration samples enriched in b-jets, c-tagged jets, or light-tagged jets, are applied to the simulated event samples.

Hadronic τ-lepton decays produce a neutrino and visible decay products, mostly one or three charged pions and up to two neutral pions. The reconstruction of the visible products of hadronically decaying τ-leptons ($\tau_{\text{had-vis}}$) is seeded by jets reconstructed using the anti-k_t algorithm [93, 94] where topological clusters of calorimeter energy deposits are used as inputs with a distance parameter of $R = 0.4$. BDTs are used to determine if tracks originate from a $\tau_{\text{had-vis}}$, and one (1-prong) or three (3-prong) tracks with a total charge of ± 1 are required. An RNN algorithm [103] using calorimeter and tracking-based variables is employed to identify $\tau_{\text{had-vis}}$ candidates and reject quark or gluon jets. The chosen "*Medium*" identification WP has an efficiency of 75% (60%) for 1-(3-) prong τ_{had} decays. A separate BDT is then used to reject $\tau_{\text{had-vis}}$ candidates with one associated track that originate from electrons, with a rejection factor of $\sim 30 - 100$ depending on η and p_{T} while reaching an efficiency of about 95% for real $\tau_{\text{had-vis}}$. The $\tau_{\text{had-vis}}$ energy scale is determined by combining information from the associated tracks, calorimeter energy clusters and reconstructed neutral

[8] 'Light-jet' refers to a jet originating from the hadronisation of a light quark (u, d, s) or a gluon.

JHEP05(2026)183

pions [104] using a multivariate regression technique [105] trained in MC samples. The $\tau_{\text{had-vis}}$ candidates with $p_{\text{T}} > 20$ GeV and $|\eta| < 2.5$, excluding the electromagnetic calorimeter transition region, are selected.

Ambiguities between independently reconstructed electrons, muons, $\tau_{\text{had-vis}}$ and jets can arise. A sequential "overlap removal" procedure is performed to resolve these ambiguities and thus avoid double counting of detector signatures. This procedure is applied to leptons satisfying the L criteria. If two electrons share the same track, only the one with the higher p_{T} is kept. A $\tau_{\text{had-vis}}$ candidate within $\Delta R < 0.2$ of an electron or a muon is removed. If an electron and a muon share the same ID track, the muon is removed if it is reconstructed only from an ID track and calorimeter energy deposits consistent with a minimum-ionising particle (i.e. if it is "calo-tagged"), otherwise the electron is removed. If an electron and a selected jet are found within $\Delta R < 0.2$, the jet is removed if it is not a $b^{70\%}$ jet or if it has $p_{\text{T}} > 200$ GeV. Muons ghost-associated [106] with an $R = 0.4$ jet must satisfy a jet-muon separation of $\Delta R < 0.4$. If the overlapping jet is not a $b^{70\%}$ jet and contains less than three tracks with $p_{\text{T}} > 500$ MeV, the jet is removed, otherwise the muon is removed. If a $\tau_{\text{had-vis}}$ and a jet are found within $\Delta R < 0.2$ the object is interpreted as a $\tau_{\text{had-vis}}$ and the matched jet candidate is removed. For each lepton in the event a lepton-p_{T}-dependent variable-size cone of maximum size $\Delta R = 0.4$ is defined. If a selected jet, surviving all previous overlap criteria, is found in this cone, the lepton is removed.

The missing transverse momentum $\boldsymbol{p}_{\text{T}}^{\text{miss}}$ (with magnitude $E_{\text{T}}^{\text{miss}}$) is defined as the negative vector sum of the $\boldsymbol{p}_{\text{T}}$ of all selected and calibrated objects in the event, including a term to account for the momenta of soft particles that are not associated with any of the selected objects [107]. This soft term is calculated from ID tracks matched to the primary vertex, which makes it more resilient to contamination from pile-up interactions.

5 Event selection and categorisation

The analysis strategy is based on six different channels, corresponding to final states differentiated by the number and charge of loose light leptons of each flavour, and number of $\tau_{\text{had-vis}}$ candidates. The considered channels are displayed in figure 2(a) and are:

- $2\ell\text{SS}0\tau_{\text{had}}$: two same-charge light leptons and no $\tau_{\text{had-vis}}$ candidates;
- $3\ell 0\tau_{\text{had}}$: three light leptons and no $\tau_{\text{had-vis}}$ candidates;
- 4ℓ: four light leptons regardless of the number of $\tau_{\text{had-vis}}$ candidates;
- $2\ell\text{SS}1\tau_{\text{had}}$: two same-charge light leptons and one $\tau_{\text{had-vis}}$ candidate;
- $1\ell 2\tau_{\text{had}}$: one light lepton and two $\tau_{\text{had-vis}}$ candidates;
- $2\ell 2\tau_{\text{had}}$: two light leptons and two $\tau_{\text{had-vis}}$ candidates.

These lepton selection criteria ensure orthogonality so that no event is classified in multiple channels. To increase the signal sensitivity, further requirements on the lepton, $\tau_{\text{had-vis}}$ and jet properties are imposed in each channel, as shown in table 3 and detailed below. Figure 2(b) shows the expected contribution in each channel from the different Higgs

JHEP05(2026)183

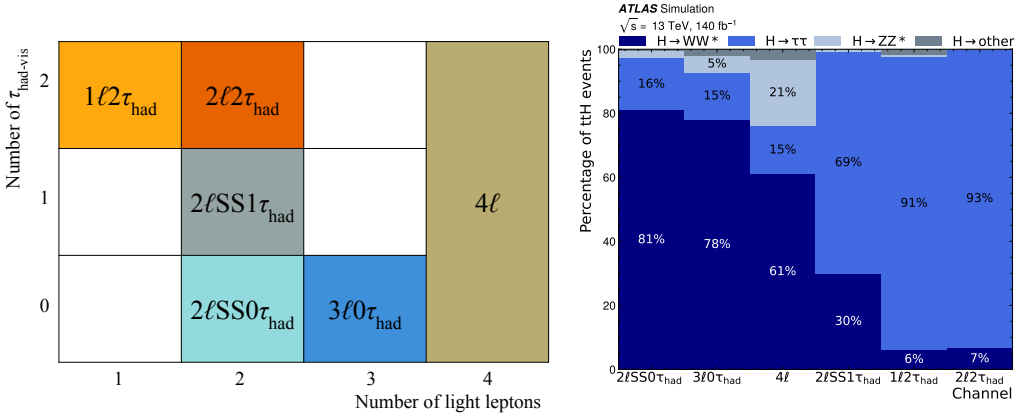

(a) (b)

Figure 2. (a) Analysis channel definition in terms of light lepton and $\tau_{\text{had-vis}}$ multiplicities. (b) Fraction of the expected $t\bar{t}H$ signal arising from different Higgs boson decay modes in each signal channel.

boson decay modes in the $t\bar{t}H$ signal. The light leptons and $\tau_{\text{had-vis}}$, as well as the jets in the event, can originate either from the Higgs boson decay products (τ-lepton, W or Z bosons) or from the W bosons in top-quark decays. In addition, multiple neutrinos can be produced in these decays together with the light leptons and $\tau_{\text{had-vis}}$, thus an attempt to fully reconstruct the Higgs boson or top quarks is difficult. Instead, the properties of the objects (such as multiplicity, p_{T}, angular separation or invariant mass) in the event are exploited to separate the signal from the main backgrounds. The jet multiplicity distribution for each channel is shown in figure 3, illustrating the background composition and signal contribution before any categorisation is applied. The background processes are described in section 6 and, as detailed there, some of the event selection requirements in table 3 are loosened or inverted to define background control regions.

Multivariate analysis (MVA) algorithms, either BDTs or deep neural networks (DNNs), are used to further separate the signal from the relevant backgrounds. The modelling of the input variables used in the training of the MVAs was studied and no significant discrepancies between data and simulation were observed. The output scores from these BDTs or DNNs are used to define separate event categories in the $2\ell\text{SS}0\tau_{\text{had}}$, $3\ell 0\tau_{\text{had}}$ and 4ℓ channels, and are the final discriminants in most categories. The signal-enriched categories are the signal regions (SRs) in the analysis, while the categories enriched in the different background processes are used as CRs for their estimation, as detailed in section 6.

In the STXS stage-1.2 formalism, $t\bar{t}H$ production is measured in bins of the generator-level p_{T}^{H} prior to Higgs-boson decay. These bins are denoted as STXS 1–6 and correspond to p_{T}^{H} values in the range 0–60 GeV, 60–120 GeV, 120–200 GeV, 200–300 GeV, 300–450 GeV and >450 GeV. In the $2\ell\text{SS}0\tau_{\text{had}}$ and $3\ell 0\tau_{\text{had}}$ channels, a GNN is trained to estimate p_{T}^{H} and is used to further categorise the events according to the $t\bar{t}H$ STXS regions. The input features for this GNN include: the four-momenta of leptons, jets, and $E_{\text{T}}^{\text{miss}}$; the jet b-tagging information; the angular separation, invariant mass and p_{T} for all combinations of leptons, jets, and $E_{\text{T}}^{\text{miss}}$; the jet multiplicity, and the scalar sum of the p_{T} of all combinations of

JHEP05(2026)183

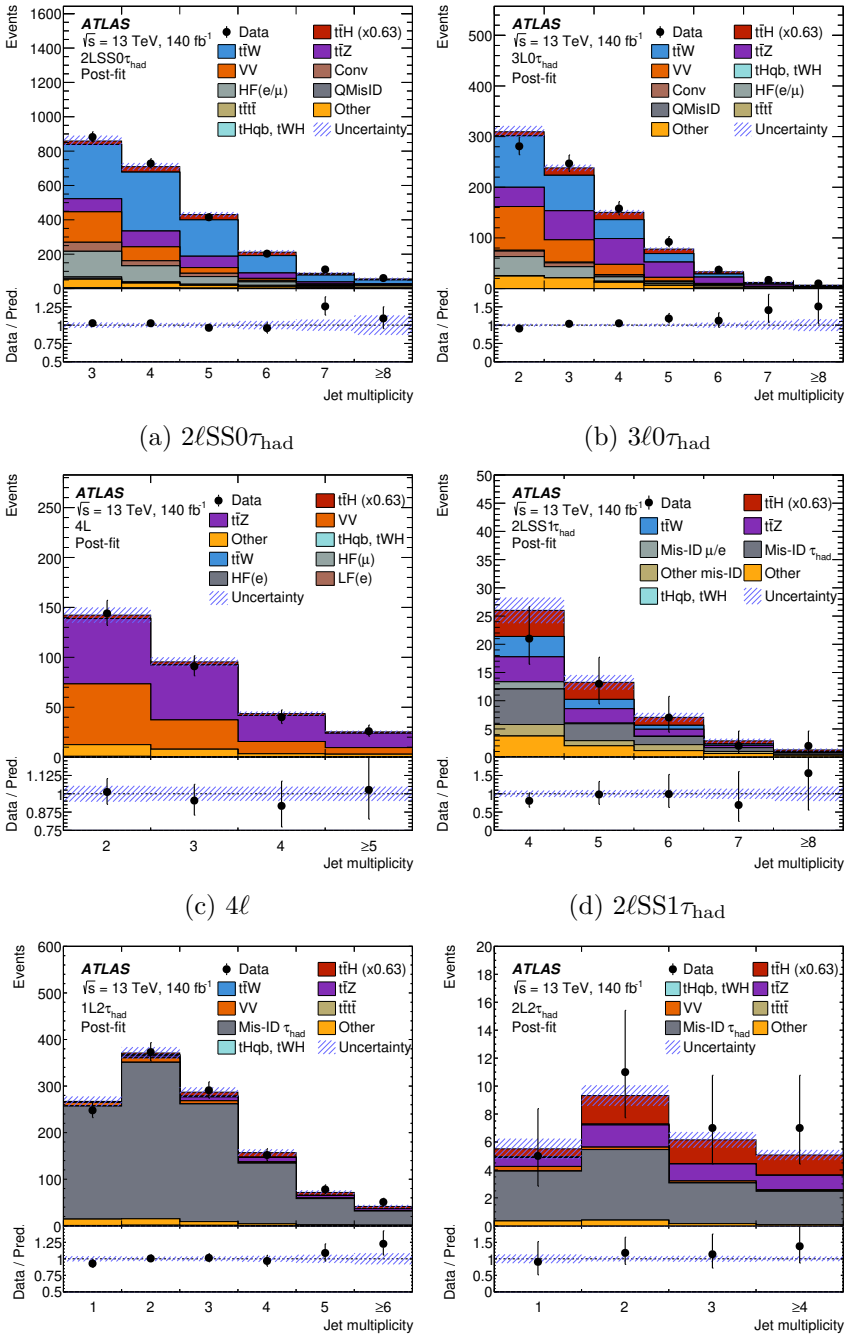

(a) $2\ell\text{SS}0\tau_{\text{had}}$ (b) $3\ell 0\tau_{\text{had}}$

(c) 4ℓ (d) $2\ell\text{SS}1\tau_{\text{had}}$

(e) $1\ell 2\tau_{\text{had}}$ (f) $2\ell 2\tau_{\text{had}}$

Figure 3. Comparison between data and the signal-plus-background prediction for the distribution of jet multiplicity in the (a) $2\ell SS0\tau_{\text{had}}$, (b) $3\ell 0\tau_{\text{had}}$, (c) 4ℓ, (d) $2\ell SS1\tau_{\text{had}}$, (e) $1\ell 2\tau_{\text{had}}$, and (f) $2\ell 2\tau_{\text{had}}$ channels. The signal and background normalisation factors and the nuisance parameters are set to their best-fit values as described in section 8. The shaded band indicates the total uncertainty, including correlations.

JHEP05(2026)183

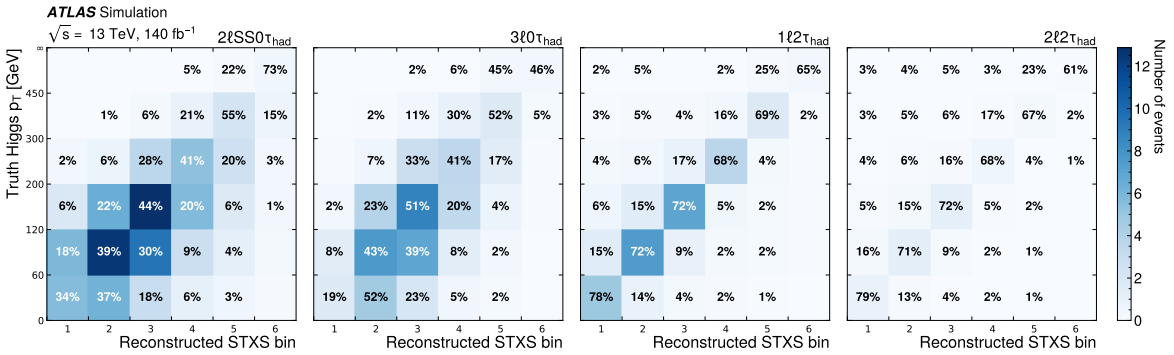

Figure 4. STXS migration matrices evaluated in the $t\bar{t}H$ MC sample for the analysis channels featuring a p_{T}^{H} estimation. Colours denote the overall fraction of events in each STXS bin, while numbers display the predicted yield fractions normalised to each truth STXS bin.

leptons and jets. In the $1\ell 2\tau_{\mathrm{had}}$ and $2\ell 2\tau_{\mathrm{had}}$ channels, p_{T}^{H} is estimated using a BDT that takes as input the p_{T} of the two $\tau_{\text{had-vis}}$ in the event as well as their angular separation and invariant mass. Figure 4 shows the migration across STXS bins for the different channels estimated in the $t\bar{t}H$ MC sample. No p_{T}^{H} reconstruction is performed in the 4ℓ and $2\ell\mathrm{SS}1\tau_{\mathrm{had}}$ channels. Due to significant migration effects and limited statistics, some reconstructed p_{T}^{H} bins are merged depending on the channel: in the $2\ell\mathrm{SS}0\tau_{\mathrm{had}}$, $3\ell 0\tau_{\mathrm{had}}$, and $1\ell 2\tau_{\mathrm{had}}$ channels, bins 5 and 6 are merged together; in the $2\ell 2\tau_{\mathrm{had}}$ channels, bins 1 and 2 on one hand, and bins 3, 4, 5, and 6 on the other hand, are merged together. As described in section 8, some truth p_{T}^{H} bins are also merged, such that the measurement is done with the following three bins: 0–120 GeV, 120–200 GeV, and >200 GeV.

5.1 $2\ell SS0\tau_{\mathrm{had}}$ channel

Events in this channel must contain two same-charge light leptons with $p_{\mathrm{T}} > 15$ GeV satisfying the T requirements in table 2. To reject backgrounds like diboson or $t\bar{t}W$ production, selected events contain at least three jets with at least one of them being b-tagged with the 85% b-tagging WP and no $\tau_{\text{had-vis}}$ candidates. Categories in this channel are defined using a multi-class BDT considering separate classes for the $t\bar{t}H$ and $tHqb$ signal processes and the main $t\bar{t}W$ background. A fourth class is included in the training containing the contributions from all other background processes, such as $t\bar{t}Z$, $t\bar{t}$ and $t\bar{t}t\bar{t}$. This BDT uses 20 input variables describing the kinematics of the leptons, jets and $E_{\mathrm{T}}^{\mathrm{miss}}$. The most discriminating variables[9] are the jet multiplicity, the invariant mass of the dilepton pair, and the average angular separation between the jets in the event.

Events are classified into categories according to the highest BDT output score and, in the case of $t\bar{t}H$ and $t\bar{t}W$, the total charge of the leptons (denoted as '++' or '−−') to exploit the relative charge asymmetry between $t\bar{t}W^{+}$ and $t\bar{t}W^{-}$ production. To reduce the contamination from $t\bar{t}t\bar{t}$ production, events with at least six jets and with at least three b-tagged jets at the 77% working point are discarded from the $t\bar{t}H$ categories. Furthermore, the $t\bar{t}H$ categories are

[9]In the MVA algorithms in this paper, the most discriminating variables are determined using the permutation importance method [108, 109].

JHEP05(2026)183

	$2\ell\text{SS}0\tau_{\text{had}}$	$3\ell0\tau_{\text{had}}$	4ℓ	$2\ell\text{SS}1\tau_{\text{had}}$	$1\ell2\tau_{\text{had}}$	$2\ell2\tau_{\text{had}}$
Light leptons						
N_ℓ	2	3	4	2	1	2
Lepton definition	T	ℓ_0,ℓ_1,ℓ_2: L,T,T	L	M	L	L
Lepton p_{T} [GeV]	> 15	ℓ_0,ℓ_1,ℓ_2: > 10, 15, 15	> 10	> 15	> 27	> 10
$\sum q_\ell$	±2	±1	0	±2	±1	0
$\lvert m_{\ell\ell} - m_Z\rvert$ [GeV]	—	> 10 (SFOS)	—	> 10 (SF)	—	> 10
$m_{\ell\ell}$ [GeV]	—	> 12 (SFOS)	> 12 (SFOS)	—	—	> 12
$m(4\ell)$ [GeV]	—	—	<115 or >130	—	—	—
$\tau_{\text{had-vis}}$ and jets						
$N_{\tau_{\text{had-vis}}}$	0	0	—	1	2	2
$\sum q_{\tau_{\text{had-vis}}}$	—	—	—	±1	0	0
N_{jets}	≥ 3	≥ 2	≥ 2	≥ 4	≥ 1	≥ 1
$N_{b^{85\%}}$	≥ 1	≥ 1	≥ 1	≥ 1	—	—
$N_{b^{77\%}}$	—	—	—	—	≥ 1	≥ 1
Number of categories	14	11	2	1	6	2

Table 3. Summary of the channel definitions, with the requirements placed on the number of light leptons (N_ℓ), $\tau_{\text{had-vis}}$ ($N_{\tau_{\text{had-vis}}}$) and jets ($N_{\text{jets}}$), as well as the lepton p_{T}, invariant masses and total charge of the light leptons ($\sum q_\ell$) or $\tau_{\text{had-vis}}$ ($\sum q_{\tau_{\text{had-vis}}}$). Some of the dilepton invariant mass requirements are only applied for pairs of same-flavour (SF) or SF opposite-sign (SFOS) leptons. The requirements on 'lepton definition' are summarised in table 2. The symbol '—' denotes that no requirement is applied for a given variable and channel.

split into five categories each according to the reconstructed p_{T}^H values. In total, 14 categories are considered in this channel, whose observed and expected yields are shown in figure 5.

5.2 $3\ell0\tau_{\text{had}}$ channel

Events in this channel must contain three light leptons with total a charge of ±1. The lepton with charge opposite to the other two is denoted as ℓ_0, while the two leptons in the event with the same electric charge (denoted ℓ_1 and ℓ_2, with ℓ_1 being the closest to ℓ_0 in ΔR) are required to fulfil the T requirements in table 2 and have $p_{\text{T}} > 15$ GeV. Additional requirements on the invariant mass of same-flavour opposite-sign (SFOS) dilepton pairs are applied to suppress Z-boson and other resonant backgrounds, and events also should have at least two jets with at least one of them being b-tagged with the 85% b-tagging WP to reject the diboson, $t\bar{t}W$ and $t\bar{t}Z$ backgrounds.

As in the previous channel, event categories are defined using a multi-class BDT with six output nodes for the $t\bar{t}H$ and $tHqb$ signals as well as the $t\bar{t}W$, $t\bar{t}Z$, diboson and $t\bar{t}$ backgrounds. A total of 25 input variables related to the multiplicities and properties of leptons, jets, b-jets and $E_{\text{T}}^{\text{miss}}$ are employed in the BDT training. The most discriminating variables include the jet multiplicity, the invariant masses of the $\ell_1\ell_2$ and $\ell_1\ell_0$ systems, and the average angular separation between leptons and jets.

Seven categories, each dedicated to enhancing a given process, are built by applying selections in the output scores to maximise its statistical significance, with the remaining

JHEP05(2026)183

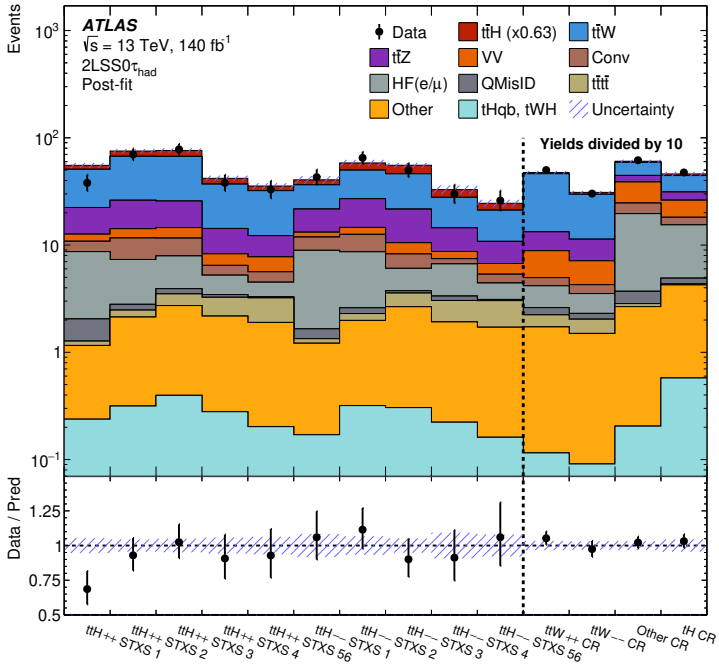

Figure 5. Observed and expected event yields in all the categories in the 2ℓSS0τ_{had} channel. The signal and background normalisation factors and the nuisance parameters are set to their best-fit values as described in section 8. The categories denoted as 'STXS n' correspond to the n-th bin in the STXS formalism described in section 5. When several STXS bins are merged together, all numbers are quoted (e.g. 'STXS 56' corresponds to STXS bins 5 and 6). The notation '++' or '−−' correspond to the total charge of the leptons in the category. The shaded band indicates the total uncertainty, including correlations. The vertical line indicates the bins in which the event yields have been scaled down by a factor 10.

events included in a separate category. The $t\bar{t}H$ category is further split into five categories according to the reconstructed p_{T}^{H} values. In total, 11 categories are considered in the $3\ell0\tau_{\text{had}}$ channel whose observed and expected yields are shown in figure 6.

5.3 4ℓ channel

Events in this channel are required to have four light leptons with total charge equal to zero, regardless of the number of $\tau_{\text{had-vis}}$ candidates. Requirements are imposed in the invariant mass of any SFOS pair to reduce the contribution from low-mass resonances, as well as a veto on the four-lepton invariant mass close to the Higgs boson mass to ensure orthogonality with the $H \to ZZ^* \to 4\ell$ analysis [21]. Events are also required to have at least two jets with at least one of them being b-tagged with the 85% b-tagging WP.

This channel uses a DNN with three output nodes for the $t\bar{t}H$ signals as well as the $t\bar{t}Z$ and ZZ backgrounds. The DNN training is performed using 22 input variables, with the most discriminating ones including the $E_{\text{T}}^{\text{miss}}$ and the invariant masses of the different dilepton pairs in the event. Using the DNN ZZ output score, two separate categories are built enhanced in $t\bar{t}H$ and ZZ production as shown in figure 7. Since the low part of the DNN distribution in the $t\bar{t}H$ category features a good purity in $t\bar{t}Z$ events, no explicit $t\bar{t}Z$ category is defined.

JHEP05(2026)183

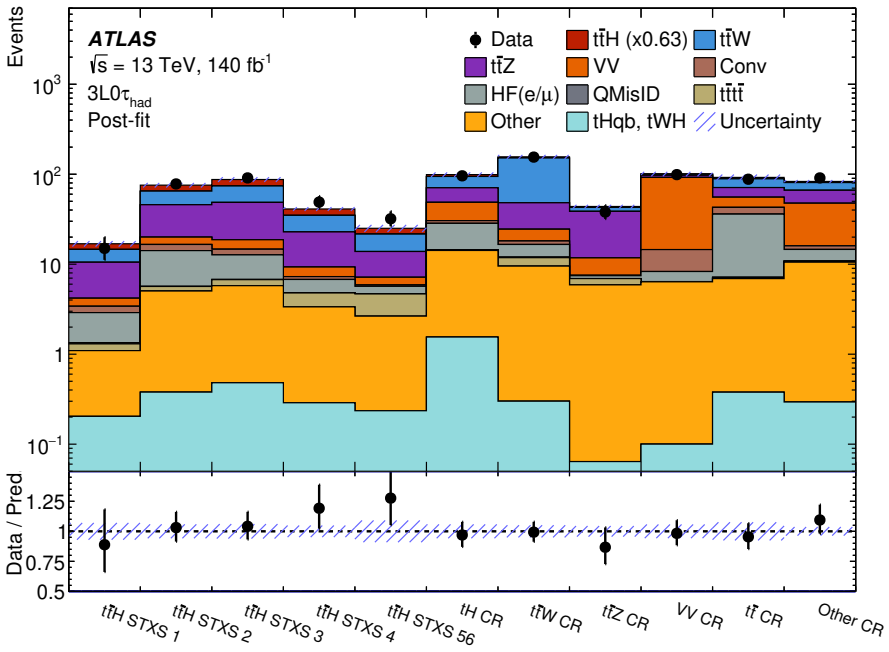

Figure 6. Observed and expected event yields in all the categories in the $3\ell 0\tau_{\text{had}}$ channel. The signal and background normalisation factors and the nuisance parameters are set to their best-fit values as described in section 8. The categories denoted as 'STXS n' correspond to the n-th bin in the STXS formalism described in section 5. When several STXS bins are merged together, all numbers are quoted (e.g. 'STXS 56' corresponds to STXS bins 5 and 6). The shaded band indicates the total uncertainty, including correlations.

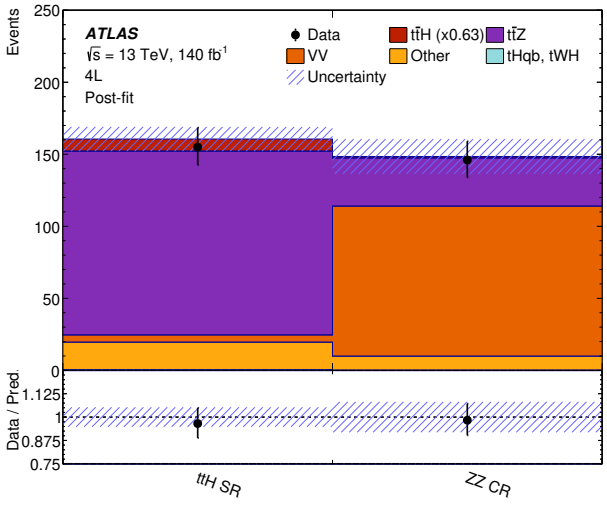

Figure 7. Observed and expected event yields in all the categories in the 4ℓ channel. The signal and background normalisation factors and the nuisance parameters are set to their best-fit values as described in section 8. The shaded band indicates the total uncertainty, including correlations.

JHEP05(2026)183

5.4 $2\ell SS1\tau_{\text{had}}$ channel

Events in this channel are required to have two light leptons fulfilling the M requirements in table 2, with $p_{\text{T}} > 15$ GeV and the same electric charge, plus one $\tau_{\text{had-vis}}$ candidate with $p_{\text{T}} > 20$ GeV. For the events where both light leptons have the same flavour, their invariant mass must not be within 10 GeV of the Z-boson mass to suppress backgrounds featuring Z-boson decays. In addition, further rejection of the main backgrounds is obtained by requiring events to have at least four jets and at least one of them must be b-tagged with the 85% b-tagging WP.

A total of 17 input variables are used to train a multi-class BDT with three output nodes for the $t\bar{t}H$ signal as well as the $t\bar{t}W$ and $t\bar{t}$ backgrounds. The BDT training is performed with a relaxed event selection accepting events with at least three jets to increase the available MC statistics. The most discriminating variables in the BDT, evaluated at the training selection level, are the jet multiplicity, the invariant mass of the system formed by the leptons and the $E_{\text{T}}^{\text{miss}}$, and the scalar sum of the transverse momenta of jets, leptons and $\tau_{\text{had-vis}}$ candidates in the event. Since it was found not to improve the sensitivity, no further categorisation is performed in this channel but the BDT output score for the $t\bar{t}H$ class is used as discriminant variable.

5.5 $1\ell 2\tau_{\text{had}}$ channel

Events in this channel are required to have one light lepton with $p_{\text{T}} > 27$ GeV fulfilling the L requirements in table 2, plus two $\tau_{\text{had-vis}}$ candidates with $p_{\text{T}} > 20$ GeV and opposite electric charge. Events must also have at least one jet fulfilling the 77% b-tagging WP requirements. Two separate categories are built depending on the number of jets in the event: a first category enhanced in $tHqb$ signal contains all the events with one or two jets, while events with at least three jets constitute a second category enhanced in $t\bar{t}H$ signal events. Similarly to the $2\ell\text{SS}0\tau_{\text{had}}$ channel, the $t\bar{t}H$ category is split into five categories each according to the reconstructed p_{T}^{H} values. In total, 6 categories are considered in this channel, whose observed and expected yields are shown in figure 8.

Separate binary BDT classifiers are trained in each category to improve the signal separation from the background, and are used as discriminant variable in the analysis. For the $tHqb$-enhanced category, 17 input variables are used for the BDT training with the most relevant being minimum angular distance between the jets and $\tau_{\text{had-vis}}$, and the azimuthal angle between the top-quark candidate (reconstructed with the lepton, $E_{\text{T}}^{\text{miss}}$ and leading b-jet) and the di-$\tau_{\text{had-vis}}$ system. For the $t\bar{t}H$-enhanced category, 12 input variables are used, the most relevant ones being the azimuthal separation between the di-$\tau_{\text{had-vis}}$ system and the $E_{\text{T}}^{\text{miss}}$, and the largest $|\eta|$ value of the two $\tau_{\text{had-vis}}$ candidates.

5.6 $2\ell 2\tau_{\text{had}}$ channel

Events in this channel are required to have two light leptons fulfilling the L requirements in table 2 with opposite electric charge and two $\tau_{\text{had-vis}}$ candidates with $p_{\text{T}} > 20$ GeV and opposite electric charge. Requirements are imposed on the dilepton invariant mass to reduce the contribution from Z boson and other light resonances. Events must also have at least one jet fulfilling the 77% b-tagging WP requirements. Figure 8 shows the observed

JHEP05(2026)183

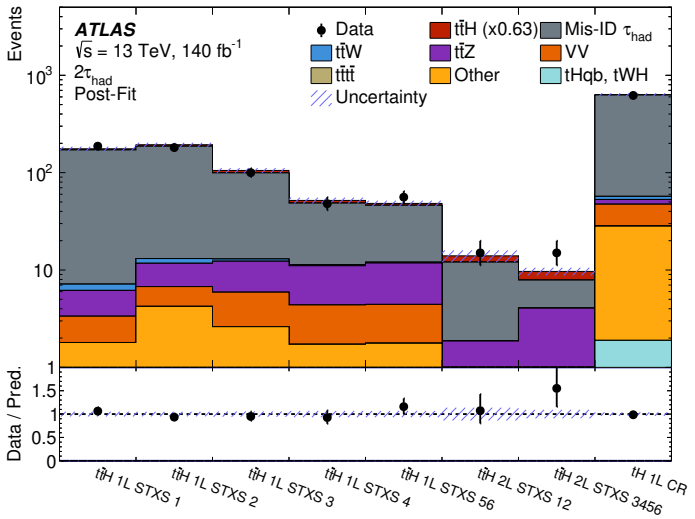

Figure 8. Observed and expected event yields in all the categories in the $1\ell 2\tau_{\text{had}}$ and $2\ell 2\tau_{\text{had}}$ channels. The signal and background normalisation factors and the nuisance parameters are set to their best-fit values as described in section 8. The shaded band indicates the total uncertainty, including correlations.

and expected yields in this channel. Two separate categories are built according to the reconstructed p_{T}^{H} value.

A binary BDT classifier is used to improve the channel sensitivity, which is trained to separate the $t\bar{t}H$ signal from the background, which is dominated by events with misidentified τ_{had}. This BDT uses 10 input variables, the most discriminating ones being the largest $|\eta|$ value of the two $\tau_{\text{had-vis}}$ candidates, the azimuthal separation between the di-$\tau_{\text{had-vis}}$ system and the $E_{\text{T}}^{\text{miss}}$ and the angular separation between $\tau_{\text{had-vis}}$ and jets. No further categorisation is performed in this channel although the BDT output score for the $t\bar{t}H$ class is used as discriminant variable in the analysis.

6 Background estimation

Background processes are categorised as either irreducible or reducible. Irreducible backgrounds are defined as events in which all selected leptons are prompt, i.e. are produced in W or Z boson decays, leptonic τ-lepton decays, or photon internal conversions. Events containing at least one selected non-prompt lepton, a misidentified τ_{had}, or a light lepton with a mis-assigned charge (QMisID), are considered reducible.

The misidentified τ_{had} background is estimated with data-driven techniques. All other backgrounds, including non-prompt leptons, are estimated from MC, with the yields of $t\bar{t}W$, $t\bar{t}Z$, WZ, WW/ZZ, and non-prompt lepton backgrounds being adjusted via normalisation factors that are determined by performing a likelihood fit to data across all event categories described in section 5 as well as dedicated control regions defined specifically to help constraining a particular background. Table 4 shows the definition of the control regions used in the $2\ell\text{SS}0\tau_{\text{had}}$, $3\ell 0\tau_{\text{had}}$, and 4ℓ channels. Table 5 shows the definition of the control regions used in the $2\ell\text{SS}1\tau_{\text{had}}$, $1\ell 2\tau_{\text{had}}$ and $2\ell 2\tau_{\text{had}}$ channels. For some backgrounds, like

JHEP05(2026)183

	2ℓSS0τ_{had} and $3\ell0\tau_{\text{had}}$ channels				4ℓ channel	
Region	3ℓVV	$3\ell t\bar{t}Z$	3ℓIntC, 3ℓMatC	$2\ell\text{tt(e)}_{TM_{\text{ex}}}$, $2\ell\text{tt(e)}_{M_{\text{ex}}T}$, $2\ell\text{tt}(\mu)_{TM_{\text{ex}}}$, $2\ell\text{tt}(\mu)_{M_{\text{ex}}T}$, $2\ell\text{tt(e)}_{M_{\text{ex}}M_{\text{ex}}}$, $2\ell\text{tt}(\mu)_{M_{\text{ex}}M_{\text{ex}}}$	3ℓ μ HF, 3ℓ e HF	3ℓ e LF
Lepton requirement	3ℓ		$\mu\mu e^*$	2ℓSS	$e^{\mp}\mu^{\pm}\mu^{\pm}$, $\mu^{\mp}e^{\pm}e^{\pm}$	$\mu^{\pm}\mu^{\mp}e^{\mp}$
Lepton definition	(L or L', M, M)		(L, M, M)	(T, M_{ex}) or (M_{ex}, T) or (M_{ex}, M_{ex})	L	
Lepton p_{T} [GeV]	(10, 15, 15)			(15, 15)	(10,10,10)	
$\lvert m^{\text{SF}}_{\ell^+\ell^-} - m_Z\rvert$ [GeV]	< 10		> 10	—	—	< 10
$\lvert m_{\ell\ell\ell} - m_Z\rvert$ [GeV]	> 10		< 10	—	—	> 15
$m_{\text{T}}(\ell_0, E_{\text{T}}^{\text{miss}})$ [GeV]	—			< 250 for TM_{ex} and $M_{\text{ex}}T$ pairs	—	
$E_{\text{T}}^{\text{miss}}$ [GeV]	—			—	—	< 20
N_{jets}	2 or 3	≥ 4	—	≥ 2	≥ 1	
$N_{b\text{-jets}}$	1 $b^{85\%}$	≥ 1 $b^{85\%}$	0 $b^{85\%}$	1 $b^{85\%}$	≥ 1 $b^{85\%}$	0 $b^{85\%}$
$\tau_{\text{had-vis}}$ candidates	0			0	—	
$3\ell0\tau_{\text{had}}$ channel veto	—			—	Yes	
Region split	—	—	internal, material	sub-leading e/μ $\times$ (TM_{ex}, $M_{\text{ex}}T$, $M_{\text{ex}}M_{\text{ex}}$)	$e^{\mp}\mu^{\pm}\mu^{\pm}$, $\mu^{\mp}e^{\pm}e^{\pm}$	—

Table 4. Event selection summary of the control regions in the 2ℓSS0τ_{had}, $3\ell0\tau_{\text{had}}$, and 4ℓ channels. The lepton types L, L', M, M_{ex}, and T correspond to the definitions described in table 2. The L' category is only used in the 3ℓVV and $3\ell t\bar{t}Z$ regions with an opposite-sign muon. The notation e^* is used to denote material conversion or internal conversion candidates, as described in section 4.

diboson production, the simulation is improved by applying additional corrections derived from data control samples before the simultaneous fit as detailed below. The values of the normalisation factors given in this section are obtained from the combined fit for the inclusive $t\bar{t}H$ cross-section measurement presented in section 8. For background sources normalised to data, uncertainties on their predicted cross-section are ignored.

6.1 Irreducible backgrounds

Background contributions with prompt leptons originate from a wide range of physics processes with the relative importance of individual processes varying by channel. The main irreducible backgrounds originate from $t\bar{t}W$, $t\bar{t}Z/\gamma^*$ and VV. Smaller contributions originate from the following rare processes: tZ, tW, tWZ, $t\bar{t}WW$, VVV, $t\bar{t}t\bar{t}$ and $t\bar{t}t$ production. Backgrounds with prompt leptons are estimated from simulation using the samples described in section 3.

The VV simulated event sample does not model the jet multiplicity spectrum in data well. Therefore, the same N_{jets}-dependent data-driven correction as the one described in the recent ATLAS $t\bar{t}W$ measurement [31] is applied to the VV sample in the 2ℓSS0τ_{had}, $3\ell0\tau_{\text{had}}$ and 2ℓSS1τ_{had} channels. This correction is derived from an inclusive trilepton diboson-enriched region with zero b-tagged jets at the 85% WP.

JHEP05(2026)183

	2ℓSS$1\tau_{\text{had}}$ channel			$1\ell 2\tau_{\text{had}}$ and $2\ell 2\tau_{\text{had}}$ channels			
Region	CR-OS	CR-SS	$\text{VR}_{1\tau_{\text{had}}}$	FF-Z	FF-tt	$\text{VR}^{1\ell}_{2\tau_{\text{had}}}$	$\text{VR}^{2\ell}_{2\tau_{\text{had}}}$
Lepton requirement	2, OS	2, SS	2, OS	2, OS	2, OS	1	2, OS
Lepton definition	M	L'	M	L	L	L	L
$\tau_{\text{had-vis}}$ requirement	1	1	1	2, OS	2, OS	2, SS	2, SS
$\tau_{\text{had-vis}}$ definition	M	M	M	VL	VL	M	M
$\lvert m^{\text{SF}}_{\ell^+\ell^-} - m_Z\rvert$ [GeV]	—	—	—	< 10	> 10	—	—
N_{jets}	2 or 3	2 or 3	≥ 4	≥ 1	≥ 1	≥ 1	≥ 1
$N_{b\text{-jets}}$	$\geq 1\ b^{85\%}$	$\geq 1\ b^{85\%}$	$\geq 1\ b^{85\%}$	$0\ b^{77\%}$	$\geq 1\ b^{77\%}$	$\geq 1\ b^{77\%}$	$\geq 1\ b^{77\%}$
Region split	—	ee, $e\mu$, μe, $\mu\mu$	—	—	—	—	—

Table 5. Event selection summary in the control and validation regions used in the 2ℓSS$1\tau_{\text{had}}$, $1\ell 2\tau_{\text{had}}$ and $2\ell 2\tau_{\text{had}}$ channels. The lepton types correspond to the definitions in table 2. Regions with two leptons or $\tau_{\text{had-vis}}$ can require their charges to have opposite sign (OS) or same sign (SS). The $\tau_{\text{had-vis}}$ definition denoted as M is described in section 4, while the definition denoted as VL employs the "*Very loose*" ID WP of ref. [103].

In addition to the MVA-based VV and $t\bar{t}Z$ CRs defined in section 5, two additional 3ℓVV and $3\ell t\bar{t}Z$ CRs are used in the likelihood fit to improve the prediction of the background contribution from the VV and $t\bar{t}Z/\gamma^*$ processes, respectively, in the 2ℓSS$0\tau_{\text{had}}$ and $3\ell 0\tau_{\text{had}}$ channels. Both rely on the selection of an SFOS lepton pair compatible with the Z mass. The number of jets and b-jets provide good discrimination between VV and $t\bar{t}Z$: events in the 3ℓVV CR are required to have 2 or 3 jets, exactly one of which is b-tagged, whereas events in the $3\ell t\bar{t}Z$ CR must have ≥ 4 jets and at least one b-tagged jet. The three leptons must satisfy the (L, M, M) (resp. L', M, M) selection when the opposite-sign lepton is an electron (resp. a muon). The yield in the 3ℓVV CR, and the number of b-jets in the $3\ell t\bar{t}Z$ CR, are included in the likelihood fit. Two normalisation factors are used for the VV processes: one for WZ, and one for WW/ZZ. The measured normalisation factors are: $\lambda_{WZ} = 1.06 \pm 0.10$, $\lambda_{WW/ZZ} = 1.13 \pm 0.17$, and $\lambda_{t\bar{t}Z} = 1.09 \pm 0.09$.

The rate of the background from internal conversions with $\text{m}_{e^+e^-} < 1$ GeV in the 2ℓSS$0\tau_{\text{had}}$ and $3\ell 0\tau_{\text{had}}$ channels is estimated using the dedicated control region 3ℓIntC, which selects $Z \to \mu\mu\gamma$ events where the photon is reconstructed as an electron candidate falling into the internal conversion category. The total yield in the region is used in the likelihood fit to determine the normalisation factor $\lambda_{\text{IntC}} = 0.89 \pm 0.16$. The purity of internal conversions in the IntC region reaches 93%.

The $t\bar{t}W$ process is the main irreducible background in the 2ℓSS$0\tau_{\text{had}}$ and $3\ell 0\tau_{\text{had}}$ channels. Its normalisation is estimated in the likelihood fit thanks to the MVA-based CRs described in section 5. No additional CR targeting $t\bar{t}W$ is defined. Its normalisation factor is found to be $\lambda_{t\bar{t}W} = 1.18 \pm 0.07$. Although it cannot be interpreted as an inclusive cross-section measurement because some acceptance uncertainties are not included (see section 7), it is in agreement with the dedicated cross-section measurements of ATLAS [31] and CMS [110]. Fitting two distinct $t\bar{t}W$ normalisation factors for the 2ℓSS$0\tau_{\text{had}}$ and the $3\ell 0\tau_{\text{had}}$ channels

JHEP05(2026)183

leads to compatible values of the normalisation factors. The other channels do not have any significant constraining power on $t\bar{t}W$.

6.2 Reducible backgrounds

6.2.1 Non-prompt leptons in the $2\ell SS0\tau_{\text{had}}$, $3\ell0\tau_{\text{had}}$ and 4ℓ channels

The non-prompt lepton backgrounds are in general small in all SRs and are estimated from simulation, with the normalisation determined from data. The main contribution to the non-prompt-lepton background is from $t\bar{t}$ production, followed by much smaller contributions from V+jets and single-top-quark processes. The non-prompt leptons in the simulated event samples are labelled according to whether they originate from HF or light-flavour (LF) hadron decays, or from a material conversion candidate. The HF category includes leptons from bottom and charm decays, which is the dominant source of non-prompt leptons in the $2\ell\text{SS}0\tau_{\text{had}}$ and $3\ell0\tau_{\text{had}}$ channels; in the 4ℓ channel, LF non-prompt electrons also contribute significantly. Several dedicated control regions enriched in specific processes are included in the simultaneous likelihood fit to data in order to constrain several normalisation factors. Due to differences in the lepton and event selection, the nature of the non-prompt background is different in the $2\ell\text{SS}0\tau_{\text{had}}/3\ell0\tau_{\text{had}}$ channels on the one hand and in the 4ℓ channel on the other hand, thus different normalisation factors and control regions are used.

Several corrections are applied to the $t\bar{t}$ and overall non-prompt-lepton background simulations before the fit. First, the $t\bar{t}$ + $\geq$1 b-jet contribution is multiplied by a factor of 1.3 as previously measured by ATLAS [111]. Second, the shape of the b-jet multiplicity distribution in the non-prompt-lepton background simulation is corrected to match data in an orthogonal $2\ell\text{SS}0\tau_{\text{had}}$ validation region enriched in non-prompt leptons, where one of the leptons must pass a looser non-prompt-lepton BDT score but not pass the M lepton WP. In the 4ℓ channel, the non-prompt-electron candidate transverse momentum is reweighted in order to correct for a slight disagreement with data in the corresponding control region, and the correction is taken as an additional systematic uncertainty.

In the $2\ell\text{SS}0\tau_{\text{had}}$ and $3\ell0\tau_{\text{had}}$ channels, the normalisation factor for HF non-prompt leptons is estimated separately for electrons and muons, and is denoted by $\lambda_{eHF}^{2\ell\text{SS}/3\ell}$ and $\lambda_{\mu HF}^{2\ell\text{SS}/3\ell}$ respectively. There are six $2\ell\text{SS}0\tau_{\text{had}}$ CRs enriched in contributions from HF non-prompt leptons in $t\bar{t}$ events, i.e. $2\ell\text{tt(e)}_{TM_{\text{ex}}}$, $2\ell\text{tt(e)}_{M_{\text{ex}}T}$, $2\ell\text{tt(e)}_{M_{\text{ex}}M_{\text{ex}}}$, $2\ell\text{tt}(\mu)_{TM_{\text{ex}}}$, $2\ell\text{tt}(\mu)_{M_{\text{ex}}T}$, and $2\ell\text{tt}(\mu)_{M_{\text{ex}}M_{\text{ex}}}$. In these CRs, the distribution of the transverse momentum $p_{\text{T}}^{\ell 1}$ of the sub-leading lepton is used in the fit. Requiring at least one M_{ex} lepton in these CR events provides separation from the processes with prompt leptons, especially $t\bar{t}W$, and thus optimises the sensitivity to the HF non-prompt electron and muon contributions. The $t\bar{t}H$ signal contribution in these control regions is at most 8% of the total expected yield. The measured normalisation factors for the $2\ell\text{SS}0\tau_{\text{had}}/3\ell0\tau_{\text{had}}$ HF non-prompt leptons are $\lambda_{eHF}^{2\ell\text{SS}/3\ell} = 1.20 \pm 0.41$ and $\lambda_{\mu HF}^{2\ell\text{SS}/3\ell} = 1.12 \pm 0.16$.

In the 4ℓ channel, the reducible background is dominated by $t\bar{t}$ events with two non-prompt leptons. The HF electron and muon components are estimated with the normalisation factors $\lambda_{eHF}^{4\ell}$ and $\lambda_{\mu HF}^{4\ell}$, and a third one, $\lambda_{eLF}^{4\ell}$, corresponds to LF non-prompt electrons. A CR enriched in $t\bar{t} + \mu^{\text{HF}}$ (resp. $t\bar{t} + e^{\text{HF}}$) is designed by selecting 3ℓ events with three L leptons with flavour $e^{\mp}\mu^{\pm}\mu^{\pm}$ (resp. $\mu^{\mp}e^{\pm}e^{\pm}$) but not selected by the $3\ell0\tau_{\text{had}}$ channel. The

JHEP05(2026)183

same-sign lepton with the lowest transverse momentum is labelled as the non-prompt-lepton candidate, and its transverse momentum distribution is included in the combined fit. A CR enriched in electron LF from Z+jets events is designed by selecting 3ℓ events with one SFOS lepton pair with an invariant mass close to the Z mass; the $E_{\mathrm{T}}^{\mathrm{miss}}$ distribution of this CR is included in the combined fit. The measured normalisation factors for HF and LF non-prompt leptons in the 4ℓchannel are $\lambda_{\mu HF}^{4\ell} = 0.91 \pm 0.06$, $\lambda_{eHF}^{4\ell} = 0.93 \pm 0.13$, and $\lambda_{eLF}^{4\ell} = 1.17 \pm 0.22$.

Finally, a normalisation factor $\lambda_e^{\mathrm{MatC}}$ is determined for the background from material conversions. The contribution from material conversions in the 4ℓ channel is negligible, so this only applies to the $2\ell\mathrm{SS}0\tau_{\mathrm{had}}/3\ell0\tau_{\mathrm{had}}$ channels. Similarly to 3ℓIntC, the 3ℓMatC CR is enriched in material conversions using $Z \to \mu\mu\gamma$ events and only the total event yield is used in the fit. The normalisation factor is measured to be $\lambda_e^{\mathrm{MatC}} = 1.13 \pm 0.21$.

In all non-prompt normalisation factors the uncertainties are mostly statistical.

6.2.2 Electron charge mis-identification

Backgrounds due to electron QMisID primarily affect the $2\ell\mathrm{SS}0\tau_{\mathrm{had}}$ and $2\ell\mathrm{SS}1\tau_{\mathrm{had}}$ channels and arise mainly from $t\bar{t}$ production, with one electron either undergoing hard bremsstrahlung followed by an asymmetric conversion ($e^{\pm} \to e^{\pm}\gamma^* \to e^{\pm}e^+e^-$) or having mismeasured track curvature. The muon charge misassignment rate is negligible in the p_{T} range relevant to this analysis.

The QmisID background is estimated using MC simulation after applying a correction derived by comparing the predicted yield with the observed data in a sample of $Z \to e^+e^-$ events reconstructed as SS di-electron pairs. This correction decreases the MC yields by 10%, and a conservative 50% uncertainty is assigned to the QmisID background estimates. The contribution from QmisID is less than 2% of the total background in the $2\ell\mathrm{SS}0\tau_{\mathrm{had}}$ and $2\ell\mathrm{SS}1\tau_{\mathrm{had}}$ channels.

6.2.3 Non-prompt leptons and misidentified τ_{had} backgrounds in the $1\ell2\tau_{\mathrm{had}}$, $2\ell2\tau_{\mathrm{had}}$, and $2\ell SS1\tau_{\mathrm{had}}$ channels

In the $1\ell2\tau_{\mathrm{had}}$ and $2\ell2\tau_{\mathrm{had}}$ channels, the main background arises from $t\bar{t}$+jets production where one jet is misidentified as a $\tau_{\text{had-vis}}$. The dominant source of misidentified $\tau_{\text{had-vis}}$ is light-quark jets, with sizeable contributions from gluon-initiated jets and heavy-flavour jets. This background contribution is evaluated using the fake-factor (FF) technique [112]. Data events are selected if they satisfy a very loose requirement on the $\tau_{\text{had-vis}}$ identification score but do not satisfy the "Medium" WP requirements. Residual contributions from processes with real $\tau_{\text{had-vis}}$ satisfying this requirement are evaluated using simulations and subtracted. The distribution of the misidentified τ_{had} background is obtained by multiplying the contribution of data events selected with the inverted identification criterion by a fake-factor defined as the ratio of misidentified τ_{had} that respectively pass or fail the "Medium" identification WP. The fake-factors are measured in control regions with two light leptons with opposite charge and two $\tau_{\text{had-vis}}$, which are dominated by Z+jets and $t\bar{t}$ production. These fake-factors are binned in (p_{T}, η) and their values are in the range 0.20–0.45 (0.04–0.20) for 1(3)-prong $\tau_{\text{had-vis}}$. The correctness of the background estimates is assessed at low BDT score and, as

JHEP05(2026)183

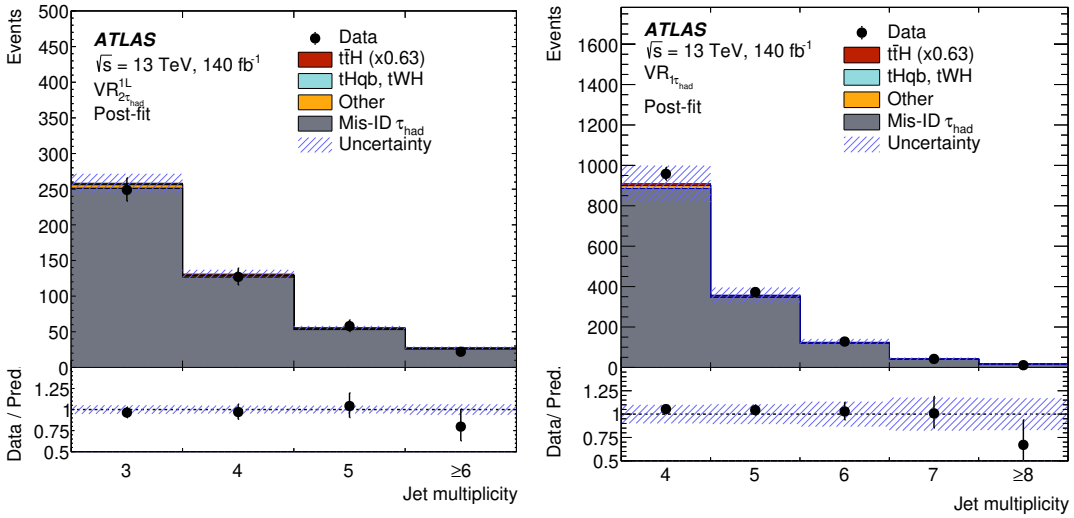

(a) (b)

Figure 9. Distribution of the jet multiplicity in the validation regions of the (a) $1\ell 2\tau_{\text{had}}$ and (b) $2\ell\text{SS}1\tau_{\text{had}}$ channels, obtained by reverting the charge requirements on the $\tau_{\text{had-vis}}$ and leptons, respectively. The signal and background normalisation factors and the nuisance parameters are set to their best-fit values as described in section 8. The shaded band indicates the total uncertainty, including correlations.

shown in figure 9(a), also in the $\text{VR}^{1\ell}_{2\tau_{\text{had}}}$ and $\text{VR}^{2\ell}_{2\tau_{\text{had}}}$ (table 5) validation regions (VRs) requiring two $\tau_{\text{had-vis}}$ with the same electric charge.

In the $2\ell\text{SS}1\tau_{\text{had}}$ channel, the method described in section 6.2.1 is extended to account for both the non-prompt lepton and the misidentified τ_{had} background contributions. Dedicated CRs are defined relaxing the jet multiplicity requirements to include only events with two or three jets. The first CR is obtained by requiring the light leptons in the event to have the same electric charge and it is dominated by the misidentified τ_{had} background. Additional CRs dominated by non-prompt light leptons are defined by loosening the lepton selections requirements and splitting according to the flavour composition (ee, $e\mu$, μe and $\mu\mu$). In the simultaneous fit, normalisation factors are obtained for the misidentified e, μ and τ_{had} contributions predicted in the MC. These normalisation factors are measure to be $\lambda^{2\ell SS1\tau_{\text{had}}}_{eHF/LF} = 0.68 \pm 0.21$, $\lambda^{2\ell SS1\tau_{\text{had}}}_{\mu HF/LF} = 1.11 \pm 0.15$ and $\lambda^{2\ell SS1\tau_{\text{had}}}_{\text{Mis-ID}\tau} = 1.01 \pm 0.07$. The results are validated in the $\text{VR}_{1\tau_{\text{had}}}$ region (table 5) with the same kinematic selection as the $2\ell\text{SS}1\tau_{\text{had}}$ except for the lepton charge requirements, as shown in figure 9(b).

7 Systematic uncertainties

Systematic uncertainties in the results arise from uncertainties in the experimental procedures, signal and background cross-sections, and the modelling of the relevant physics processes. In the different regions, each uncertainty can affect the normalisations and/or the shape of the discriminants used in the fit.

The dominant experimental uncertainties arise from the calibration of the jet energy scale and resolution [95]. The calibration of the b-tagging efficiencies and c- and light-jet rejection

JHEP05(2026)183

rates have smaller effects among the experimental uncertainties [101, 102, 113]. Uncertainties are considered for the JVT selection efficiency [96] and for the correction of the pile-up profile in the simulations to match that in data. Other detector-related systematic uncertainties include the light lepton and $\tau_{\text{had-vis}}$ reconstruction and identification efficiency, energy scale and energy resolution, $E_{\text{T}}^{\text{miss}}$ modelling, light lepton trigger efficiency and luminosity.

Several sources of uncertainties related to the signal modelling are considered. Except for $t\bar{t}H$ cross-section measurements, two cross-section uncertainties are applied accounting for the effect of varying the PDF and α_S and for missing higher-order terms in the fixed order perturbative QCD calculations. They amount to $\pm 3.6\%$ and $\pm 9.2\%$, respectively [56]. Systematic uncertainties related to the migrations of events between the Higgs boson p_{T} boundaries in the STXS scheme [114] are also included. Uncertainties in the Higgs boson decay branching fractions are also applied following the recommendation in ref. [56]. The impact of using a different parton shower and hadronisation model is evaluated by comparing the nominal Powheg+Pythia 8 sample with an alternative Powheg+Herwig 7 [115] sample. Uncertainties in the matching between the matrix element and parton shower are estimated by comparing the nominal event sample with an alternative Powheg+Pythia 8 sample where the definition of the hardness of the Powheg emission, calculated via the parameter $p_{\text{T}}^{\text{hard}}$ [116], is varied following ref. [117]. An uncertainty related to the amount of initial-state radiation (ISR) is estimated by varying independently the factorisation and renormalisation scales in the matrix element as well as considering ISR α_{s} variations taken from the A14 tune [118].

Since normalisation factors are extracted from the fit for the $t\bar{t}W$, $t\bar{t}Z$ and VV backgrounds, cross-section uncertainties for these processes are omitted. Moreover the modelling variations on $t\bar{t}W$, $t\bar{t}Z$ and VV described below are all normalised to the yield of selected events of the nominal prediction, such as not to include overall acceptance uncertainties. As a result the normalisation factors cannot be interpreted as cross-section measurements.

Systematic uncertainties in the modelling of the $t\bar{t}W$, $t\bar{t}Z$ and VV backgrounds due to missing higher-order QCD corrections are estimated by varying independently the factorisation and renormalisation scales by a factor of 0.5 and 2 with respect to the central value.

For systematic uncertainties in the modelling of the $t\bar{t}W$ background due to the matrix element and parton shower algorithm and parameter choices, the nominal Sherpa prediction is compared to a sample generated with MadGraph5_aMC@NLO+Pythia 8 using the FxFx NLO multijet merging [76]. In addition, an uncertainty related to the choice of parton shower and hadronisation model is derived by comparing the relative difference between Powheg+Pythia 8 and Powheg+Herwig 7 and applying that variation to the nominal $t\bar{t}W$ prediction. Uncertainties in the PDF modelling are also included.

Uncertainties in the modelling of additional jets for $t\bar{t}Z$ production are applied by varying the ISR α_{s} variations taken from the A14 tune. In addition, parton shower, hadronisation and underlying event modelling uncertainties are derived by comparing the nominal MadGraph5_aMC@NLO+Pythia 8 sample with an alternative MadGraph5_aMC@NLO+Herwig 7 sample.

JHEP05(2026)183

Systematic uncertainties associated to the data-driven N_{jets}-dependent correction factors applied to the VV production are derived based on the N_{jets} fit function parameter uncertainties. These are applied only in the channels where the correction factors are used ($2\ell\text{SS}0\tau_{\text{had}}$, $3\ell 0\tau_{\text{had}}$ and $2\ell\text{SS}1\tau_{\text{had}}$).

The uncertainties in higher-order cross-sections are taken into account for the rare background processes (tZ, $t\bar{t}t\bar{t}$, $t\bar{t}WW$, VH, tWZ, VVV, $t\bar{t}t$, $tHqb$ and tHW) except for those whose normalisation is measured in the fit. A $^{+70}_{-15}\%$ normalisation uncertainty is assigned to $t\bar{t}t\bar{t}$ production to account for the 15% theory uncertainty in this process [75] as well as the 70% difference of the ATLAS measurement [119] of $22.5^{+6.6}_{-5.5}$ fb with respect to the SM prediction of $13.4^{+1.0}_{-1.8}$ fb [120]. This uncertainty treatment is consistent with the recent update of that calculation at next-to-leading logarithmic accuracy of $17.4^{+1.4}_{-3.0}$ fb in ref. [121]. Additionally, uncertainties associated to the $t\bar{t}t\bar{t}$ matrix element and choice of parton shower are estimated by comparing the nominal sample to alternative Sherpa and MadGraph5_aMC@NLO+Herwig 7 samples, respectively.

The systematic uncertainties in the estimation of the non-prompt light lepton background closely follow the strategy in ref. [31], including uncertainties related to the non-prompt lepton BDT (applied in the $2\ell\text{SS}0\tau_{\text{had}}$ and $3\ell 0\tau_{\text{had}}$ channels only) and uncertainties related to the $t\bar{t}$ MC modelling. Uncertainties are estimated for the modelling of the non-prompt-lepton BDT input variables, namely the muon energy deposit in the calorimeter relative to the expected value ($E_{\text{cluster}}/E_{\text{expected}}$), the electron track p_{T} divided by the jet track p_{T}, and the secondary vertex's longitudinal significance, using tracks with $p_{\text{T}} > 500$ MeV for non-prompt muons. These uncertainties are included as variations that can affect the shape of distributions in each region, but not the normalisation. An uncertainty of $\pm 20\%$ is considered to account for non-prompt-lepton rate differences between the *Tight-not-VeryTight* and *VeryTight* non-prompt lepton BDT working points. Uncertainties in the $t\bar{t}$ parton shower are assessed by using a Powheg+Herwig 7 $t\bar{t}$ MC simulation as a variation of the nominal Powheg+Pythia 8 prediction, separately for the electron and muons channels. The following uncertainties associated to the generation of the $t\bar{t}$ MC sample are also taken into account: normalisation and factorisation scales, initial- and final-state radiation, $p_{\text{T}}^{\text{hard}}$ and h_{damp} parameters.

Uncertainties in the modelling of $t\bar{t}$ production in association with heavy-flavour jets are accounted for by assigning an uncorrelated 50% uncertainty on the $t\bar{t}+b$ and $t\bar{t}+c$ background processes. In the 4ℓ channel, due to the sizeable contribution from leptons produced in semileptonic decays of heavy-flavour jets in $t\bar{t}$ production, an additional uncertainty comparing the predictions from $t\bar{t}$ MC samples produced in the four-flavour and five-flavour schemes is included.

Uncertainties in the electron conversion background extrapolation from Z-enriched to $t\bar{t}$-enriched regions are derived from the residual data/simulation mismodelling in $2\ell\text{SS}0\tau_{\text{had}}$ validation regions built by reversing the electron conversion veto. Internal and material conversion extrapolation uncertainties of 50% and 10%, respectively, are applied.

A systematic uncertainty of 50% is assigned to the background from electrons with misidentified charge in the $2\ell\text{SS}0\tau_{\text{had}}$ and $2\ell\text{SS}1\tau_{\text{had}}$ channels.

In the $2\ell\text{SS}1\tau_{\text{had}}$ channel, the same set of uncertainties related to the non-prompt light lepton background are applied. Dedicated uncertainties of 20% for material conversions and

JHEP05(2026)183

	$\Delta\sigma_{t\bar{t}H}/\sigma^{\mathrm{SM}}$
Total uncertainty	$+0.20\ -0.19$
Statistical uncertainty	$+0.13\ -0.12$
Total systematic uncertainty	± 0.15
ttH modelling	$+0.03\ -0.02$
$t\bar{t}W$ modelling	± 0.05
$t\bar{t}$ modelling	± 0.04
$t\bar{t}t\bar{t}$ modelling	± 0.03
$t\bar{t}Z$ modelling	± 0.01
Diboson modelling	± 0.01
Other backgrounds modelling	± 0.03
$t\bar{t}W$ normalisation	$+0.07\ -0.06$
$t\bar{t}Z$ normalisation	$+0.05\ -0.05$
Non-prompt normalisation	$+0.02\ -0.02$
Diboson normalisation	$+0.01\ -0.01$
MC samples size	± 0.04
Electrons, muons and $\tau_{\text{had-vis}}$	$+0.04\ -0.03$
Jets	$+0.04\ -0.03$
Flavour tagging	< 0.01
$E_{\mathrm{T}}^{\mathrm{miss}}$	± 0.01
Misidentified τ-lepton background	± 0.03
Luminosity	< 0.01

Table 6. Summary of the different sources of uncertainty in the ratio of $\sigma_{t\bar{t}H}$ to the SM expectation. The quoted values are obtained by repeating the fit, while fixing the set of nuisance parameters of the sources corresponding to each category to their best-fit values, and subtracting in quadrature the resulting uncertainty from the total uncertainty of the nominal fit presented in the first row. Experimental uncertainties for reconstructed objects combine efficiency and energy/momentum scale and resolution uncertainties.

40% for the extrapolation between L' and M lepton definitions are also applied. Additional extrapolation uncertainties related to the difference in misidentified τ_{had} kinematics and composition between the signal and control regions are included.

The systematic uncertainties in the estimation of the misidentified τ_{had} background in the $1\ell 2\tau_{\text{had}}$ and $2\ell 2\tau_{\text{had}}$ channels include statistical uncertainties in the τ_{had} fake-factors, uncertainties due to the subtraction of processes with two real $\tau_{\text{had-vis}}$ in the control regions, and an overall 10% uncertainty due to observed non-closure in the validation region with same-sign $\tau_{\text{had-vis}}$ pairs. Additional uncertainties due to the composition differences between the signal and control regions are evaluated by comparing the fake-factors measured in data from Z+jets and $t\bar{t}$ control regions.

Table 6 summarises the impact of the different uncertainty sources on the measurement of the $t\bar{t}H$ production cross-section.

JHEP05(2026)183

8 Results

A combined profile-likelihood fit is performed on all bins in the signal and control regions to measure the $t\bar{t}H$ cross-section and the normalisation of the different background processes. Similar fits are also performed to measure the $t\bar{t}H$ cross-section in STXS bins and to measure the $t\bar{t}H$ and $tHqb$ cross-sections simultaneously. The statistical analysis is based on a likelihood function constructed as the product of Poisson probability terms (P) over the bins of the input distributions:

$$L\left(\boldsymbol{\mu}, \boldsymbol{\lambda}, \boldsymbol{\theta}, \text{data}\right) = \prod_{k \in \text{reg}} \prod_{b \in \text{bins}} P(n_{k,b} | n_{k,b}^{\text{signal}}(\boldsymbol{\mu}, \boldsymbol{\theta}) + n_{k,b}^{\text{bkg}}(\boldsymbol{\lambda}, \boldsymbol{\theta})) \prod_{\theta \in \boldsymbol{\theta}} G(\theta), \tag{8.1}$$

where $n_{k,b}$, $n_{k,b}^{\text{signal}}$ and $n_{k,b}^{\text{bkg}}$ stand for the number of observed events, the number of expected signal events and the number of expected background events in bin b of analysis region k, respectively. The systematic uncertainties (described in section 7) are incorporated in the likelihood function through nuisance parameters, $\boldsymbol{\theta}$, which are constrained by Gaussian probability terms, G. The statistical uncertainty due to the limited number of simulated events is included in the likelihood in the form of additional nuisance parameters with Poisson constraint terms. Both $\boldsymbol{\mu}$ (signal-strength parameter, defined as a multiplicative factor to the yield of expected signal events) and $\boldsymbol{\lambda}$ (normalisation factors for several backgrounds) are treated as free parameters in the likelihood fit and are estimated by maximising the likelihood. The test statistic is constructed from the profile likelihood ratio, and the confidence intervals for the parameters of interest are derived using the asymptotic approximation [122].

8.1 $t\bar{t}H$ cross-section measurements

Figures 10-12 show the data and background predictions in each bin entering the statistical analysis. An excess of events over the expected background is found with an observed (expected) significance of 3.3σ (5.3σ). The measured $t\bar{t}H$ cross-section ($\sigma_{t\bar{t}H}$) is 321^{+102}_{-99} fb, while the SM prediction (σ^{SM}) is 507^{+35}_{-50} fb. The compatibility of this result with the SM is 7.2%.

The best-fit value of $\sigma_{t\bar{t}H}/\sigma^{\text{SM}}$[10] for each individual channel and the combination of all channels are shown in figure 13. The individual channel results are extracted from the full fit but with a separate parameter of interest for each channel. The measured results are compatible with the SM prediction in most of the channels. The probability that the six fitted cross-sections are compatible with a single value is 12.4%. The largest deviation is observed in the $2\ell\text{SS}1\tau_{\text{had}}$ channel, with a fitted value of $\sigma_{t\bar{t}H}/\sigma^{\text{SM}} = -0.72^{+0.56}_{-0.59}$. As shown in figure 12, there is a downward fluctuation in data at high value of the $2\ell\text{SS}1\tau_{\text{had}}$ BDT.

The highest ranked nuisance parameters are shown in figure 14. The most relevant nuisance parameters correspond to the $t\bar{t}t\bar{t}$ background cross-section uncertainty as well as in the normalisation factors of $t\bar{t}W$ and $t\bar{t}Z$ production. Mild constraints are observed for the nuisance parameters related to the $t\bar{t}W$ modelling uncertainties and the non-closure uncertainties in the $1\ell 2\tau_{\text{had}}$ channel.

[10] Results are quoted as $\sigma_{t\bar{t}H}/\sigma^{\text{SM}}$ for convenience, but the inclusive theory systematics in σ^{SM} are not included.

JHEP05(2026)183

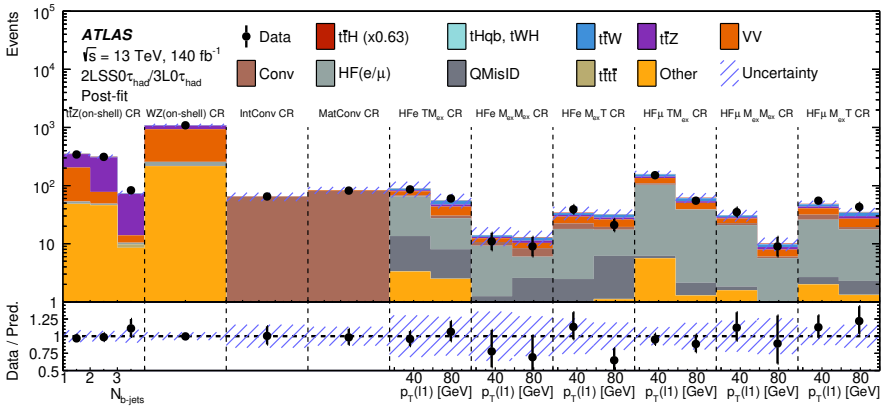

(a)

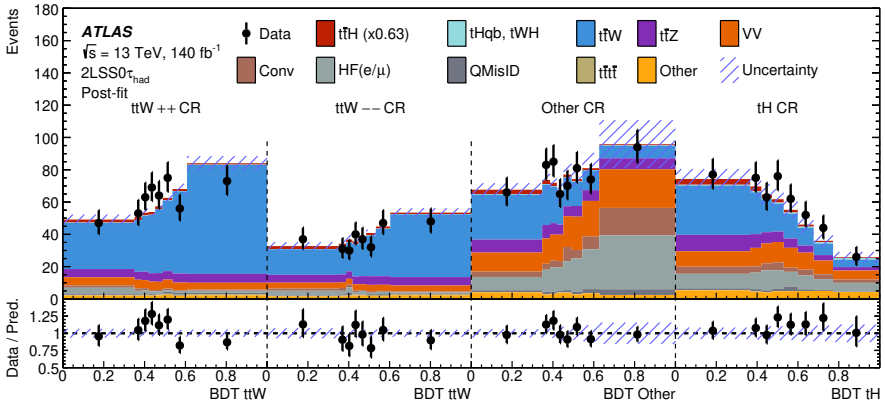

(b)

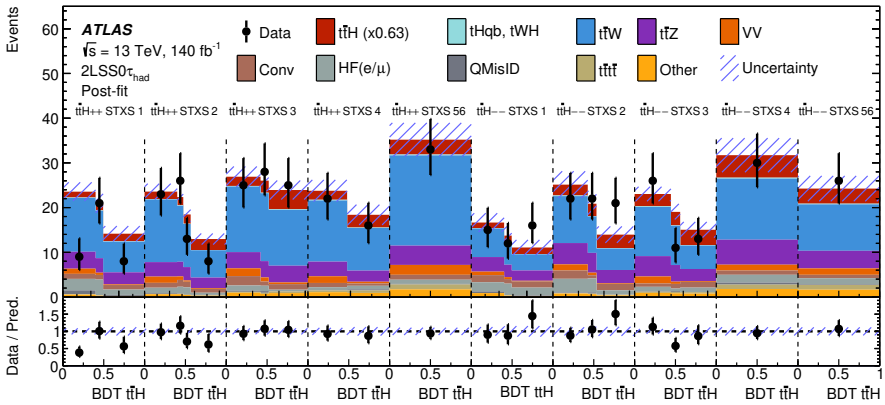

(c)

Figure 10. Comparison of the observed and expected event yields in all the regions and bins used in the statistical analysis for (a) the $2\ell\text{SS}0\tau_{\text{had}}$ and $3\ell 0\tau_{\text{had}}$ control regions, and (b,c) the $2\ell\text{SS}0\tau_{\text{had}}$ channel. The signal and background normalisation factors and the nuisance parameters are set to their best-fit values. Regions labelled 'IntConv' and 'MatConv' stand for the control regions enhanced in internal an material conversions, respectively. The regions denoted as 'STXS n' correspond to the n-th bin in the STXS formalism described in section 5. When several STXS bins are merged together, all numbers are quoted (e.g. 'STXS 56' corresponds to STXS bins 5 and 6). '++' and '−−' refer to the charge of the two leptons. The shaded band indicates the total uncertainty, including correlations.

JHEP05(2026)183

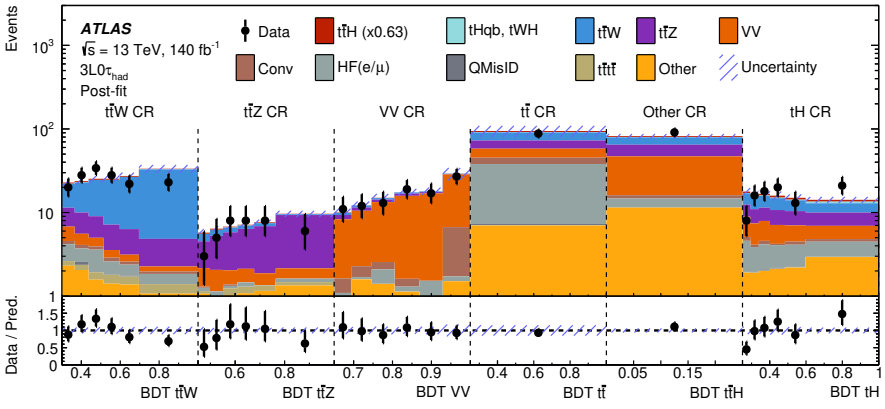

(a)

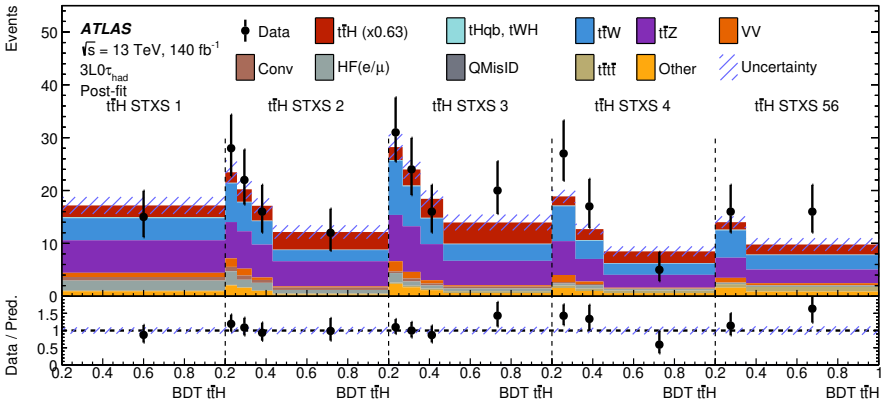

(b)

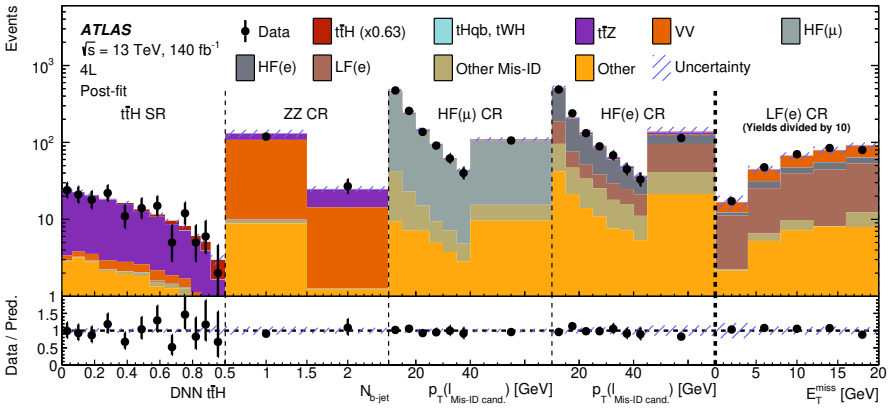

(c)

Figure 11. Comparison of the observed and expected event yields in all the regions and bins used in the statistical analysis for the (a,b) $3\ell 0\tau_{\text{had}}$ and (c) 4ℓ channels. The signal and background normalisation factors and the nuisance parameters are set to their best-fit values. The regions denoted as 'STXS n' correspond to the n-th bin in the STXS formalism described in section 5. When several STXS bins are merged together, all numbers are quoted (e.g. 'STXS 56' corresponds to STXS bins 5 and 6). The shaded band indicates the total uncertainty, including correlations.

JHEP05(2026)183

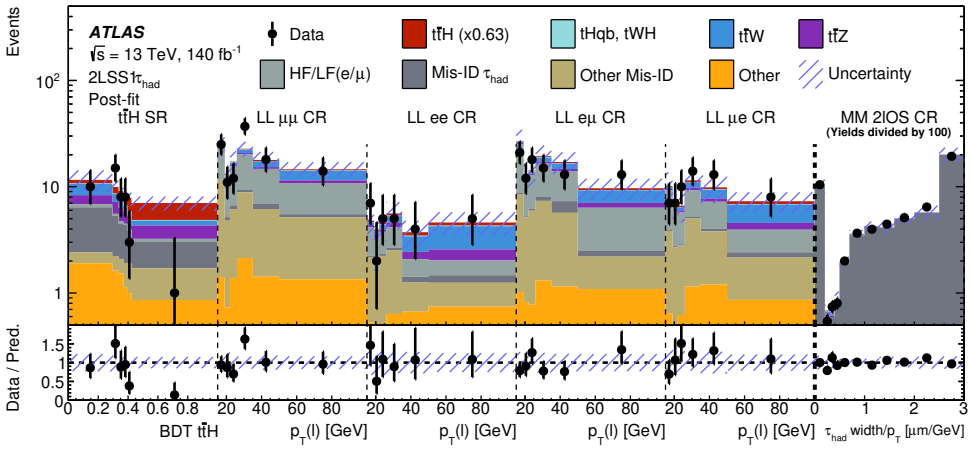

(a)

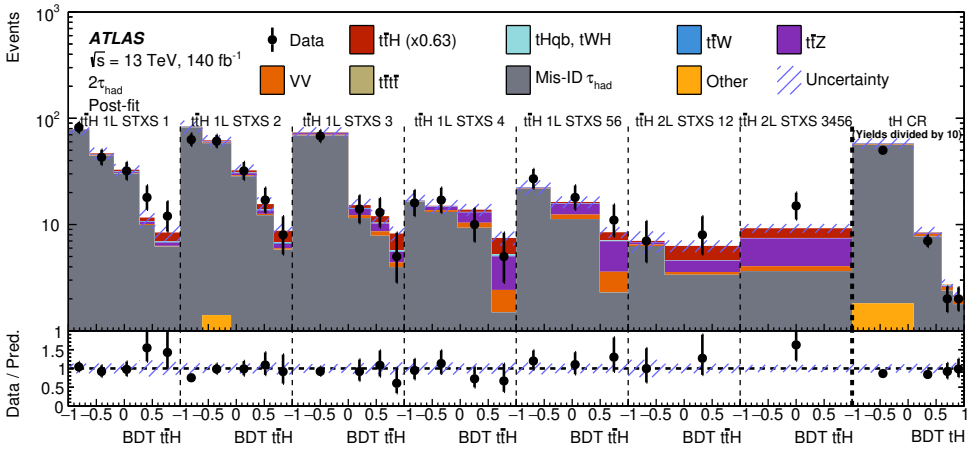

(b)

Figure 12. Comparison of the observed and expected event yields in all the regions and bins used in the statistical analysis for the (a) 2ℓSS$1\tau_{\text{had}}$, and (b) $1\ell 2\tau_{\text{had}}$ and $2\ell 2\tau_{\text{had}}$ channels. The signal and background normalisation factors and the nuisance parameters are set to their best-fit values. The regions denoted as 'STXS n' correspond to the n-th bin in the STXS formalism described in section 5. When several STXS bins are merged together, all numbers are quoted (e.g. 'STXS 3456' corresponds to STXS bins from 3 to 6). The shaded band indicates the total uncertainty, including correlations.

JHEP05(2026)183

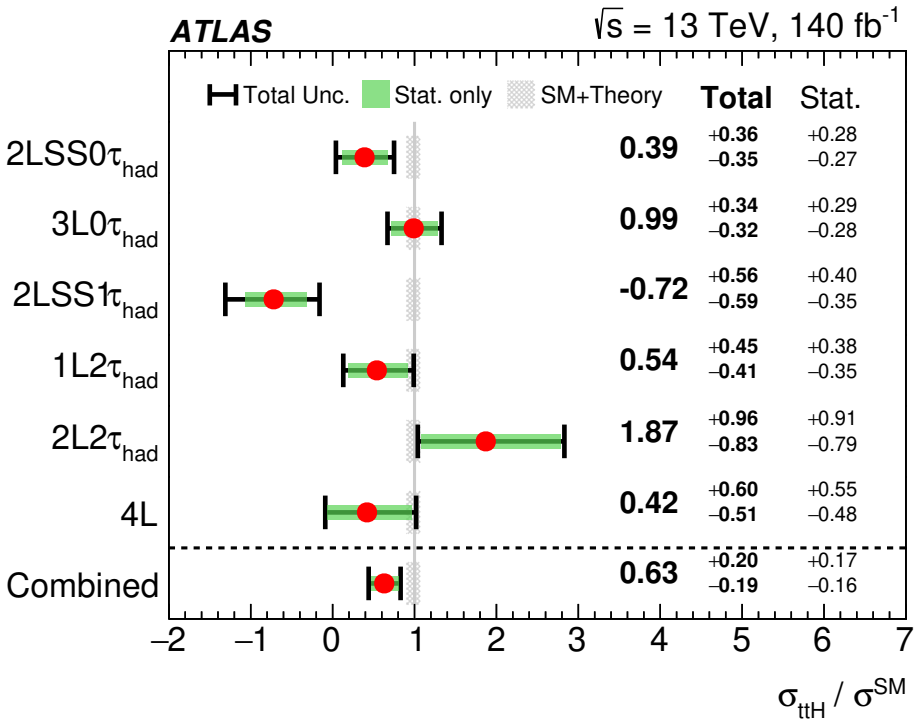

Figure 13. The observed best-fit values of the $t\bar{t}H$ cross-section relative to the SM expectation and their uncertainties by analysis channel and combined. The individual $\sigma_{t\bar{t}H}/\sigma^{\mathrm{SM}}$ values for the channels are obtained from a simultaneous fit with the cross-section parameter for each channel floating independently. The inclusive theory systematics in σ^{SM} are shown as a grey dashed band but are not included in the uncertainties of the measurement.

JHEP05(2026)183

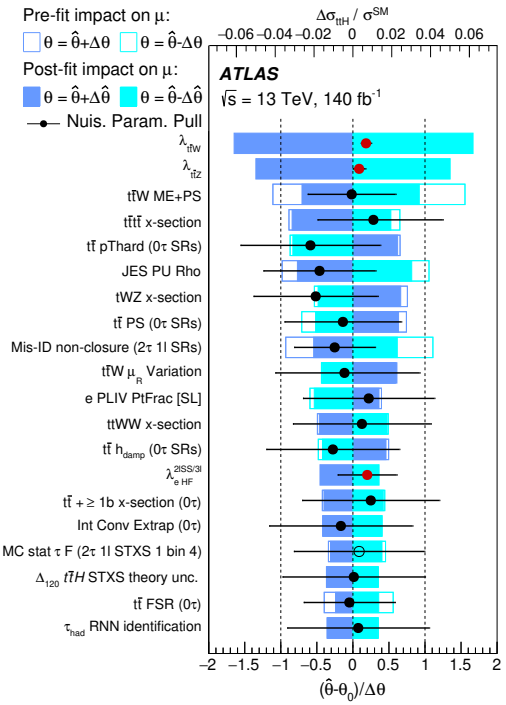

Figure 14. Ranking of the 20 modelling and experimental systematic uncertainties with the largest post-fit impact on the inclusive cross-section. The empty (filled) blue rectangles correspond to the pre-(post-)fit impact on $\sigma_{t\bar{t}H}/\sigma^{\mathrm{SM}}$ and refer to the upper scale of the plot. The impact of each nuisance parameter, $\Delta\sigma_{t\bar{t}H}/\sigma^{\mathrm{SM}}$, is computed by comparing the nominal best-fit value of $\sigma_{t\bar{t}H}/\sigma^{\mathrm{SM}}$ with the result of the fit when fixing the considered nuisance parameter to its best-fit value, $\hat{\theta}$, shifted by its pre-fit (post-fit) uncertainties $\pm\Delta\theta$ ($\pm\Delta\hat{\theta}$). The black markers show the pulls of the nuisance parameters relative to their nominal values, $\theta_0 = 0$. The red markers show the pulls of the normalisation factors relative to their nominal value, $\theta_0 = 1$. No pre-fit uncertainty is defined for the normalisation factors as they are free parameters of the fit. The pulls and their relative post-fit errors, $\Delta\hat{\theta}/\Delta\theta$, refer to the lower scale of the plot. The inclusive theory systematics in σ^{SM} are not included in the uncertainties of the measurement. For brevity, the following acronyms are used in the figure: matrix element (ME), parton shower(PS), cross-section (x-section), pile-up density (PU Rho), non-prompt-lepton BDT (PLIV), final state radiation (FSR). The STXS migration uncertainty for the bin boundary at $p_{\mathrm{T}}^{H} = 120$ GeV is denoted as Δ_{120}.

JHEP05(2026)183

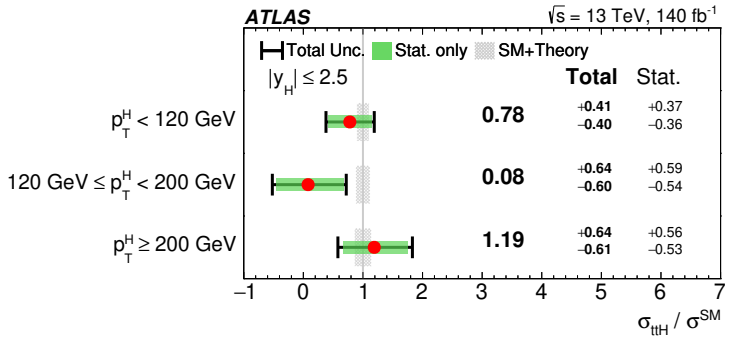

Figure 15. The observed best-fit values of the $t\bar{t}H$ cross-section relative to the SM expectation and their uncertainties in the simplified template cross-section measurement. The inclusive theory systematics in σ^{SM} are shown as a grey dashed band but are not included in the uncertainties of the measurement.

STXS bin	$\sigma_{t\bar{t}H}$ [fb]	σ^{SM} [fb]
$p_{\text{T}}^{H} < 120$ GeV	231^{+122}_{-119}	297^{+20}_{-29}
$120 \leq p_{\text{T}}^{H} < 200$ GeV	10^{+81}_{-76}	127^{+9}_{-12}
$p_{\text{T}}^{H} \geq 200$ GeV	92^{+49}_{-47}	77^{+5}_{-8}

Table 7. Observed best-fit values of the $t\bar{t}H$ cross-section and their SM expectation in the simplified template cross-section measurement.

Table 7 and figure 15 show the results of the STXS measurement of three separate p_{T}^{H} bins. These results are obtained by performing a fit using all the channels, although the sensitivity for different STXS bins comes mostly from the channels featuring p_{T}^{H} reconstruction (i.e. $2\ell\text{SS}0\tau_{\text{had}}$, $3\ell 0\tau_{\text{had}}$, $1\ell 2\tau_{\text{had}}$ and $2\ell 2\tau_{\text{had}}$). Excellent agreement with the SM is found for the $p_{\text{T}}^{H} < 120$ GeV and $p_{\text{T}}^{H} > 200$ GeV bins, although the measured cross-section value in the $120 < p_{\text{T}}^{H} < 200$ GeV bin is lower than the SM prediction. This is due to data underfluctuations in the STXS3 categories of the $2\ell\text{SS}0\tau_{\text{had}}$ and $1\ell 2\tau_{\text{had}}$ channels, as well as the effect of anti-correlations between the measurement in the different STXS bins. The compatibility of the STXS fit with the SM is 28%. The compatibility of the STXS fit with the inclusive fit is 55%.

8.2 $t\bar{t}H$ and $tHqb$ combined measurement

Sensitivity to $tHqb$ can also be achieved since the $2\ell\text{SS}0\tau_{\text{had}}$, $3\ell 0\tau_{\text{had}}$ and $1\ell 2\tau_{\text{had}}$ channels have dedicated categories enhanced in this production process. Figure 16 shows the results of a fit to all the channels with both $\mu_{t\bar{t}H}$ and μ_{tHqb} signal strengths floating freely, while the tWH process is fixed at its SM prediction. The best-fit values of the signal strengths are $\mu_{t\bar{t}H} = 0.59^{+0.22}_{-0.20}$ and $\mu_{tHqb} = 7.2^{+4.6}_{-4.0}$ (including uncertainties in the SM prediction), with a -11% correlation between them. The measured μ_{tHqb} is consistent with the dedicated tH ATLAS result that combines multilepton and $H \to b\bar{b}$ channels [30].

JHEP05(2026)183

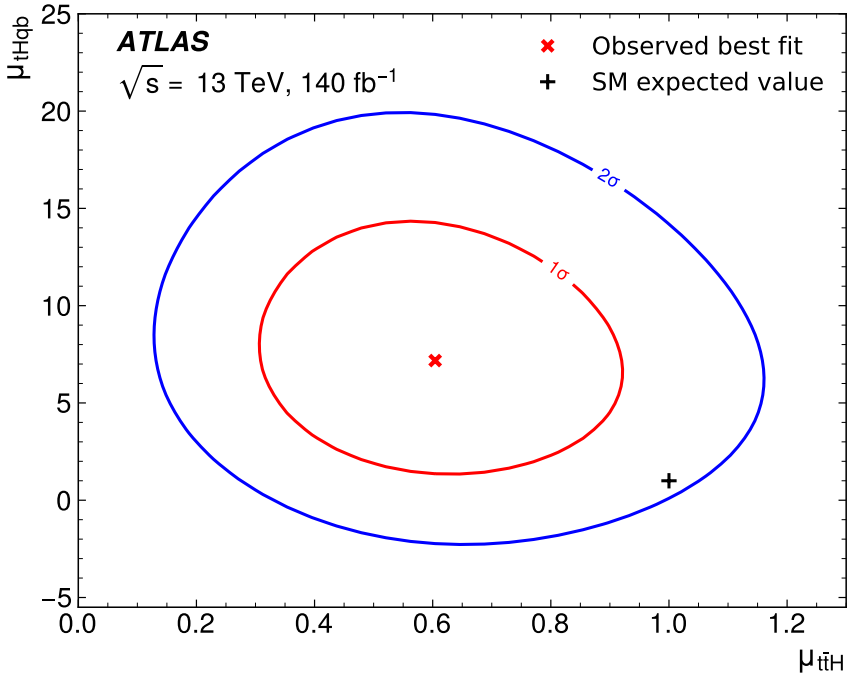

Figure 16. Observed exclusion contours in the $(\mu_{t\bar{t}H}, \mu_{tHqb})$ plane, with the best-fit values shown with the cross and the 1σ and 2σ contours shown with solid lines. Uncertainties in both the measurement and the SM prediction are included.

8.3 *CP* interpretation

To determine the α and κ_t' CP parameters, a binned profile likelihood fit is performed using only the $2\ell\text{SS}0\tau_{\text{had}}$, $3\ell0\tau_{\text{had}}$, $1\ell2\tau_{\text{had}}$ and $2\ell2\tau_{\text{had}}$ channels. In this case, the value of the likelihood in eq. (8.1) varies according to the expected $t\bar{t}H$, $tHqb$ and tWH signal yields, which are functions of α and κ_t'. By scanning the value of the test statistic in grid points in κ_t' and α, two-dimensional exclusion contours in the (κ_t', α) plane are obtained.

In the $2\ell\text{SS}0\tau_{\text{had}}$ and $3\ell0\tau_{\text{had}}$ channels, the same discriminants used in the STXS measurement are also employed for the CP interpretation. In the $1\ell2\tau_{\text{had}}$ and $2\ell2\tau_{\text{had}}$ channels, dedicated CP BDTs are trained to separate between the CP-even and CP-odd signal hypotheses. Separate BDTs are built for $t\bar{t}H$ and $tHqb$, using 17 input variables, the most relevant ones being the angular separations between τ_{had} and jets, jets and leptons, and τ_{had} and leptons. The performance of these BDTs is illustrated in figure 17. The difference in $tHqb$ yields between the CP-odd and CP-even hypothesis are due to the change of the relative sign between the Higgs-boson couplings to the top quark and the W boson in the diagrams contributing to this process. The $t\bar{t}H$ CP BDT is used as discriminant variable for the $2\ell2\tau_{\text{had}}$ channel and for the $t\bar{t}H$-enhanced category in the $1\ell2\tau_{\text{had}}$ channel, while the $tHqb$ CP BDT is employed in the $1\ell2\tau_{\text{had}}$ $tHqb$-enhanced category.

The exclusion contours in the (κ_t', α) plane are shown in figure 18. The results are compatible with the SM hypothesis, and the observed (expected) exclusion of the pure CP-odd hypothesis is at 1.8σ (3.1σ). Because the likelihood is very flat around the minimum, the best-fit value is sensitive to numerical instabilities. The observed (expected) exclusion at

JHEP05(2026)183

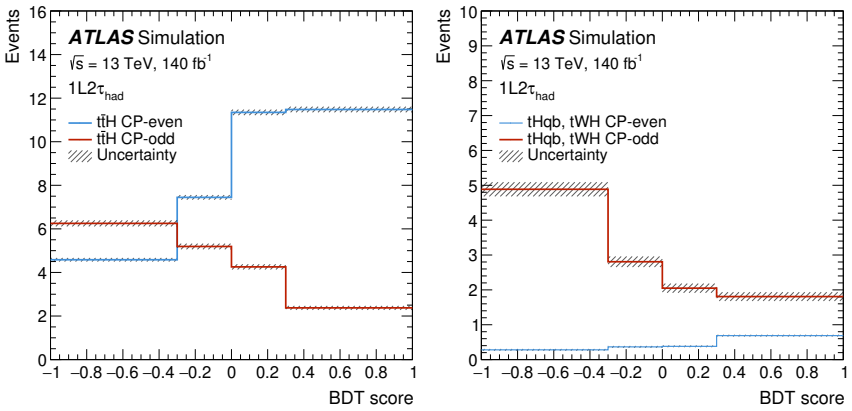

(a) (b)

Figure 17. Distributions of the scores of the CP BDT in the $1\ell 2\tau_{\text{had}}$ channels for (a) $t\bar{t}H$ and (b) $tHqb$ signals under the SM (CP-even) and CP-odd hypotheses, normalised to the expected event yields assuming the predicted cross-sections. Only MC statistical uncertainties are shown.

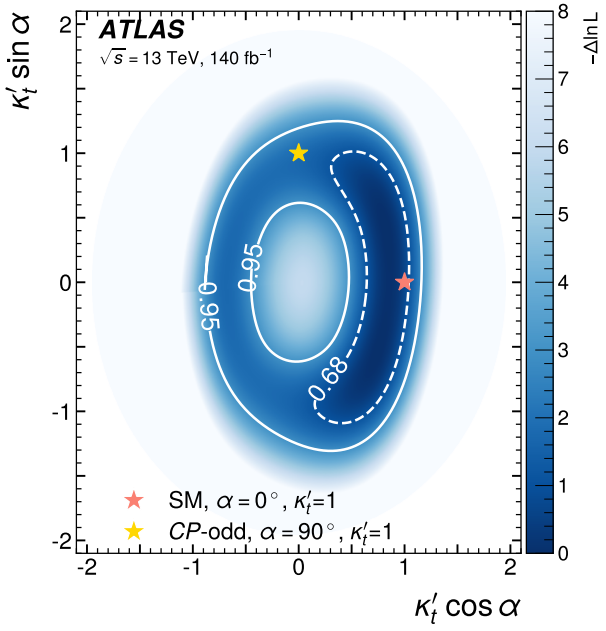

Figure 18. The observed exclusion contours in the $(\kappa_t' \cos\alpha, \kappa_t' \sin\alpha)$ plane. Regions contained in the dashed, and in the solid lines are compatible with the best-fit result at 68% and 95% confidence level, with stars representing the CP-even and CP-odd results with κ_t' =1.

68% confidence level on the CP-mixing angle is $|\alpha| > 62°$ (43°). The difference between the expected and observed exclusions is mainly coming from the low fitted cross-section in the $2\ell\text{SS}0\tau_{\text{had}}$ channel. The compatibility between the results from fits to the channels without τ_{had} ($2\ell\text{SS}0\tau_{\text{had}}$, $3\ell 0\tau_{\text{had}}$) and those with τ_{had} ($1\ell 2\tau_{\text{had}}$ and $2\ell 2\tau_{\text{had}}$) is 34%.

JHEP05(2026)183

9 Conclusion

Several measurements of the associated production of a top-quark pair with the Higgs boson ($t\bar{t}H$) in multilepton final states based on a dataset of proton-proton collisions at $\sqrt{s} = 13$ TeV recorded with the ATLAS detector at the CERN Large Hadron Collider and corresponding to an integrated luminosity of 140 fb^{-1} are presented. The inclusive $t\bar{t}H$ production cross-section is measured to be 321^{+102}_{-99} fb. This result is compatible with the Standard Model prediction of 507^{+35}_{-50} fb and corresponds to an observed (expected) significance of 3.3σ (5.3σ). The $t\bar{t}H$ cross-section is also measured differentially in bins of the Higgs boson transverse momentum in the simplified template cross-section framework. Another fit is done in which $t\bar{t}H$ and $tHqb$ are left floating freely separately, leading to signal strengths of $\mu_{t\bar{t}H} = 0.59^{+0.22}_{-0.20}$ and $\mu_{tHqb} = 7.2^{+4.6}_{-4.0}$. Finally, the CP structure of the top quark-Higgs boson Yukawa coupling is probed; the results are compatible with the SM hypothesis, and values of the CP-mixing angle of $|\alpha| > 62°$ are excluded at 68% confidence level while the expected exclusion is $|\alpha| > 43°$.

Acknowledgments

We thank CERN for the very successful operation of the LHC and its injectors, as well as the support staff at CERN and at our institutions worldwide without whom ATLAS could not be operated efficiently.

The crucial computing support from all WLCG partners is acknowledged gratefully, in particular from CERN, the ATLAS Tier-1 facilities at TRIUMF/SFU (Canada), NDGF (Denmark, Norway, Sweden), CC-IN2P3 (France), KIT/GridKA (Germany), INFN-CNAF (Italy), NL-T1 (Netherlands), PIC (Spain), RAL (U.K.) and BNL (U.S.A.), the Tier-2 facilities worldwide and large non-WLCG resource providers. Major contributors of computing resources are listed in ref. [123].

We gratefully acknowledge the support of ANPCyT, Argentina; YerPhI, Armenia; ARC, Australia; BMWFW and FWF, Austria; ANAS, Azerbaijan; CNPq and FAPESP, Brazil; NSERC, NRC and CFI, Canada; CERN; ANID, Chile; CAS, MOST and NSFC, China; Minciencias, Colombia; MEYS CR, Czech Republic; DNRF and DNSRC, Denmark; IN2P3-CNRS and CEA-DRF/IRFU, France; SRNSFG, Georgia; BMFTR, HGF and MPG, Germany; GSRI, Greece; RGC and Hong Kong SAR, China; ICHEP and Academy of Sciences and Humanities, Israel; INFN, Italy; MEXT and JSPS, Japan; CNRST, Morocco; NWO, Netherlands; RCN, Norway; MNiSW, Poland; FCT, Portugal; MNE/IFA, Romania; MSTDI, Serbia; MSSR, Slovakia; ARIS and MVZI, Slovenia; DSI/NRF, South Africa; MICIU/AEI, Spain; SRC and Wallenberg Foundation, Sweden; SERI, SNSF and Cantons of Bern and Geneva, Switzerland; NSTC, Taipei; TENMAK, Türkiye; STFC/UKRI, United Kingdom; DOE and NSF, United States of America.

Individual groups and members have received support from BCKDF, CANARIE, CRC and DRAC, Canada; CERN-CZ, FORTE and PRIMUS, Czech Republic; COST, ERC, ERDF, Horizon 2020 and Marie Skℓodowska-Curie Actions, European Union; Investissements d'Avenir Labex, Investissements d'Avenir Idex and ANR, France; DFG and AvH Foundation, Germany; Herakleitos, Thales and Aristeia programmes co-financed by EU-ESF and the Greek NSRF, Greece; BSF-NSF and MINERVA, Israel; NCN and NAWA, Poland; La Caixa

JHEP05(2026)183

Banking Foundation, CERCA Programme Generalitat de Catalunya and PROMETEO and GenT Programmes Generalitat Valenciana, Spain; Göran Gustafssons Stiftelse, Sweden; The Royal Society and Leverhulme Trust, United Kingdom.

In addition, individual members wish to acknowledge support from Chile: Agencia Nacional de Investigación y Desarrollo (FONDECYT 1230812, FONDECYT 1240864, Fondecyt 3240661, Fondecyt Regular 1240721); China: Chinese Ministry of Science and Technology (MOST-2023YFA1605700, MOST-2023YFA1609300), National Natural Science Foundation of China (NSFC — 12175119, NSFC 12275265); Czech Republic: Czech Science Foundation (GACR — 24-11373S), Ministry of Education Youth and Sports (ERC-CZ-LL2327, FORTE CZ.02.01.01/00/22_008/0004632), PRIMUS Research Programme (PRIMUS/21/SCI/017); EU: H2020 European Research Council (ERC — 101002463); European Union: European Research Council (BARD No. 101116429, ERC — 948254, ERC 101089007), European Regional Development Fund (SMASH COFUND 101081355, SLO ERDF), European Union, Future Artificial Intelligence Research (FAIR-NextGenerationEU PE00000013); France: Agence Nationale de la Recherche (ANR-21-CE31-0022, ANR-22-EDIR-0002, ANR-24-CE31-0504-01); Germany: Deutsche Forschungsgemeinschaft (DFG — 469666862, DFG — CR 312/5-2); China: Research Grants Council (GRF); Italy: Ministero dell'Università e della Ricerca (NextGenEU 153D23001490006 M4C2.1.1, NextGenEU I53D23000820006 M4C2.1.1, NextGenEU I53D23001490006 M4C2.1.1, SOE2024_0000023); Japan: Japan Society for the Promotion of Science (JSPS KAKENHI JP22H01227, JSPS KAKENHI JP22H04944, JSPS KAKENHI JP22KK0227, JSPS KAKENHI JP24K23939, JSPS KAKENHI JP24KK0251, JSPS KAKENHI JP25H00650, JSPS KAKENHI JP25H01291, JSPS KAKENHI JP25K01023); Norway: Research Council of Norway (RCN-314472); Poland: Ministry of Science and Higher Education (IDUB AGH, POB8, D4 no 9722), Polish National Science Centre (NCN 2021/42/E/ST2/00350, NCN OPUS 2023/51/B/ST2/02507, NCN UMO-2019/34/E/ST2/00393, UMO-2022/47/O/ST2/00148, UMO-2023/49/B/ST2/04085, UMO-2023/51/B/ST2/00920, UMO-2024/53/N/ST2/00869); Portugal: Foundation for Science and Technology (FCT); Spain: Ministry of Science and Innovation (RYC2019-028510-I, RYC2020-030254-I, RYC2021-031273-I, RYC2022-038164-I); Sweden: Carl Trygger Foundation (Carl Trygger Foundation CTS 22:2312), Swedish Research Council (Swedish Research Council 2023-04654, VR 2021-03651, VR 2022-03845, VR 2022-04683, VR 2023-03403, VR 2024-05451), Knut and Alice Wallenberg Foundation (KAW 2018.0458, KAW 2022.0358, KAW 2023.0366); Switzerland: Swiss National Science Foundation (SNSF — PCEFP2_194658); United Kingdom: The Binks Trust, Royal Society (NIF-R1-231091); United States of America: U.S. Department of Energy (ECA DE-AC02-76SF00515), Neubauer Family Foundation.

Data Availability Statement. The public release of data supporting the findings of this article will follow the CERN Open Data Policy [124]. Inquiries about plots and tables associated with this article can be addressed to atlas.publications@cern.ch.

Code Availability Statement. The ATLAS Collaboration's Athena software, including the configuration of the event generators, is open source (`http://gitlab.cern.ch/atlas/athena`).

JHEP05(2026)183

References

[1] ATLAS collaboration, *Observation of a new particle in the search for the Standard Model Higgs boson with the ATLAS detector at the LHC*, *Phys. Lett. B* **716** (2012) 1 [arXiv:1207.7214] [INSPIRE].

[2] CMS collaboration, *Observation of a new boson at a mass of 125 GeV with the CMS experiment at the LHC*, *Phys. Lett. B* **716** (2012) 30 [arXiv:1207.7235] [INSPIRE].

[3] L. Evans and P. Bryant, *LHC machine*, 2008 *JINST* **3** S08001 [INSPIRE].

[4] ATLAS collaboration, *A detailed map of Higgs boson interactions by the ATLAS experiment ten years after the discovery*, *Nature* **607** (2022) 52 [*Erratum ibid.* **612** (2022) E24] [arXiv:2207.00092] [INSPIRE].

[5] CMS collaboration, *Combination and interpretation of differential Higgs boson production cross sections in proton-proton collisions at* $\sqrt{s} = 13$ *TeV*, *JHEP* **04** (2026) 093 [arXiv:2504.13081] [INSPIRE].

[6] J.F. Gunion and X.-G. He, *Determining the CP nature of a neutral Higgs boson at the LHC*, *Phys. Rev. Lett.* **76** (1996) 4468 [hep-ph/9602226] [INSPIRE].

[7] J. Ellis, D.S. Hwang, K. Sakurai and M. Takeuchi, *Disentangling Higgs-top couplings in associated production*, *JHEP* **04** (2014) 004 [arXiv:1312.5736] [INSPIRE].

[8] X.-G. He, G.-N. Li and Y.-J. Zheng, *Probing Higgs boson CP properties with* $t\bar{t}H$ *at the LHC and the 100 TeV pp collider*, *Int. J. Mod. Phys. A* **30** (2015) 1550156 [arXiv:1501.00012] [INSPIRE].

[9] F. Boudjema, R.M. Godbole, D. Guadagnoli and K.A. Mohan, *Lab-frame observables for probing the top-Higgs interaction*, *Phys. Rev. D* **92** (2015) 015019 [arXiv:1501.03157] [INSPIRE].

[10] ATLAS collaboration, *Study of the spin and parity of the Higgs boson in diboson decays with the ATLAS detector*, *Eur. Phys. J. C* **75** (2015) 476 [*Erratum ibid.* **76** (2016) 152] [arXiv:1506.05669] [INSPIRE].

[11] CMS collaboration, *Constraints on the spin-parity and anomalous HVV couplings of the Higgs boson in proton collisions at 7 and 8 TeV*, *Phys. Rev. D* **92** (2015) 012004 [arXiv:1411.3441] [INSPIRE].

[12] ATLAS collaboration, *Measurement of the CP properties of Higgs boson interactions with* τ*-leptons with the ATLAS detector*, *Eur. Phys. J. C* **83** (2023) 563 [arXiv:2212.05833] [INSPIRE].

[13] CMS collaboration, *Constraints on anomalous Higgs boson couplings to vector bosons and fermions from the production of Higgs bosons using the* $\tau\tau$ *final state*, *Phys. Rev. D* **108** (2023) 032013 [arXiv:2205.05120] [INSPIRE].

[14] D. Fontes, J.C. Romão, R. Santos and J.P. Silva, *Large pseudoscalar Yukawa couplings in the complex 2HDM*, *JHEP* **06** (2015) 060 [arXiv:1502.01720] [INSPIRE].

JHEP05(2026)183

[15] ATLAS collaboration, *Observation of Higgs boson production in association with a top quark pair at the LHC with the ATLAS detector*, *Phys. Lett. B* **784** (2018) 173 [arXiv:1806.00425] [INSPIRE].

[16] CMS collaboration, *Observation of $t\bar{t}H$ production*, *Phys. Rev. Lett.* **120** (2018) 231801 [arXiv:1804.02610] [INSPIRE].

[17] ATLAS collaboration, *CP properties of Higgs boson interactions with top quarks in the $t\bar{t}H$ and tH processes using $H \to \gamma\gamma$ with the ATLAS detector*, *Phys. Rev. Lett.* **125** (2020) 061802 [arXiv:2004.04545] [INSPIRE].

[18] ATLAS collaboration, *Measurement of the properties of Higgs boson production at $\sqrt{s} = 13$ TeV in the $H \to \gamma\gamma$ channel using 139 fb^{-1} of pp collision data with the ATLAS experiment*, *JHEP* **07** (2023) 088 [arXiv:2207.00348] [INSPIRE].

[19] CMS collaboration, *Measurements of Higgs boson production cross sections and couplings in the diphoton decay channel at $\sqrt{s} = 13$ TeV*, *JHEP* **07** (2021) 027 [arXiv:2103.06956] [INSPIRE].

[20] CMS collaboration, *Measurements of $t\bar{t}H$ production and the CP structure of the Yukawa interaction between the Higgs boson and top quark in the diphoton decay channel*, *Phys. Rev. Lett.* **125** (2020) 061801 [arXiv:2003.10866] [INSPIRE].

[21] ATLAS collaboration, *Higgs boson production cross-section measurements and their EFT interpretation in the 4ℓ decay channel at $\sqrt{s} = 13$ TeV with the ATLAS detector*, *Eur. Phys. J. C* **80** (2020) 957 [*Erratum ibid.* **81** (2021) 29] [arXiv:2004.03447] [INSPIRE].

[22] CMS collaboration, *Constraints on anomalous Higgs boson couplings to vector bosons and fermions in its production and decay using the four-lepton final state*, *Phys. Rev. D* **104** (2021) 052004 [arXiv:2104.12152] [INSPIRE].

[23] ATLAS collaboration, *Differential cross-section measurements of Higgs boson production in the $H \to \tau^+\tau^-$ decay channel in pp collisions at $\sqrt{s} = 13$ TeV with the ATLAS detector*, *JHEP* **03** (2025) 010 [arXiv:2407.16320] [INSPIRE].

[24] ATLAS collaboration, *Probing the CP nature of the top-Higgs Yukawa coupling in $t\bar{t}H$ and tH events with $H \to b\bar{b}$ decays using the ATLAS detector at the LHC*, *Phys. Lett. B* **849** (2024) 138469 [arXiv:2303.05974] [INSPIRE].

[25] ATLAS collaboration, *Measurement of the associated production of a top-antitop-quark pair and a Higgs boson decaying into a $b\bar{b}$ pair in pp collisions at $\sqrt{s} = 13$ TeV using the ATLAS detector at the LHC*, *Eur. Phys. J. C* **85** (2025) 210 [arXiv:2407.10904] [INSPIRE].

[26] CMS collaboration, *Measurement of the $t\bar{t}H$ and tH production rates in the $H \to b\bar{b}$ decay channel using proton-proton collision data at $\sqrt{s} = 13$ TeV*, *JHEP* **02** (2025) 097 [arXiv:2407.10896] [INSPIRE].

[27] ATLAS collaboration, *Evidence for the associated production of the Higgs boson and a top quark pair with the ATLAS detector*, *Phys. Rev. D* **97** (2018) 072003 [arXiv:1712.08891] [INSPIRE].

[28] CMS collaboration, *Measurement of the Higgs boson production rate in association with top quarks in final states with electrons, muons, and hadronically decaying tau leptons at $\sqrt{s} = 13$ TeV*, *Eur. Phys. J. C* **81** (2021) 378 [arXiv:2011.03652] [INSPIRE].

[29] CMS collaboration, *Search for CP violation in ttH and tH production in multilepton channels in proton-proton collisions at $\sqrt{s} = 13$ TeV*, *JHEP* **07** (2023) 092 [arXiv:2208.02686] [INSPIRE].

JHEP05(2026)183

[30] ATLAS collaboration, *Search for the production of a Higgs boson in association with a single top quark in pp collisions at $\sqrt{s} = 13$ TeV with the ATLAS detector*, *JHEP* **10** (2025) 093 [arXiv:2508.14695] [INSPIRE].

[31] ATLAS collaboration, *Measurement of the total and differential cross-sections of $t\bar{t}W$ production in pp collisions at $\sqrt{s} = 13$ TeV with the ATLAS detector*, *JHEP* **05** (2024) 131 [*Erratum ibid.* **11** (2025) 127] [arXiv:2401.05299] [INSPIRE].

[32] ATLAS collaboration, *Inclusive and differential cross-section measurements of $t\bar{t}Z$ production in pp collisions at $\sqrt{s} = 13$ TeV with the ATLAS detector, including EFT and spin-correlation interpretations*, *JHEP* **07** (2024) 163 [arXiv:2312.04450] [INSPIRE].

[33] J.R. Andersen et al., *Les Houches 2015: physics at TeV colliders Standard Model working group report*, in the proceedings of the *9th Les Houches Workshop on Physics at TeV Colliders*, Les Houches, France, June 01–19 (2015) [arXiv:1605.04692] [INSPIRE].

[34] N. Berger et al., *Simplified template cross sections — stage 1.1 and 1.2*, arXiv:1906.02754 [DOI:10.21468/SciPostPhysCommRep.15] [INSPIRE].

[35] H. Bahl et al., *Indirect CP probes of the Higgs-top-quark interaction: current LHC constraints and future opportunities*, *JHEP* **11** (2020) 127 [arXiv:2007.08542] [INSPIRE].

[36] F. Demartin et al., *Higgs characterisation at NLO in QCD: CP properties of the top-quark Yukawa interaction*, *Eur. Phys. J. C* **74** (2014) 3065 [arXiv:1407.5089] [INSPIRE].

[37] ATLAS collaboration, *The ATLAS experiment at the CERN Large Hadron Collider*, 2008 *JINST* **3** S08003 [INSPIRE].

[38] ATLAS collaboration, *ATLAS Insertable B-Layer technical design report*, CERN-LHCC-2010-013 (2010) [INSPIRE].

[39] ATLAS IBL collaboration, *Production and integration of the ATLAS Insertable B-Layer*, 2018 *JINST* **13** T05008 [arXiv:1803.00844] [INSPIRE].

[40] G. Avoni et al., *The new LUCID-2 detector for luminosity measurement and monitoring in ATLAS*, 2018 *JINST* **13** P07017 [INSPIRE].

[41] ATLAS collaboration, *Performance of the ATLAS trigger system in 2015*, *Eur. Phys. J. C* **77** (2017) 317 [arXiv:1611.09661] [INSPIRE].

[42] ATLAS collaboration, *Software and computing for run 3 of the ATLAS experiment at the LHC*, *Eur. Phys. J. C* **85** (2025) 234 [arXiv:2404.06335] [INSPIRE].

[43] ATLAS collaboration, *ATLAS data quality operations and performance for 2015–2018 data-taking*, 2020 *JINST* **15** P04003 [arXiv:1911.04632] [INSPIRE].

[44] ATLAS collaboration, *Luminosity determination in pp collisions at $\sqrt{s} = 13$ TeV using the ATLAS detector at the LHC*, *Eur. Phys. J. C* **83** (2023) 982 [arXiv:2212.09379] [INSPIRE].

[45] ATLAS collaboration, *Performance of electron and photon triggers in ATLAS during LHC run 2*, *Eur. Phys. J. C* **80** (2020) 47 [arXiv:1909.00761] [INSPIRE].

[46] ATLAS collaboration, *Performance of the ATLAS muon triggers in run 2*, 2020 *JINST* **15** P09015 [arXiv:2004.13447] [INSPIRE].

[47] ATLAS collaboration, *ATLAS Pythia 8 tunes to 7 TeV data*, ATL-PHYS-PUB-2014-021 (2014) [INSPIRE].

[48] P. Golonka and Z. Was, *PHOTOS Monte Carlo: a precision tool for QED corrections in Z and W decays*, *Eur. Phys. J. C* **45** (2006) 97 [hep-ph/0506026] [INSPIRE].

JHEP05(2026)183

[49] R.D. Ball et al., *Parton distributions with LHC data*, *Nucl. Phys. B* **867** (2013) 244 [arXiv:1207.1303] [INSPIRE].

[50] J. Pumplin et al., *New generation of parton distributions with uncertainties from global QCD analysis*, *JHEP* **07** (2002) 012 [hep-ph/0201195] [INSPIRE].

[51] P. Nason and C. Oleari, *NLO Higgs boson production via vector-boson fusion matched with shower in POWHEG*, *JHEP* **02** (2010) 037 [arXiv:0911.5299] [INSPIRE].

[52] S. Alioli, P. Nason, C. Oleari and E. Re, *A general framework for implementing NLO calculations in shower Monte Carlo programs: the POWHEG BOX*, *JHEP* **06** (2010) 043 [arXiv:1002.2581] [INSPIRE].

[53] P. Nason, *A new method for combining NLO QCD with shower Monte Carlo algorithms*, *JHEP* **11** (2004) 040 [hep-ph/0409146] [INSPIRE].

[54] S. Frixione, P. Nason and C. Oleari, *Matching NLO QCD computations with parton shower simulations: the POWHEG method*, *JHEP* **11** (2007) 070 [arXiv:0709.2092] [INSPIRE].

[55] NNPDF collaboration, *Parton distributions for the LHC run II*, *JHEP* **04** (2015) 040 [arXiv:1410.8849] [INSPIRE].

[56] LHC Higgs Cross Section Working Group collaboration, *Handbook of LHC Higgs cross sections: 4. Deciphering the nature of the Higgs sector*, *CERN Yellow Rep. Monogr.* **2** (2017) 1 [arXiv:1610.07922] [INSPIRE].

[57] W. Beenakker et al., *NLO QCD corrections to $t\bar{t}H$ production in hadron collisions*, *Nucl. Phys. B* **653** (2003) 151 [hep-ph/0211352] [INSPIRE].

[58] S. Dawson et al., *Associated Higgs production with top quarks at the Large Hadron Collider: NLO QCD corrections*, *Phys. Rev. D* **68** (2003) 034022 [hep-ph/0305087] [INSPIRE].

[59] Y. Zhang et al., *QCD NLO and EW NLO corrections to $t\bar{t}H$ production with top quark decays at hadron collider*, *Phys. Lett. B* **738** (2014) 1 [arXiv:1407.1110] [INSPIRE].

[60] S. Frixione et al., *Weak corrections to Higgs hadroproduction in association with a top-quark pair*, *JHEP* **09** (2014) 065 [arXiv:1407.0823] [INSPIRE].

[61] J. Alwall et al., *The automated computation of tree-level and next-to-leading order differential cross sections, and their matching to parton shower simulations*, *JHEP* **07** (2014) 079 [arXiv:1405.0301] [INSPIRE].

[62] P. Artoisenet, R. Frederix, O. Mattelaer and R. Rietkerk, *Automatic spin-entangled decays of heavy resonances in Monte Carlo simulations*, *JHEP* **03** (2013) 015 [arXiv:1212.3460] [INSPIRE].

[63] S. Frixione et al., *Single-top hadroproduction in association with a W boson*, *JHEP* **07** (2008) 029 [arXiv:0805.3067] [INSPIRE].

[64] F. Demartin et al., *tWH associated production at the LHC*, *Eur. Phys. J. C* **77** (2017) 34 [arXiv:1607.05862] [INSPIRE].

[65] ATLAS collaboration, *Studies on top-quark Monte Carlo modelling for Top2016*, ATL-PHYS-PUB-2016-020 (2016) [INSPIRE].

[66] Sherpa collaboration, *Event generation with Sherpa 2.2*, *SciPost Phys.* **7** (2019) 034 [arXiv:1905.09127] [INSPIRE].

[67] T. Gleisberg and S. Hoeche, *Comix, a new matrix element generator*, *JHEP* **12** (2008) 039 [arXiv:0808.3674] [INSPIRE].

JHEP05(2026)183

[68] F. Cascioli, P. Maierhofer and S. Pozzorini, *Scattering amplitudes with OpenLoops*, *Phys. Rev. Lett.* **108** (2012) 111601 [arXiv:1111.5206] [INSPIRE].

[69] A. Denner, S. Dittmaier and L. Hofer, *Collier: a fortran-based Complex One-Loop LIbrary in Extended Regularizations*, *Comput. Phys. Commun.* **212** (2017) 220 [arXiv:1604.06792] [INSPIRE].

[70] F. Buccioni et al., *OpenLoops 2*, *Eur. Phys. J. C* **79** (2019) 866 [arXiv:1907.13071] [INSPIRE].

[71] S. Schumann and F. Krauss, *A parton shower algorithm based on Catani-Seymour dipole factorisation*, *JHEP* **03** (2008) 038 [arXiv:0709.1027] [INSPIRE].

[72] S. Hoeche, F. Krauss, M. Schonherr and F. Siegert, *QCD matrix elements + parton showers: the NLO case*, *JHEP* **04** (2013) 027 [arXiv:1207.5030] [INSPIRE].

[73] S. Kallweit et al., *NLO QCD+EW predictions for V + jets including off-shell vector-boson decays and multijet merging*, *JHEP* **04** (2016) 021 [arXiv:1511.08692] [INSPIRE].

[74] C. Gütschow, J.M. Lindert and M. Schönherr, *Multi-jet merged top-pair production including electroweak corrections*, *Eur. Phys. J. C* **78** (2018) 317 [arXiv:1803.00950] [INSPIRE].

[75] R. Frederix, D. Pagani and M. Zaro, *Large NLO corrections in $t\bar{t}W^{\pm}$ and $t\bar{t}t\bar{t}$ hadroproduction from supposedly subleading EW contributions*, *JHEP* **02** (2018) 031 [arXiv:1711.02116] [INSPIRE].

[76] R. Frederix and I. Tsinikos, *On improving NLO merging for $t\bar{t}W$ production*, *JHEP* **11** (2021) 029 [arXiv:2108.07826] [INSPIRE].

[77] L. Buonocore et al., *Precise predictions for the associated production of a W boson with a top-antitop quark pair at the LHC*, *Phys. Rev. Lett.* **131** (2023) 231901 [arXiv:2306.16311] [INSPIRE].

[78] S. Frixione, E. Laenen, P. Motylinski and B.R. Webber, *Angular correlations of lepton pairs from vector boson and top quark decays in Monte Carlo simulations*, *JHEP* **04** (2007) 081 [hep-ph/0702198] [INSPIRE].

[79] S. Catani, F. Krauss, R. Kuhn and B.R. Webber, *QCD matrix elements + parton showers*, *JHEP* **11** (2001) 063 [hep-ph/0109231] [INSPIRE].

[80] S. Hoeche, F. Krauss, S. Schumann and F. Siegert, *QCD matrix elements and truncated showers*, *JHEP* **05** (2009) 053 [arXiv:0903.1219] [INSPIRE].

[81] T. Sjöstrand et al., *An introduction to PYTHIA 8.2*, *Comput. Phys. Commun.* **191** (2015) 159 [arXiv:1410.3012] [INSPIRE].

[82] D.J. Lange, *The EvtGen particle decay simulation package*, *Nucl. Instrum. Meth. A* **462** (2001) 152 [INSPIRE].

[83] T. Sjostrand, S. Mrenna and P.Z. Skands, *A brief introduction to PYTHIA 8.1*, *Comput. Phys. Commun.* **178** (2008) 852 [arXiv:0710.3820] [INSPIRE].

[84] ATLAS collaboration, *The Pythia 8 A3 tune description of ATLAS minimum bias and inelastic measurements incorporating the Donnachie-Landshoff diffractive model*, ATL-PHYS-PUB-2016-017 (2016) [INSPIRE].

[85] A.D. Martin, W.J. Stirling, R.S. Thorne and G. Watt, *Parton distributions for the LHC*, *Eur. Phys. J. C* **63** (2009) 189 [arXiv:0901.0002] [INSPIRE].

[86] ATLAS collaboration, *The ATLAS simulation infrastructure*, *Eur. Phys. J. C* **70** (2010) 823 [arXiv:1005.4568] [INSPIRE].

JHEP05(2026)183

[87] GEANT4 collaboration, *GEANT4 — a simulation toolkit*, *Nucl. Instrum. Meth. A* **506** (2003) 250 [INSPIRE].

[88] ATLAS collaboration, *Vertex reconstruction performance of the ATLAS detector at* $\sqrt{s} = 13$ *TeV*, ATL-PHYS-PUB-2015-026 (2015) [INSPIRE].

[89] ATLAS collaboration, *Electron and photon efficiencies in LHC run 2 with the ATLAS experiment*, *JHEP* **05** (2024) 162 [arXiv:2308.13362] [INSPIRE].

[90] ATLAS collaboration, *Muon reconstruction and identification efficiency in ATLAS using the full Run 2 pp collision data set at* $\sqrt{s} = 13$ *TeV*, *Eur. Phys. J. C* **81** (2021) 578 [arXiv:2012.00578] [INSPIRE].

[91] ATLAS collaboration, *Electron and photon performance measurements with the ATLAS detector using the 2015–2017 LHC proton-proton collision data*, 2019 *JINST* **14** P12006 [arXiv:1908.00005] [INSPIRE].

[92] ATLAS collaboration, *Jet reconstruction and performance using particle flow with the ATLAS detector*, *Eur. Phys. J. C* **77** (2017) 466 [arXiv:1703.10485] [INSPIRE].

[93] M. Cacciari, G.P. Salam and G. Soyez, *The anti-*k_t *jet clustering algorithm*, *JHEP* **04** (2008) 063 [arXiv:0802.1189] [INSPIRE].

[94] M. Cacciari, G.P. Salam and G. Soyez, *FastJet user manual*, *Eur. Phys. J. C* **72** (2012) 1896 [arXiv:1111.6097] [INSPIRE].

[95] ATLAS collaboration, *Jet energy scale and resolution measured in proton–proton collisions at* $\sqrt{s} = 13$ *TeV with the ATLAS detector*, *Eur. Phys. J. C* **81** (2021) 689 [arXiv:2007.02645] [INSPIRE].

[96] ATLAS collaboration, *Performance of pile-up mitigation techniques for jets in pp collisions at* $\sqrt{s} = 8$ *TeV using the ATLAS detector*, *Eur. Phys. J. C* **76** (2016) 581 [arXiv:1510.03823] [INSPIRE].

[97] ATLAS collaboration, *Forward jet vertex tagging using the particle flow algorithm*, ATL-PHYS-PUB-2019-026 (2019) [INSPIRE].

[98] ATLAS collaboration, *Selection of jets produced in 13 TeV proton-proton collisions with the ATLAS detector*, ATLAS-CONF-2015-029 (2015) [INSPIRE].

[99] ATLAS collaboration, *ATLAS flavour-tagging algorithms for the LHC run 2 pp collision dataset*, *Eur. Phys. J. C* **83** (2023) 681 [arXiv:2211.16345] [INSPIRE].

[100] ATLAS collaboration, *ATLAS b-jet identification performance and efficiency measurement with* $t\bar{t}$ *events in pp collisions at* $\sqrt{s} = 13$ *TeV*, *Eur. Phys. J. C* **79** (2019) 970 [arXiv:1907.05120] [INSPIRE].

[101] ATLAS collaboration, *Measurement of the c-jet mistagging efficiency in* $t\bar{t}$ *events using pp collision data at* $\sqrt{s} = 13$ *TeV collected with the ATLAS detector*, *Eur. Phys. J. C* **82** (2022) 95 [arXiv:2109.10627] [INSPIRE].

[102] ATLAS collaboration, *Calibration of the light-flavour jet mistagging efficiency of the b-tagging algorithms with Z+jets events using 139 fb*$^{-1}$ *of ATLAS proton–proton collision data at* $\sqrt{s} = 13$ *TeV*, *Eur. Phys. J. C* **83** (2023) 728 [arXiv:2301.06319] [INSPIRE].

[103] ATLAS collaboration, *Identification of hadronic tau lepton decays using neural networks in the ATLAS experiment*, ATL-PHYS-PUB-2019-033 (2019) [INSPIRE].

[104] ATLAS collaboration, *Reconstruction of hadronic decay products of tau leptons with the ATLAS experiment*, *Eur. Phys. J. C* **76** (2016) 295 [arXiv:1512.05955] [INSPIRE].

JHEP05(2026)183

[105] ATLAS collaboration, *Measurement of the tau lepton reconstruction and identification performance in the ATLAS experiment using pp collisions at* $\sqrt{s} = 13$ *TeV*, ATLAS-CONF-2017-029 (2017) [INSPIRE].

[106] M. Cacciari, G.P. Salam and G. Soyez, *The catchment area of jets*, *JHEP* **04** (2008) 005 [arXiv:0802.1188] [INSPIRE].

[107] ATLAS collaboration, *The performance of missing transverse momentum reconstruction and its significance with the ATLAS detector using* $140\,fb^{-1}$ *of* $\sqrt{s} = 13$ *TeV pp collisions*, *Eur. Phys. J. C* **85** (2025) 606 [arXiv:2402.05858] [INSPIRE].

[108] L. Breiman, *Random forests*, *Mach. Learn.* **45** (2001) 5 [INSPIRE].

[109] A. Altmann, L. Toloşi, O. Sander and T. Lengauer, *Permutation importance: a corrected feature importance measure*, *Bioinformatics* **26** (2010) 1340.

[110] CMS collaboration, *Measurement of the cross section of top quark-antiquark pair production in association with a W boson in proton-proton collisions at* $\sqrt{s} = 13$ *TeV*, *JHEP* **07** (2023) 219 [arXiv:2208.06485] [INSPIRE].

[111] ATLAS collaboration, *Measurement of Higgs boson decay into b-quarks in associated production with a top-quark pair in pp collisions at* $\sqrt{s} = 13$ *TeV with the ATLAS detector*, *JHEP* **06** (2022) 097 [arXiv:2111.06712] [INSPIRE].

[112] ATLAS collaboration, *Tools for estimating fake/non-prompt lepton backgrounds with the ATLAS detector at the LHC*, 2023 *JINST* **18** T11004 [arXiv:2211.16178] [INSPIRE].

[113] ATLAS collaboration, *Identification of jets containing b-hadrons with recurrent neural networks at the ATLAS experiment*, ATL-PHYS-PUB-2017-003 (2017) [INSPIRE].

[114] ATLAS collaboration, *Evaluation of QCD uncertainties for Higgs boson production through gluon fusion and in association with two top quarks for simplified template cross-section measurements*, ATL-PHYS-PUB-2023-031 (2023) [INSPIRE].

[115] J. Bellm et al., *Herwig 7.0/Herwig++ 3.0 release note*, *Eur. Phys. J. C* **76** (2016) 196 [arXiv:1512.01178] [INSPIRE].

[116] S. Höche et al., *A study of QCD radiation in VBF Higgs production with Vincia and Pythia*, *SciPost Phys.* **12** (2022) 010 [arXiv:2106.10987] [INSPIRE].

[117] ATLAS collaboration, *Studies on the improvement of the matching uncertainty definition in top-quark processes simulated with Powheg+Pythia 8*, ATL-PHYS-PUB-2023-029 (2023) [INSPIRE].

[118] ATLAS collaboration, *Study of top-quark pair modelling and uncertainties using ATLAS measurements at* $\sqrt{s} = 13$ *TeV*, ATL-PHYS-PUB-2020-023 (2020) [INSPIRE].

[119] ATLAS collaboration, *Observation of four-top-quark production in the multilepton final state with the ATLAS detector*, *Eur. Phys. J. C* **83** (2023) 496 [*Erratum ibid.* **84** (2024) 156] [arXiv:2303.15061] [INSPIRE].

[120] M. van Beekveld, A. Kulesza and L.M. Valero, *Threshold resummation for the production of four top quarks at the LHC*, *Phys. Rev. Lett.* **131** (2023) 211901 [arXiv:2212.03259] [INSPIRE].

[121] M. van Beekveld, A. Kulesza and L.M. Valero, *Threshold resummation for the production of four top quarks at the LHC*, arXiv:2212.03259v2.

[122] G. Cowan, K. Cranmer, E. Gross and O. Vitells, *Asymptotic formulae for likelihood-based tests of new physics*, *Eur. Phys. J. C* **71** (2011) 1554 [*Erratum ibid.* **73** (2013) 2501] [arXiv:1007.1727] [INSPIRE].

JHEP05(2026)183

[123] ATLAS collaboration, *ATLAS computing acknowledgements*, ATL-SOFT-PUB-2025-001 (2025) [INSPIRE].

[124] ATLAS collaboration, *CERN open data policy for the LHC experiments*, CERN-OPEN-2020-013 (2020).

JHEP05(2026)183

The ATLAS collaboration

G. Aad[103], E. Aakvaag[17], B. Abbott[122], S. Abdelhameed[118a], K. Abeling[55], N.J. Abicht[49], S.H. Abidi[30], M. Aboelela[45], A. Aboulhorma[36e], H. Abramowicz[156], B.S. Acharya[69a,69b,a], A. Ackermann[63a], C. Adam Bourdarios[4], L. Adamczyk[86a], S.V. Addepalli[148], M. J. Addison[102], J. Adelman[117], A. Adiguzel[22c], T. Adye[136], A.A. Affolder[138], Y. Afik[40], M.N. Agaras[13], A. Aggarwal[101], C. Agheorghiesei[28c], F. Ahmadov[39,b], S. Ahuja[96], S. Ahuja[168], X. Ai[142b], G. Aielli[76a,76b], A. Aikot[168], M. Ait Tamlihat[36e], B. Aitbenchikh[36a], T.P.A. Åkesson[99], D. Akiyama[173], N.N. Akolkar[25], S. Aktas[171], G.L. Alberghi[24b], J. Albert[170], U. Alberti[20], P. Albicocco[53], G.L. Albouy[60], S. Alderweireldt[52], Z.L. Alegria[123], M. Aleksa[37], C. Alexa[28b], I.N. Aleksandrov[39], T. Alexopoulos[10], F. Alfonsi[24b], M. Algren[56], M. Alhroob[172], B. Ali[134], H. M. J. Ali[92,c], S. Ali[32], S.W. Alibocus[93], M. Aliev[34c], G. Alimonti[71a], W. Alkakhi[55], C. Allaire[66], B.M.M. Allbrooke[151], D. R. Allen[123], J. S. Allen[102], J.F. Allen[52], A. Aloisio[72a,72b], F. Alonso[91], C. Alpigiani[141], Z.M.K. Alsolami[92], A. Alvarez Fernandez[101], M. Alves Cardoso[56], M.G. Alviggi[72a,72b], M. Aly[102], A. Ambler[105], C. Amelung[37], M. Amerl[102], C.G. Ames[110], T. Amezza[129], B. Amini[54], K. Amirie[160], A. Amirkhanov[39], S.P. Amor Dos Santos[132a], D. Amperiadou[157], S. An[83], C. Anastopoulos[144], T. Andeen[11], J.K. Anders[93], A. C. Anderson[59], A. Andreazza[71a,71b], S. Angelidakis[9], A. Angerami[42], A.V. Anisenkov[39], A. Annovi[74a], C. Antel[37], E. Antipov[150], M. Antonelli[53], F. Anulli[75a], M. Aoki[83], T. Aoki[158], M.A. Aparo[13], L. Aperio Bella[48], M. Apicella[31], C. Appelt[156], A. Apyan[27], M. Arampatzi[10], S. J. Arbiol Val[87], C. Arcangeletti[53], A.T.H. Arce[51], J-F. Arguin[109], S. Argyropoulos[157], J.-H. Arling[48], O. Arnaez[4], H. Arnold[150], G. Artoni[75a,75b], H. Asada[112], K. Asai[120], S. Asatryan[178], N.A. Asbah[37], R. A. Ashby Pickering[172], A. M. Aslam[96], K. Assamagan[30], R. Astalos[29a], K. S. V. Astrand[99], S. Atashi[164], R.J. Atkin[34a], H. Atmani[36f], P.A. Atmasiddha[130], K. Augsten[134], A.D. Auriol[41], V.A. Austrup[102], A.S. Avad[95], G. Avolio[37], K. Axiotis[56], A. Azzam[13], D. Babal[29b], H. Bachacou[137], K. Bachas[157,d], A. Bachiu[35], E. Bachmann[50], M. J. Backes[63a], A. Badea[40], T.M. Baer[107], P. Bagnaia[75a,75b], M. Bahmani[19], D. Bahner[54], K. Bai[125], J.T. Baines[136], L. Baines[95], O.K. Baker[177], E. Bakos[16], D. Bakshi Gupta[8], L.E. Balabram Filho[82b], V. Balakrishnan[122], R. Balasubramanian[4], E.M. Baldin[38], P. Balek[86a], E. Ballabene[24b,24a], F. Balli[137], L.M. Baltes[63a], W.K. Balunas[33], J. Balz[101], I. Bamwidhi[118b], E. Banas[87], M. Bandieramonte[131], A. Bandyopadhyay[25], S. Bansal[25], L. Barak[156], M. Barakat[48], E.L. Barberio[106], D. Barberis[18b], M. Barbero[103], M. Z. Barel[116], T. Barillari[111], M-S. Barisits[37], T. Barklow[148], P. Baron[135], D.A. Baron Moreno[102], A. Baroncelli[62], A.J. Barr[128], J.D. Barr[97], F. Barreiro[100], J. Barreiro Guimarães da Costa[14], M.G. Barros Teixeira[132a], R.F. Coelho Barrue[132a], S. Barsov[38], F. Bartels[63a], R. Bartoldus[148], A.E. Barton[92], P. Bartos[29a], M. Baselga[49], S. Bashiri[87], A. Bassalat[66,e], M.J. Basso[161a], S. Bataju[45], R. Bate[169], R.L. Bates[59], S. Batlamous[100], M. Battaglia[138], D. Battulga[19], M. Bauce[75a,75b], L. Bauckhage[48], P. Bauer[25], L. T. Bayer[48], L.T. Bazzano Hurrell[31], J.B. Beacham[111], T. Beau[129], J.Y. Beaucamp[91], P.H. Beauchemin[163], P. Bechtle[25], H.P. Beck[20,f], K. Becker[172], A.J. Beddall[81], V.A. Bednyakov[39], C.P. Bee[150], L.J. Beemster[16], M. Begalli[82d], M. Begel[30], J.K. Behr[48], J.F. Beirer[37], F. Beisiegel[25],

JHEP05(2026)183

M. Belfkir[118b], G. Bella[156], L. Bellagamba[24b], A. Bellerive[35], C.D. Bellgraph[68], P. Bellos[21], K. Beloborodov[38], I. Benaoumeur[21], D. Benchekroun[36a], F. Bendebba[36a], Y. Benhammou[156], K.C. Benkendorfer[61], L. Beresford[48], M. Beretta[53], E. Bergeaas Kuutmann[166], N. Berger[4], B. Bergmann[134], J. Beringer[18a], G. Bernardi[5], C. Bernius[148], F.U. Bernlochner[25], A. Berrocal Guardia[13], T. Berry[96], P. Berta[135], A. Berti[132a], R. Bertrand[103], S. Bethke[111], A. Betti[75a,75b], A.J. Bevan[95], L. Bezio[56], N.K. Bhalla[54], S. Bharthuar[111], S. Bhatta[150], P. Bhattarai[148], Z.M. Bhatti[119], K. D. Bhide[54], V.S. Bhopatkar[123], R.M. Bianchi[131], G. Bianco[24b,24a], O. Biebel[110], M. Biglietti[77a], C. S. Billingsley[45], Y. Bimgdi[36f], M. Bindi[55], A. Bingham[176], A. Bingul[22b], C. Bini[75a,75b], G.A. Bird[33], M. Birman[174], M. Biros[135], S. Biryukov[151], T. Bisanz[49], E. Bisceglie[24b,24a], J.P. Biswal[136], D. Biswas[146], I. Bloch[48], A. Blue[59], U. Blumenschein[95], V.S. Bobrovnikov[39], L. Boccardo[57b,57a], M. Boehler[54], D. Bogavac[13], A.G. Bogdanchikov[38], L. S. Boggia[129], B. Boehm[171], V. Boisvert[96], P. Bokan[166], T. Bold[86a], M. Bomben[5], M. Bona[95], M. Boonekamp[137], A.G. Borbély[59], I.S. Bordulev[38], G. Borissov[92], D. Bortoletto[128], D. Boscherini[24b], K. Bouaouda[36a], N. Bouchhar[168], L. Boudet[4], J. Boudreau[131], E.V. Bouhova-Thacker[92], D. Boumediene[41], R. Bouquet[57b,57a], A. Boveia[121], J. Boyd[37], D. Boye[30], I.R. Boyko[39], L. Bozianu[56], J. Bracinik[21], N. Brahimi[4], G. Brandt[176], O. Brandt[33], B. Brau[104], L. Brenner[116], R. Brenner[166], S. Bressler[174], G. Brianti[116], D. Britton[59], D. Britzger[111], I. Brock[25], R. Brock[108], G. Brooijmans[42], A.J. Brooks[68], E. M. Brooks[161b], E. Brost[30], L.M. Brown[170,161a], L.E. Bruce[61], T.L. Bruckler[128], P.A. Bruckman de Renstrom[87], B. Brüers[48], A. Bruni[24b], G. Bruni[24b], D. Brunner[47a,47b], M. Bruschi[24b], N. Bruscino[75a,75b], T. Buanes[17], Q. Buat[141], D. Buchin[111], A.G. Buckley[59], V. Büscher[101], O. Bulekov[81], B.A. Bullard[148], S. Burdin[93], C.D. Burgard[49], A.M. Burger[90], B. Burghgrave[8], O. Burlayenko[54], J. Burleson[167], J.C. Burzynski[147], P.J. Bussey[59], O. But[25], J.M. Butler[26], C.M. Buttar[59], J.M. Butterworth[97], P. Butti[37], W. Buttinger[136], C.J. Buxo Vazquez[108], A.R. Buzykaev[39], S. Cabrera Urbán[168], L. Cadamuro[66], H. Cai[37], Y. Cai[24b,113c,24a], Y. Cai[113a], V.M.M. Cairo[37], O. Cakir[3a], N. Calace[37], P. Calafiura[18a], G. Calderini[129], P. Calfayan[35], L. Calic[99], G. Callea[59], L.P. Caloba[82b], D. Calvet[41], S. Calvet[41], R. Camacho Toro[129], S. Camarda[37], D. Camarero Munoz[27], P. Camarri[76a,76b], C. Camincher[37], M. Campanelli[97], A. Camplani[43], V. Canale[72a,72b], A.C. Canbay[3a], E. Canonero[96], J. Cantero[168], Y. Cao[167], F. Capocasa[27], M. Capua[44b,44a], A. Carbone[71a,71b], R. Cardarelli[76a], J.C.J. Cardenas[8], M. P. Cardiff[27], J.M. Silva[52], G. Carducci[44b,44a], T. Carli[37], G. Carlino[72a], J.I. Carlotto[13], B.T. Carlson[131,g], E.M. Carlson[170], L. Carminati[71a,71b], A. Carnelli[4], M. Carnesale[37], S. Caron[115], E. Carquin[139g], I.B. Carr[106], S. Carrá[73a,73b], G. Carratta[24b,24a], C. Carrion Martinez[168], A.M. Carroll[125], M.P. Casado[13,h], P. Casolaro[72a,72b], M. Caspar[48], W.R. Castiglioni[40], F.L. Castillo[4], L. Castillo Garcia[13], V. Castillo Gimenez[168], N.F. Castro[132a,132e], M.C.N. Fiolhais[132a,132c,i], A. Catinaccio[37], J.R. Catmore[127], T. Cavaliere[4], V. Cavaliere[30], L.J. Caviedes Betancourt[23b], E. Celebi[81], S. Cella[37], V. Cepaitis[56], K. Cerny[124], A. Cerri[74a,74b,j], L. Cerrito[76a,76b], F. Cerutti[18a], B. Cervato[71a,71b], A. Cervelli[24b], G. Cesarini[53], S.A. Cetin[81], P.M. Chabrillat[129], R. Chakkappai[66], S. Chakraborty[172], A. Chambers[61], J. Chan[18a], W.Y. Chan[158],

JHEP05(2026)183

J.D. Chapman[33], E. Chapon[137], B. Chargeishvili[154b], D.G. Charlton[21], C. Chauhan[135], Y. Che[113a], S. Chekanov[6], B. Chen[170], H. Chen[30], J. Chen[143a], J. Chen[147], M. Chen[128], S. Chen[88], S.J. Chen[113a], X. Chen[143a], X. Chen[15,k], Z. Chen[62], C.L. Cheng[175], H.C. Cheng[64a], S. Cheong[148], A. Cheplakov[39], E. Cherepanova[116], E. Cheu[7], K. Cheung[65], L. Chevalier[137], V. Chiarella[53], G. Chiarelli[74a], G. Chiodini[70a], A.S. Chisholm[21], A. Chitan[28b], M. Chitishvili[168], M.V. Chizhov[39,l], K. Choi[11], Y. Chou[141], E.Y.S. Chow[115], V.A. Schegelsky[38], K.L. Chu[174], M.C. Chu[64a], Z. Chubinidze[53], J. Chudoba[133], J.J. Chwastowski[87], D. Cieri[111], K.M. Ciesla[86a], V. Cindro[94], A. Ciocio[18a], F. Cirotto[72a,72b], Z.H. Citron[174], M. Citterio[71a], D.A. Ciubotaru[28b], A. Clark[56], P.J. Clark[52], N. Clarke Hall[97], C. Clarry[160], S.E. Clawson[48], C. Clement[47a,47b], L. Clissa[24b,24a], Y. Coadou[103], M. Cobal[69a,69c], A. Coccaro[57b], R. Coelho Lopes De Sa[104], S. Coelli[71a], M.M. Cohen[130], L. S. Colangeli[160], B. Cole[42], P. Collado Soto[100], J. Collot[60], R. Coluccia[70a,70b], P. Conde Muiño[132a,132g], M.P. Connell[34c], S.H. Connell[34c], E.I. Conroy[128], M. Contreras Cossio[11], F. Conventi[72a,m], L. Corazzina[75a,75b], F. A. Corchia[24b,24a], A. Cordeiro Oudot Choi[141], L.D. Corpe[41], M. Corradi[75a,75b], F. Corriveau[105,n], A. Cortes-Gonzalez[158], M.J. Costa[168], F. Costanza[4], D. Costanzo[144], J. Couthures[4], G. Cowan[96], K. Cranmer[175], L. Cremer[49], D. Cremonini[24b,24a], S. Crépé-Renaudin[60], F. Crescioli[129], T. Cresta[73a,73b], M. Cristinziani[146], M. Cristoforetti[78a,78b], E. Critelli[97], G. Crosetti[44b,44a], A. Cueto[100], H. Cui[97], Z. Cui[7], B.M. Cunnett[151], W.R. Cunningham[59], F. Curcio[168], J. R. Curran[52], G. D'amen[30], V. D'Amico[110], M. D'Andrea[57b,57a], G. D'anniballe[74a,74b], S. D'Auria[71a,71b], A. D'Avanzo[72a,72b], L. D'Eramo[41], A. D'Onofrio[72a,72b], M. D'Onofrio[93], M. D'uffizi[102], J.V. Da Fonseca Pinto[82b], A. Gomes[132a,132b], C. Da Via[102], W. Dabrowski[86a], T. Dado[37], S. Dahbi[153], T. Dai[107], D. Dal Santo[20], C. Dallapiccola[104], M. Dam[43], J.R. Dandoy[35], D. Dannheim[37], M. Danninger[147], V. Dao[150], G. Darbo[57b], S.J. Das[30], F. Dattola[48], T. Davidek[135], J. Davidson[172], I. Dawson[95], K. De[8], F.A. Dias[116], C. De Almeida Rossi[160], R. De Asmundis[72a], N. De Biase[48], S. De Castro[24b,24a], N. De Groot[115], P. de Jong[116], H. De la Torre[117], A. De Maria[113a], A. De Salvo[75a], U. De Sanctis[76a,76b], F. De Santis[70a,70b], A. De Santo[151], J.B. De Vivie De Regie[60], J. Debevc[94], D.V. Dedovich[39], J. Degens[93], A.M. Deiana[45], J. Del Peso[100], L. Delagrange[129], F. Deliot[137], C.M. Delitzsch[49], A. Dell'Acqua[37], L. Dell'Asta[71a,71b], M. Della Pietra[72a,72b], D. Della Volpe[56], M. Delmastro[4], C.C. Delogu[57b,57a], P.A. Delsart[60], S. Demers[177], M. Demichev[39], S.P. Denisov[38], H. Denizli[22a,o], M.G. Depala[93], D. Derendarz[87], F. Derue[129], P. Dervan[93,†], A. M. Desai[1], K. Desch[25], F.A. Di Bello[74a,74b], A. Di Ciaccio[76a,76b], L. Di Ciaccio[4], A. Di Domenico[75a,75b], C. Di Donato[72a,72b], A. Di Girolamo[37], G. Di Gregorio[66], A. Di Luca[78a,78b], B. Di Micco[77a,77b], R. Di Nardo[77a,77b], K.F. Di Petrillo[40], M. Diamantopoulou[35], M.A. Diaz[139a,139b], A. R. Didenko[39], M. Didenko[168], S.D. Diefenbacher[18a], E.B. Diehl[107], S. Díez Cornell[48], C. Diez Pardos[146], C. Dimitriadi[149], A. Dimitrievska[21], A. Dimri[150], Y. Ding[62], J. Dingfelder[25], T. Dingley[128], I-M. Dinu[28b], S.J. Dittmeier[63b], F. Dittus[37], M. Divisek[135], B. Dixit[93], F. Djama[103], T. Djobava[154b], Y. Amaral Coutinho[82b], C. Doglioni[102,99], A. Dohnalova[29a], Z. Dolezal[135], K. Domijan[86a], K.M. Dona[40], M. Donadelli[82d], B. Dong[108], D. Qichen[128], J. Donini[41], J. Dopke[136], A. Doria[72a],

JHEP05(2026)183

N. Dos Santos Fernandes[132a], I.A. Dos Santos Luz[82e], P. Dougan[45], M.T. Dova[91], A.T. Doyle[59], M.P. Drescher[55], E. Dreyer[174], I. Drivas-koulouris[10], M. Drnevich[119], D. Du[62], T.A. du Pree[116], Z. Duan[113a], M. Dubau[4], F. Dubinin[39], M. Dubovsky[29a], E. Duchovni[174], G. Duckeck[110], P. K. Duckett[97], O.A. Ducu[28b], D. Duda[52], A. Dudarev[37], M.M. Dudek[87], E. R. Duden[27], M. Dührssen[37], L. Duflot[66], I. Duminica[28g], A.E. Dumitriu[28b], M. Dunford[63a], A. Duperrin[103], A. Durglishvili[154b], G.I. Dyckes[18a], M. Dyndal[86a], B.S. Dziedzic[37], Z.O. Earnshaw[151], G.H. Eberwein[128], B. Eckerova[29a], S. Eggebrecht[55], G. Eigen[17], K. Einsweiler[18a], T. Ekelof[166], P.A. Ekman[99], S. El Farkh[36b], Y. El Ghazali[62], H. El Jarrari[105], A. El Moussaouy[36a], D. Elitez[37], M. Ellert[166], F. Ellinghaus[176], T.A. Elliot[96], J. Elmsheuser[30], M. Elsawy[118a], M. Elsing[37], D. Emeliyanov[136], Y. Enari[83], S. Epari[109], D. Ernani Martins Neto[87], F. Ernst[37], M. Escalier[66], C. Escobar[168], E. Etzion[156], H. Evans[68], L.S. Evans[48], A. Ezhilov[38], S. Ezzarqtouni[36a], F. Fabbri[24b,24a], L. Fabbri[24b,24a], G. Facini[97], V. Fadeyev[138], R.M. Fakhrutdinov[38], D. Fakoudis[101], S. Falciano[75a], L.F. Falda Ulhoa Coelho[27], P.J. Falke[25], F. Fallavollita[111], G. Falsetti[44b,44a], J. Faltova[135], C. Fan[167], K. Y. Fan[64b], Y. Fan[14], Y. Fang[14,113c], M. Fanti[71a,71b], M. Faraj[69a,69c], Z. Farazpay[98], A. Farbin[8], A. Farilla[77a], K. Farman[153], J. N. Farr[177], M. S. Farrington[61], S.M. Farrington[136,52], F. Fassi[36e], D. Fassouliotis[9], L. Fayard[66], P. Federic[135], P. Federicova[133], O.L. Fedin[38,p], M. Feickert[175], L. Feligioni[103], D.E. Fellers[18a], C. Feng[142a], Y. Feng[14], Z. Feng[116], B. Fernandez Barbadillo[92], P. Fernandez Martinez[67], M. Bosman[13], M.J.V. Fernoux[103], J. Ferrando[92], A. Ferrari[166], P. Ferrari[116,115], R. Ferrari[73a], D. Ferrere[56], C. Ferretti[107], M. P. Fewell[1], D. Fiacco[75a,75b], F. Fiedler[101], P. Fiedler[134], S. Filimonov[39], M.S. Filip[28b,q], A. Filipčič[94], E.K. Filmer[161a], F. Filthaut[115], L. Fiorini[168], W.C. Fisher[108], T. Fitschen[102], P. M. Fitzhugh[137], I. Fleck[146], P. Fleischmann[107], T. Flick[176], M. Flores[34d,r], L.R. Flores Castillo[64a], M. Foll[127], F.M. Follega[78a,78b], N. Fomin[33], J.H. Foo[160], A. Formica[137], A.C. Forti[102], E. Fortin[37], A.W. Fortman[18a], L. Foster[18a], L. Fountas[9,s], H. Fox[92], P. Francavilla[74a,74b], S. Francescato[61], S. Franchellucci[56], M. Franchini[24b,24a], S. Franchino[63a], D. Francis[37], L. Franco[48], L. Franconi[48], M. Franklin[61], G. Frattari[27], Y.Y. Frid[156], J. Friend[59], N. Fritzsche[37], A. Froch[56], D. Froidevaux[37], J.A. Frost[136], Y. Fu[108], S. Fuenzalida Garrido[139g], M. Fujimoto[150], K. Y. Fung[64a], M. Furukawa[158], M. Fuste Costa[48], J. Fuster[168], A. Gaa[55], A. Gabrielli[24b,24a], A. Gabrielli[160], P. Gadow[37], G. Gagliardi[57b,57a], L.G. Gagnon[18a], S. Gaid[84b], S. Galantzan[156], J. Gallagher[1], E.J. Gallas[128], A.L. Gallen[166], B.J. Gallop[136], K.K. Gan[121], Y. Gao[52], A. Garabaglu[141], F.M. Garay Walls[139a,139b], C. García[168], A. Garcia Alonso[116], A.G. Garcia Caffaro[177], J.E. García Navarro[168], M. A. Garcia Ruiz[23b], M. Garcia-Sciveres[18a], G.L. Gardner[130], R.W. Gardner[40], N. Garelli[163], R.B. Garg[148], J.M. Gargan[33], C.A. Garner[160], C.M. Garvey[34a], G. Evans[132a,132b], V. K. Gassmann[163], G. Gaudio[73a], V. Gautam[13], P. Gauzzi[75a,75b], J. Gavranovic[94], I.L. Gavrilenko[132a], A. Gavrilyuk[38], C. Gay[169], G. Gaycken[125], A. Gekow[121], C. Gemme[57b], M.H. Genest[60], S. Gentile[75b], A. D. Gentry[114], S. George[96], T. Geralis[46], A. A. Gerwin[122], P. Gessinger-Befurt[37], M. Ghani[172], K. Ghorbanian[95], A. Ghosal[146], A. Ghosh[164], A. Ghosh[7], B. Giacobbe[24b], S. Giagu[75a,75b], T. Giani[116], A. Giannini[62], S.M. Gibson[96], D.T. Gil[86b], A.K. Gilbert[86a],

JHEP05(2026)183

B.J. Gilbert[42], D. Gillberg[35], G. Gilles[116], D.M. Gingrich[2,t], M.P. Giordani[69a,69c], P.F. Giraud[137], G. Giugliarelli[69a,69c], D. Giugni[71a], F. Giuli[76a,76b], I. Gkialas[9,s], L.K. Gladilin[38], C. Glasman[100], M. Glazewska[20], R. M. Gleason[164], G. Glemža[48], M. Glisic[125], I. Gnesi[44b], Y. Go[30], M. Goblirsch-Kolb[37], B. Gocke[49], D. Godin[109], B. Gokturk[22a], S. Goldfarb[106], T. Golling[56], M.G.D. Gololo[34c], A. Golub[141], D. Golubkov[38], J.P. Gombas[108], G. Gomes Da Silva[146], A.J. Gomez Delegido[37], A. Gongadze[154c], F. Gonnella[21], J.L. Gonski[148], R.Y. González Andana[52], S. González de la Hoz[168], M. V. Gonzalez Rodrigues[48], S. Gonzalez-Sevilla[56], R. Gonzalez Suarez[166], L. Goossens[37], B. Gorini[37], E. Gorini[70a,70b], A. Gorišek[94], T.C. Gosart[130], A.T. Goshaw[51], M.I. Gostkin[39], S. Goswami[123], C.A. Gottardo[37], S. A. Gotz[110], M. Gouighri[36b], A.G. Goussiou[141], N. Govender[34c], R. P. Grabarczyk[128], I. Grabowska-Bold[86a], K. Graham[35], E. Gramstad[127], S. Grancagnolo[70a,70b], C.M. Grant[1], P.M. Gravila[28f], F.G. Gravili[70a,70b], H.M. Gray[18a], M. Greco[111], M. J. Green[1], C. Grefe[25], A. S. Grefsrud[17], I.M. Gregor[48], R.R. Marcelo Gregorio[95], K.T. Greif[164], P. Grenier[148], S.G. Grewe[111], K. Grimm[32], S. Grinstein[13,u], E. Gross[174], J. Grosse-Knetter[55], L.H. Grossman[18b], L. Guan[107], G. Guerrieri[37], R. Guevara[127], R. Gugel[101], J.A.M. Guhit[107], A. Guida[19], E. Guilloton[172], S. Guindon[37], F. Guo[14,113c], J. Guo[143a], L. Guo[48], L. Guo[113b,v], Y. Guo[107], Y. Guo[42], A. Gupta[49], R. Gupta[131], S. Gupta[27], S. Gurbuz[25], S.S. Gurdasani[48], G. Gustavino[75a,75b], P. Gutierrez[122], L.F. Gutierrez Zagazeta[130], M. Gutsche[50], C. Gutschow[97], C. Gwenlan[128], C.B. Gwilliam[93], E.S. Haaland[127], A. Haas[119], M. Habedank[59], C. Haber[18a], H.K. Hadavand[8], A. Haddad[41], A. Hadef[50], A.I. Hagan[92], J. J. Hahn[146], E.H. Haines[97], M. Haleem[171], J. Haley[123], G.D. Hallewell[103], J.A. Hallford[48], K. Hamano[170], H. Hamdaoui[166], M. Hamer[25], S. E. D. Hammoud[66], E.J. Hampshire[96], L. Han[113a], L. Han[62], S. Han[14], K. Hanagaki[83], M. Hance[138], D.A. Hangal[42], H. Hanif[147], M.D. Hank[130], J.B. Hansen[43], P.H. Hansen[43], T. Harenberg[176], S. Harkusha[178], M.L. Harris[104], Y.T. Harris[25], J. Harrison[13], P.F. Harrison[172], M. L. E. Hart[97], N.M. Hartman[111], R. Z. Hasan[96,136], Y. Hasegawa[145], D. Hashimoto[112], F. Haslbeck[128], S. Hassan[17], R. Hauser[108], M. Haviernik[135], C.M. Hawkes[21], R.J. Hawkings[37], Y. Hayashi[158], D. Hayden[108], R.L. Hayes[116], C.P. Hays[128], J.M. Hays[95], H.S. Hayward[93], M. He[14,113c], Y. He[48], Y. He[97], N.B. Heatley[95], V. Hedberg[99], J. Heilman[35], S. Heim[48], T. Heim[18a], J.J. Heinrich[125], L. Heinrich[111], J. Hejbal[133], M. Helbig[50], A. Held[175], S. Hellesund[17], C.M. Helling[169], H. Herde[99], Y. Hernández Jiménez[150], L.M. Herrmann[25], G. Herten[54], R. Hertenberger[110], L. Hervas[37], M.E. Hesping[101], N.P. Hessey[161a], J. Hessler[111], M. Hidaoui[36b], N. Hidic[135], Y. Nakahama[83], E. Hill[160], T. S. Hillersoy[17], S.J. Hillier[21], J.R. Hinds[108], F. Hinterkeuser[25], M. Hirose[126], S. Hirose[162], D. Hirschbuehl[176], T.G. Hitchings[102], B. Hiti[94], J. Hobbs[150], R. Hobincu[28e], A.M. Hodges[167], M.C. Hodgkinson[144], B.H. Hodkinson[128], A. Hoecker[37], D. D. Hofer[107], J. Hofer[168], J. Hofner[101], M. Holzbock[37], L.B.A.H. Hommels[33], V. Homsak[128], J. J. Hong[68], T.M. Hong[131], B.H. Hooberman[167], W.H. Hopkins[6], M. C. Hoppesch[167], Y. Horii[112], M. E. Horstmann[111], S. Hou[153], M. R. Housenga[167], J. Howarth[59], J. Hoya[6], M. Hrabovsky[124], T. Hryn'ova[4], P.J. Hsu[65], S.-C. Hsu[141], T. Hsu[66], M. Hu[18a], Q. Hu[62], S. Huang[33], X. Huang[14,113c],

JHEP05(2026)183

Y. Huang[135], Y. Huang[113b], Y. Huang[14], Z. Huang[66], Z. Hubacek[134], F. Huegging[25], T.B. Huffman[128], M. Hufnagel Maranha De Faria[82a], C. A. Hugli[48], M. Huhtinen[37], S.K. Huiberts[127], R. Hulsken[105], C. E. Hultquist[18a], D.L. Humphreys[104], N. Huseynov[12], J. Huston[108], J. Huth[61], L. Huth[48], R. Hyneman[7], G. Iacobucci[56], G. Iakovidis[30], L. Iconomidou-Fayard[66], J. P. Iddon[37], P. Iengo[72a,72b], Y. Iiyama[158], T. Iizawa[158], Y. Ikegami[83], D. Iliadis[157], N. Ilic[160], H. Imam[36a], G. Inacio Goncalves[82d], S. A. Infante Cabanas[139c], T. Ingebretsen Carlson[47a,47b], J. M. Inglis[95], G. Introzzi[73a,73b], M. Iodice[77a], V. Ippolito[75a,75b], R. K. Irwin[93], M. Ishino[158], W. Islam[175], C. Issever[19], S. Istin[22a,w], K. Itabashi[126], H. Ito[173], R. Iuppa[78a,78b], A. Ivina[174], S. Izumiyama[112], V. Izzo[72a], P. Jacka[134], P. Jackson[1], P. R. Jacobson[51], P. Jain[48], K. Jakobs[54], T. Jakoubek[174], J. Jamieson[59], W. Jang[158], S. Jankovych[116], M. Javurkova[104], P. Jawahar[102], L. Jeanty[125], J. Jejelava[154a,x], P. Jenni[54,y], C.E. Jessiman[35], H. Jia[169], J. Jia[150], X. Jia[111,113c], Z. Jia[113a], C. Jiang[52], Q. Jiang[64b], S. Jiggins[48], M. Jimenez Ortega[168], J. Jimenez Pena[13], S. Jin[113a], A. Jinaru[28b], O. Jinnouchi[140], P. Johansson[144], K.A. Johns[7], J.W. Johnson[138], F. A. Jolly[48], D.M. Jones[151], E. Jones[48], K.S. Jones[8], P. Jones[33], R.W.L. Jones[92], T.J. Jones[93], H.L. Joos[55], R. Joshi[121], J. Jovicevic[16], X. Ju[18a], J.J. Junggeburth[37], T. Junkermann[63a], A. Juste Rozas[13,u], M.K. Juzek[87], S. Kabana[139f], A. Kaczmarska[87], S. A. Kadir[148], M. Kado[111], H. Kagan[121], M. Kagan[148], A. Kahn[130], C. Kahra[101], T. Kaji[158], E. Kajomovitz[155], N. Kakati[174], N. Kakoty[13], S. Kandel[8], N. Kanellos[10], N.J. Kang[138], D. Kar[34j], E. Karentzos[25], K. Karki[8], O. Karkout[116], S.N. Karpov[39], Z.M. Karpova[39], V. Kartvelishvili[92,154b], A.N. Karyukhin[38], E. Kasimi[157], J. Katzy[48], S. Kaur[35], K. Kawade[145], M.P. Kawale[122], C. Kawamoto[88], E.F. Kay[37], S. Kazakos[108], K. Kazakova[103], V.F. Kazanin[38], J.M. Keaveney[34a], R. Keeler[170], G.V. Kehris[61], J.S. Keller[35], J. M. Kelly[170], J.J. Kempster[151], O. Kepka[133], J. Kerr[161b], B.P. Kerridge[136], B.P. Kerševan[94], L. Keszeghova[29a], R. A. Khan[131], A. Khanov[123], A.G. Kharlamov[38], T. Kharlamova[38], M. Kholodenko[132a], T.J. Khoo[19], G. Khoriauli[171], Y. Khoulaki[36a], Y.A.R. Khwaira[129], D. Kim[6], D.W. Kim[18b], Y.K. Kim[40], N. Kimura[97], M.K. Kingston[55], C. Kirfel[25], F. Kirfel[25], J. Kirk[136], A.E. Kiryunin[111], S. Kita[162], O. Kivernyk[25], M. Klassen[163], C. Klein[35], L. Klein[171], M.H. Klein[45], S.B. Klein[56], U. Klein[93], A. Klimentov[30], P. Kluit[116], S. Kluth[111], E. Kneringer[79], T.M. Knight[160], A. Knue[49], M. Kobel[50], D. Kobylianskii[174], S.F. Koch[37], M. Kocian[148], D.M. Koeck[125], P. Kodyš[135], K. Köneke[55], T. Koffas[35], O. Kolay[50], I. Koletsou[4], T. Komarek[87], A.X.Y. Kong[1], T. Kono[120], N. Konstantinidis[97], P. Kontaxakis[56], B. Konya[99], R. Kopeliansky[42], S. Koperny[86a], R. Koppenhofer[54], K. Korcyl[87], K. Kordas[157,z], A. Korn[97], S. Korn[55], I. Korolkov[13], N. Korotkova[38], B. Kortman[116], O. Kortner[111], S. Kortner[111], W.H. Kostecka[117], M. Kostov[29a], V.V. Kostyukhin[146], A. Kotsokechagia[37], A. Kotwal[51], A. Koulouris[37], Y. Kulchitsky[39], A. Kourkoumeli-Charalampidi[73a,73b], E. Kourlitis[111], O. Kovanda[125], R. Kowalewski[170], W. Kozanecki[125], A.S. Kozhin[38], V.A. Kramarenko[38], G. Kramberger[94], P. Kramer[25], M.W. Krasny[129], A. Krasznahorkay[104], A. C. Kraus[117], J.W. Kraus[176], J.A. Kremer[48], N. B. Krengel[146], T. Kresse[50], L. Kretschmann[176], J. Kretzschmar[93], P. Krieger[160], K. Krizka[21], K. Kroeninger[49], H. Kroha[111], J. Kroll[133], J. Kroll[130], K.S. Krowpman[108], U. Kruchonak[39], H. Krüger[25], N.M. Hartmann[110],

JHEP05(2026)183

N. Krumnack[80], M.C. Kruse[51], O. Kuchinskaia[39], S. Kuday[3a], S. Kuehn[37], T. Kuhl[48], V. Kukhtin[39], S. Kuleshov[139d,139b], J. Kull[1], E. V. Kumar[110], M. Kumar[34j], N. Kumari[48], P. Kumari[161b], A. Kupco[133], A. Kupich[38], O. Kuprash[54], H. Kurashige[85], L.L. Kurchaninov[161a], O. Kurdysh[4], A. Kurova[38], R. Kuesters[54], M. Kuze[140], A.K. Kvam[104], J. Kvita[124], N.G. Kyriacou[141], M. Laassiri[30], C. Lacasta[168], F. Lacava[75a,75b], H. Lacker[19], D. Lacour[129], E. Ladygin[39], A. Lafarge[41], B. Laforge[129], T. Lagouri[177], F.Z. Lahbabi[36a], S. Lai[55,37], W. S. Lai[97], I.K. Lakomiec[55], J.E. Lambert[170], S. Lammers[68], W. Lampl[7], C. Lampoudis[157], G. Lamprinoudis[171], A.N. Lancaster[117], U. Landgraf[54], M.P.J. Landon[95], V.S. Lang[54], A.J. Lankford[164], F. Lanni[37], C. S. Lantz[167], K. Lantzsch[25], A. Lanza[73a], M. Lanzac Berrocal[168], T. Lari[71a], D. Larsen[17], L. Larson[11], F. Lasagni Manghi[24b], M. Lassnig[37], S.D. Lawlor[144], R. Lazaridou[164], M. Lazzaroni[71a,71b], E. T. T. Le[164], H. D. M. Le[108], E.M. Le Boulicaut[177], L.T. Le Pottier[18a], B. Leban[24b,24a], F. Ledroit-Guillon[60], T.F. Lee[161b], L.L. Leeuw[34h], M. Lefebvre[170], C. Leggett[18a], G. Lehmann Miotto[37], M. Leigh[56], W.A. Leight[104], W. Leinonen[115], A. Leisos[157,aa], C.E. Leitgeb[19], R. Leitner[135], K.J.C. Leney[45], T. Lenz[25], S. Leone[74a], C. Leonidopoulos[52], A. Leopold[149], J.H. Lepage Bourbonnais[35], R. Les[108], C.G. Lester[33], M. Levchenko[38], J. Levêque[4], L.J. Levinson[174], G. Levrini[24b,24a], M.P. Lewicki[87], C. Lewis[141], D.J. Lewis[4], L. Lewitt[144], A. Li[30], B. Li[142a], C. Li[107], C-Q. Li[111], H. Li[142a], H. Li[102], H. Li[15], H. Li[62], H. Li[142a], J. Li[143a], L. Li[143a], R. Li[177], S. Li[143b,143a], T. Li[5], Y. Li[14], Z. Li[14,113c], Z. Li[62], S. Liang[14,113c], Z. Liang[14], M. Liberatore[137], B. Liberti[76a], G. B. Libotte[82d], K. Lie[64c], J. Lieber Marin[82e], H. Lien[68], H. Lin[107], S. F. Lin[150], L. Linden[110], R.E. Lindley[7], J.H. Lindon[37], J. Ling[61], E. Lipeles[130], A. Lipniacka[17], M.A.L. Leite[82c], A. Lister[169], J.D. Little[68], B. Liu[14], B.X. Liu[113b], D. Liu[155], D. Liu[138], E. H. L. Liu[21], J.K.K. Liu[119], K. Liu[143b], K. Liu[143b], M. Liu[62], M.Y. Liu[62], P. Liu[142a], Q. Liu[148], S. Liu[150], X. Liu[142a], Y. Liu[113b,113c], Y. Liu[167], Y.L. Liu[142a], Y.W. Liu[62], Z. Liu[66,ab], S.L. Lloyd[95], E.M. Lobodzinska[48], P. Loch[7], E. Lodhi[160], G. Löschcke Centeno[4], K. Lohwasser[144], E. Loiacono[48], J. D. Lomas[21], I. Longarini[164], R. Longo[167], A. Lopez Solis[13], N.A. Lopez-canelas[7], N. Lorenzo Martinez[4], A.M. Lory[110], M. Losada[118a], X. Lou[47a,47b], X. Lou[14,113c], P.A. Love[92], M. Lu[66], S. Lu[130], Y.J. Lu[153], H.J. Lubatti[141], C. Luci[75a,75b], F.L. Lucio Alves[113a], F. Luehring[68], B. S. Lunday[130], O. Lundberg[149], J. Lunde[37], N.A. Luongo[6], M.S. Lutz[170], A.B. Lux[26], D. Lynn[30], R. Lysak[133], V. Lysenko[134], E. Lytken[99], V. Lyubushkin[39], T. Lyubushkina[39], M.M. Lyukova[150], H. Ma[30], K. Ma[62], L.L. Ma[142a], W. Ma[62], Y. Ma[123], J.C. MacDonald[101], B. Maček[94], P.C. Machado De Abreu Farias[82e], D. Macina[37], R. Madar[41], T. Madula[97], J. Maeda[85], T. Maeno[30], P.T. Mafa[34f], H. Maguire[144], M. Maheshwari[33], V. Maiboroda[66], A. Maio[132a,132b,132d], K. Maj[86a], O. Majersky[48], S. Majewski[125], R. Makhmanazarov[38], N. Makovec[66], V. Maksimovic[16], B. Malaescu[129], J. Malamant[127], Pa. Malecki[87], V.P. Maleev[38], F. Malek[60,ac], M. Mali[94], D. Malito[96], A. Maloizel[5], A. Malvezzi Lopes[82d], S. Malyukov[39], J. Mamuzic[94], G. Mancini[53], M. N. Mancini[27], G. Manco[73a,73b], S.S. Mandarry[151], I. Mandić[94], L. Manhaes de Andrade Filho[82a], I.M. Maniatis[174], J. Manjarres Ramos[90], D.C. Mankad[174], A. Mann[110], T. Manoussos[37], M.N. Mantinan[40], S. Manzoni[37], L. Mao[143a],

JHEP05(2026)183

X. Mapekula[34c], A. Marantis[157], G. Marchiori[5], C. Marcon[71a], E. Maricic[16], M. Marinescu[48], S. Marium[48], M. Marjanovic[122], A. Markhoos[54], M. Markovitch[66], M. K. Maroun[104], M. C. Marr[147], T. L. Marsault[137], G. T. Marsden[102], E.J. Marshall[92], Z. Marshall[18a], S. Marti-Garcia[168], J. Martin[97], T.A. Martin[136], V.J. Martin[52], B. Martin dit Latour[17], S. Martin-Haugh[136], L. Martinelli[75a,75b], P. Martinez Agullo[168], V.I. Martinez Outschoorn[104], P. Martinez Suarez[37], G. Martinovicova[135], V.S. Martoiu[28b], A.C. Martyniuk[97], A. Marzin[37], D. Mascione[78a,78b], L. Masetti[101], J. Masik[102], A.L. Maslennikov[39], S.L. Mason[42], P. Massarotti[72a,72b], P. Mastrandrea[74a,74b], A. Mastroberardino[44b,44a], T. Masubuchi[126], T.T. Mathew[125], G. Pinheiro Matos[42], J. Matousek[135], D.M. Mattern[49], K. Mauer[48], J. Maurer[28b], T. Maurin[59], A.J. Maury[66], C. Mavungu Tsava[103], D.A. Maximov[38], A. E. May[102], E. Mayer[41], R. Mazini[34j], S.M. Mazza[138], E. Mazzeo[37], R.P. McGovern[130], J.P. Mc Gowan[170], S.P. Mc Kee[107], C.C. McCracken[169], E.F. McDonald[106], L. F. Mcelhinney[92], J.A. Mcfayden[151], R.P. Mckenzie[34j], D.J. Mclaughlin[97], S.J. McMahon[136], C.M. Mcpartland[93], R.A. McPherson[170,n], S. Mehlhase[110], A. Mehta[93], D. Melini[168], B.R. Mellado Garcia[34j], A.H. Melo[55], F. Meloni[48], A.M. Mendes Jacques Da Costa[102], J.G. Saraiva[132a,132d], L. Meng[92], S. Menke[111], M. Mentink[37], E. Meoni[44b,44a], G. Mercado[117], S. Merianos[157], C. Merlassino[69a,69c], C. Meroni[71a,71b], J. Metcalfe[6], A.S. Mete[6], E. Meuser[101], C. Meyer[68], J-P. Meyer[137], Y. Miao[113a], R.P. Middleton[136], M. Mihovilovic[66], K. Petukhova[37], L. Mijović[52], G. Mikenberg[174], M. Mikestikova[133], M. Mikuž[94], H. Mildner[101], A. Milic[37], D.W. Miller[40], E. H. Miller[148], A. Milov[174], D.A. Milstead[47a,47b], T. Min[113a], A.A. Minaenko[38], I.A. Minashvili[154b], A.I. Mincer[119], B. Mindur[86a], M. Mineev[39], Y. Mino[88], L.M. Mir[13], M. Miralles Lopez[59], M. Mironova[18a], M. Missio[41], A. Mitra[172], V.A. Mitsou[168], Y. Mitsumori[112], P.S. Miyagawa[95], T. Mkrtchyan[37], M. Mlinarevic[97], T. Mlinarevic[97], M. Mlynarikova[135], L. Mlynarska[86a], C. Mo[143a], S. Mobius[20], M. H. Mohamed Farook[114], S. Mohapatra[42], S. Mohiuddin[123], G. Mokgatitswane[34j], L. Moleri[174], U. Molinatti[128], L.G. Mollier[20], B. Mondal[133], S. Mondal[135], K. Mönig[48], E. Monnier[103], L. Monsonis Romero[168], A. Montella[47a,47b], M. Montella[121], F. Montereali[77a,77b], F. Monticelli[91], S. Monzani[69a,69c], R. Gonçalo[132a], A. Morancho Tarda[43], N. Morange[66], M. Moreno Llácer[168], C. Moreno Martinez[56], J.M. Moreno Perez[23b], P. Morettini[57b], S. Morgenstern[37], M. Morii[61], M. Morinaga[158], F. Morodei[75a,75b], P. Moschovakos[37], B. Moser[54], M. Mosidze[154b], T. Moskalets[45], P. Moskvitina[115], J. Moss[32], T. Motta Quirino[82d], A. Moussa[36d], Y. Moyal[174], H. Moyano Gomez[13], E.J.W. Moyse[104], T.G. Mroz[87], S. Muanza[103], M. Mucha[25], J. Mueller[131], R. Müller[37], G.A. Mullier[166], A.J. Mullin[33], J.J. Mullin[51], A.C. Mullins[45], A.E. Mulski[61], D.P. Mungo[160], D. Munoz Perez[168], F.J. Munoz Sanchez[102], W.J. Murray[172,136], E. Musajan[62], M. Muškinja[94], C. Mwewa[48], A.G. Myagkov[38,p], A.J. Myers[8], G. Myers[107], M. Myska[134], B.P. Nachman[148], K. Nagai[128], K. Nagano[83], R. Nagasaka[158], J.L. Nagle[30,ad], E. Nagy[103], A.M. Nairz[37], K. Nakamura[83], K. Nakkalil[5], A. Nandi[63b], H. Nanjo[126], E.A. Narayanan[45], Y. Narukawa[158], I. Naryshkin[38], L. Nasella[71a,71b], S. Nasri[118b], C. Nass[25], G. Navarro[23a], A. Nayaz[19], P.Y. Nechaeva[38], S. Nechaeva[24b,24a], F. Nechansky[133], L. Nedic[128], A. Negri[73a,73b], M. Negrini[24b], C. Nellist[116], C. Nelson[105], K. Nelson[107], S. Nemecek[133], M. Nessi[37,ae],

JHEP05(2026)183

M.S. Neubauer[167], J. Newell[93], P.R. Newman[21], Y.W.Y. Ng[167], B. Ngair[118a], H.D.N. Nguyen[109], J.D. Nichols[122], R.B. Nickerson[128], J. Nielsen[138], M. Niemeyer[55], J. Niermann[37], N. Nikiforou[37], V. Nikolaenko[38,p], R. Nicolaidou[137], I. Nikolic-Audit[129], P. Nilsson[30], G. Ninio[156], A. Nisati[75a], R. Nisius[111], N. Nitika[174], E.K. Nkadimeng[34b], T. Nobe[158], D. Noll[148], T. Nommensen[152], M.B. Norfolk[144], B.J. Norman[35], L.C. Nosler[18a], M. Noury[36a], J. Novak[94], T. Novak[94], P. Novotny[174], R. Novotny[134], L. Nozka[124], K. Ntekas[164], D. Ntounis[148], N.M.J. Nunes De Moura Junior[82b], A.P. O'Neill[20], J. Ocariz[129], I. Ochoa[132a], A. Odella Rodriguez[13], J.T. Offermann[40], A. Ogrodnik[87], A. Oh[102], C.C. Ohm[149], H. Oide[83], M.L. Ojeda[37], Y. Okumura[158], I. Oleksiyuk[56], G. Oliveira Correa[13], D. Oliveira Damazio[30], J.L. Oliver[1], R. Omar[68], Ö.O. Öncel[54], A. Onofre[132a,132e,af], P.U.E. Onyisi[11], S. Oerdek[48,ag], M.J. Oreglia[40], D. Orestano[77a,77b], R. Orlandini[77a,77b], R.S. Orr[160], L.M. Osojnak[42], Y. Osumi[112], G. Otero y Garzon[31], H. Otono[89], M. Ouchrif[36d], F. Ould-Saada[127], T. Ovsiannikova[141], M. Owen[59], R.E. Owen[136], V.E. Ozcan[22a], F. Ozturk[87], N. Ozturk[8], S. Ozturk[81], H.A. Pacey[128], K. Pachal[161a], A. Pacheco Pages[13], C. Padilla Aranda[13], G. Padovano[75a,75b], S. Pagan Griso[18a], J. Pampel[25], J. Pan[177], D.K. Panchal[11], C.E. Pandini[60], J.G. Panduro Vazquez[136], H.D. Pandya[1], H. Pang[137], P. Pani[48], G. Panizzo[69a,69c], L. Panwar[129], L. Paolozzi[56], S. Parajuli[167], A. Paramonov[6], C. Paraskevopoulos[53], D. Paredes Hernandez[64b], S.R. Paredes Saenz[52], A. Pareti[73a,73b], K.R. Park[42], T.H. Park[111], F. Parodi[57b,57a], J.A. Parsons[42], U. Parzefall[54], B. Pascual Dias[41], L. Pascual Dominguez[100], E. Pasqualucci[75a], S. Passaggio[57b], F. Pastore[96], P. Patel[87], U.M. Patel[51], J.R. Pater[102], T. Pauly[37], F. Pauwels[135], C.I. Pazos[163], M. Pedersen[127], R. Pedro[132a], A.P. Pereira Peixoto[141], S.V. Peleganchuk[38], O. Penc[133], S. Peng[15], G. D. Penn[177], K.E. Penski[110], M. Penzin[38], B.C. Pinheiro Pereira[132a], L. Pereira Sanchez[148], D.V. Perepelitsa[30,ad], G. Perera[104], E. Perez Codina[37], M. Perganti[10], H. Pernegger[37], S. Perrella[75a,75b], K. Peters[48], R.F.Y. Peters[102], B.A. Petersen[37], T.C. Petersen[43], E. Petit[103], V. Petousis[134], A. R. Petri[71a,71b], T. Petru[135], M. Pettee[18a], A. Petukhov[81], R. Pezoa[139g], L. Pezzotti[24b,24a], G. Pezzullo[177], L. Pfaffenbichler[37], A. J. Pfleger[79], T.M. Pham[175], T. Pham[106], P.W. Phillips[136], G. Piacquadio[150], E. Pianori[18a], F. Piazza[125], R. Piegaia[31], D. Pietreanu[28b], A.D. Pilkington[102], M. Pinamonti[69a,69c], J.L. Pinfold[2], J. Pinol Bel[13], A. E. Pinto Pinoargote[129], L. Pintucci[69a,69c], K. M. Piper[151], A. Pirttikoski[56], D.A. Pizzi[35], L. Pizzimento[64b], A. Plebani[33], M.-A. Pleier[30], V. Pleskot[135], E. Plotnikova[39], G. Poddar[95], L. Poggioli[129], S. Polacek[135], G. Polesello[73a], A. Poley[147], A. Polini[24b], C.S. Pollard[172], Z.B. Pollock[121], E. Pompa Pacchi[122], N. I. Pond[97], D. Ponomarenko[68], L. Pontecorvo[37], S. Popa[28a], G.A. Popeneciu[28d], A. Poreba[37], D.M. Portillo Quintero[161a], S. Pospisil[134], M. A. Postill[144], P. Postolache[28c], K. Potamianos[172], P.A. Potepa[86a], I.N. Potrap[39], C.J. Potter[33], R. Poettgen[99], H. Potti[152], J. Poveda[168], M.E. Pozo Astigarraga[37], R. Pozzi[37], A. Prades Ibanez[76a,76b], S.R. Pradhan[144], J. Pretel[170], D. Price[102], M. Primavera[70a], L. Primomo[69a,69c], M.A. Principe Martin[100], R. Privara[124], T. Procter[86b], M.L. Proffitt[141], N. Proklova[130], K. Prokofiev[64c], G. Proto[111], J. Proudfoot[6], M. Przybycien[86a], W.W. Przygoda[86b], A. Psallidas[46], J.E. Puddefoot[144], D. Pudzha[53], E. Egidio Purcino De Souza[82e],

JHEP05(2026)183

H. I. Purnell[1], D. Pyatiizbyantseva[115], J. Qian[107], R. Qian[108], Y. Qin[13], T. Qiu[52], A. Quadt[55], M. Queitsch-Maitland[102], G. Quetant[56], R.P. Quinn[169], G. Rabanal Bolanos[61], D. Rafanoharana[111], F. Raffaeli[76a,76b], J.L. Rainbolt[40], S. Rajagopalan[30], E. Ramakoti[39], L. Rambelli[57b,57a], I.A. Ramirez-Berend[35], K. Ran[107,113c], D. S. Rankin[130], N.P. Rapheeha[34j], H. Rasheed[28b], A. Rastogi[18a], S. Rave[101], S. Ravera[57b,57a], B. Ravina[37], I. Ravinovich[174], M. Raymond[37], A.L. Read[127], N.P. Readioff[144], D.M. Rebuzzi[73a,73b], A. S. Reed[59], K. Reeves[27], D. Reikher[37], A. Rej[49], C. Rembser[37], H. Ren[62], M. Renda[28b], F. Renner[48], A.G. Rennie[59], M. Repik[56], A.L. Rescia[57b,57a], S. Resconi[71a], M. Ressegotti[57b,57a], S. Rettie[116], W.F. Rettie[35], M. M. Revering[33], O.L. Rezanova[39], P. Reznicek[135], H. Riani[36d], N. Ribaric[51], B. Ricci[69a,69c], E. Ricci[78a,78b], R. Richter[111], S. Richter[47a,47b], E. Richter-Was[86b], M. Ridel[129], S. Ridouani[36d], P. Rieck[119], P. Riedler[37], E.M. Riefel[47a,47b], J. O. Rieger[116], M. Rimoldi[34c], L. Rinaldi[24b,24a], P. Rincke[166,55], G. Ripellino[166], I. Riu[13], J.C. Rivera Vergara[170], F. Rizatdinova[123], E. Rizvi[95], B.R. Roberts[40], S.S. Roberts[138], D. Robinson[33], A. Robson[59], A. Rocchi[76a,76b], C. Roda[74a,74b], F.A. Rodriguez[117], S. Rodriguez Bosca[37], Y. Rodriguez Garcia[23a], A.M. Rodríguez Vera[117], S. Roe[37], J.T. Roemer[37], O. Røhne[127], R.A. Rojas[37], C.P.A. Roland[129], A. Romaniouk[79], E. Romano[73a,73b], M. Romano[24b], A.C. Romero Hernandez[167], N. Rompotis[93], L. Roos[129], S. Rosati[75a], B.J. Rosser[40], E. Rossi[128], E. Rossi[72a,72b], L.P. Rossi[61], L. Rossini[54], R. Rosten[121], M. Rotaru[28b], D. Rousseau[66], D. Rousso[48], S. Roy-Garand[160], A. Rozanov[103], Z. M. A. Rozario[59], Y. Rozen[155], A. Rubio Jimenez[168], V.H. Ruelas Rivera[19], T.A. Ruggeri[1], A. Ruggiero[128], A. Ruiz-Martinez[168], A. Rummler[37], G.B. Rupnik Boero[37], Z. Rurikova[54], N.A. Rusakovich[39], S. Ruscelli[49], H.L. Russell[170], G. Russo[75a,75b], J.P. Rutherfoord[7], S. Rutherford Colmenares[119], M. Rybar[135], P. Rybczynski[86a], A. Ryzhov[45], F. Safai Tehrani[75a], S. Saha[1], B. Sahoo[174], A. Saibel[168], B. T. Saifuddin[122], M. Saimpert[137], G.T. Saito[82c], M. Saito[158], T. Saito[158], A. Sala[71a,71b], A. Salnikov[148], J. Salt[168], A. Salvador Salas[156], F. Salvatore[151], A. Salzburger[37], D. Sammel[54], E. Sampson[92], D. Sampsonidis[157,z], D. Sampsonidou[125], M.A.A. Samy[59], J. Sánchez[168], V. Sanchez Sebastian[168], H. Sandaker[127], C.O. Sander[48], J.A. Sandesara[175], M. Sandhoff[176], C. Sandoval[23b], L. Sanfilippo[63a], D.P.C. Sankey[136], T. Sano[88], A. Sansoni[53], M. Santana Queiroz[18b], L. Santi[37], A.S. Cerqueira[82a], C. Santoni[41], H. Santos[132a,132b], E. Sanzani[24b,24a], K.A. Saoucha[84b], J. Sardain[7], A.M. Cooper-Sarkar[128], O. Sasaki[83], K. Sato[162], C. Sauer[37], E. Sauvan[4], P. Savard[160,t], R. Sawada[158], C. Sawyer[136], L. Sawyer[98], A. M. Sayed[27], C. Sbarra[24b], A. Sbrizzi[24b,24a], T. Scanlon[97], J. Schaarschmidt[141], U. Schäfer[101], A.C. Schaffer[66,45], D. Schaile[110], R.D. Schamberger[150], C. Scharf[19], M.M. Schefer[20], D. Scheirich[135], M. Schernau[139f], C. Scheulen[56], C. Schiavi[57b,57a], R. Brener[174], M. Schioppa[44b,44a], B. Schlag[148], S. Schlenker[37], J. Schmeing[176], E. Schmidt[111], M. A. Schmidt[176], K. Schmieden[25], C. Schmitt[101], N. Schmitt[101], S. Schmitt[48], N.A. Schneider[110], L. Schoeffel[137], A. Schoening[63b], P.G. Scholer[35], E. Schopf[146], M. Schott[25], S. Schramm[56], T. Schroer[56], H-C. Schultz-Coulon[63a], M. Schumacher[54], B.A. Schumm[138], Ph. Schune[137], H.R. Schwartz[7], A. Schwartzman[148], T.A. Schwarz[107], Ph. Schwemling[137], R. Schwienhorst[108], F.G. Sciacca[20], A. Sciandra[30], G. Sciolla[27], S. A. Scoville[131],

JHEP05(2026)183

F. Scuri[74a], L.F. Oleiro Seabra[132a], C.D. Sebastiani[37], K. Sedlaczek[117], S.C. Seidel[114], B.D. Seidlitz[42], C. Seitz[48], J.M. Seixas[82b], G. Sekhniaidze[72a], L. Selem[129], N. Semprini-Cesari[24b,24a], A. Semushin[178], D. Sengupta[56], V. Senthilkumar[168], L. Serin[66], M. Sessa[72a,72b], H. Severini[122], F. Sforza[57b,57a], A. Sfyrla[56], Q. Sha[14], H. Shaddix[117], A.H. Shah[33], R. Shaheen[149], J.D. Shahinian[130], M. Shamim[37], L.Y. Shan[14], M. Shapiro[18a], A. Sharma[37], A.S. Sharma[169], P. Sharma[30], P.B. Shatalov[38], K. Shaw[151], S.M. Shaw[102], G.A. Chelkov[39,p], Q. Shen[14], D.J. Sheppard[147], P. Sherwood[97], L. Shi[97], X. Shi[14], S. Shimizu[83], I.P.J. Shipsey[128,†], S. Shirabe[89], M. Shiyakova[39,ah], M.J. Shochet[40], D.R. Shope[127], B. Shrestha[122], S. Shrestha[121,ai], I. Shreyber[39], M.J. Shroff[105], P. Sicho[133], A.M. Sickles[167], E. Sideras Haddad[34j,165], A. C. Sidley[116], A. Sidoti[24b], F. Siegert[50], Dj. Sijacki[16], F. Sili[62], I. Silva Ferreira[82b], M.V. Silva Oliveira[30], S.B. Silverstein[47a], E. Furtado De Simas Filho[82e], S. Simion[66], R. Simoniello[37], E.L. Simpson[102], H. Simpson[151], L.R. Simpson[6], S. Simsek[81], S. Sindhu[55], S. N. Singh[27], S. Singh[30], S. Sinha[48], S. Sinha[102], M. Sioli[24b,24a], K. Sioulas[9], I. Siral[37], E. Sitnikova[48], J. Sjölin[47a,47b], A. Skaf[55], E. Skorda[21], P. Skubic[122], M. Slawinska[87], I. Slazyk[17], I. Sliusar[127], V. Smakhtin[174], B.H. Smart[136], S.Yu. Smirnov[139b], Y. Smirnov[34c], L.N. Smirnova[38,p], O. Smirnova[99], A.C. Smith[42], J.L. Smith[102], M. B. Smith[35], R. Smith[148], H. Smitmanns[101], M. Smizanska[92], K. Smolek[134], P. Smolyanskiy[134], A.A. Snesarev[39], H.L. Snoek[116], R. M. Snyder[51], S. Snyder[30], M.F. Mohd Soberi[52], R. Sobie[170,n], A. Soffer[156], C.A. Solans Sanchez[37], E.Yu. Soldatov[39], U. Soldevila[168], A.A. Solodkov[34j], S. Solomon[27], A. Soloshenko[39], K. Solovieva[54], O.V. Solovyanov[41], P. Sommer[50], A. Sonay[13], A. Sopczak[134], A.L. Sopio[52], F. Sopkova[29b], J. D. Sorenson[114], I.R. Sotarriva Alvarez[140], V. Sothilingam[63a], O. J. Soto Sandoval[139c,139b], B.S. Peralva[82d], S. Sottocornola[68], R. Soualah[84a], Z. Soumaimi[36e], M.J. Da Cunha Sargedas De Sousa[57b,57a], D. South[48], N. Soybelman[174], S. Spagnolo[70a,70b], D. Sperlich[54], B. Spisso[72a,72b], L. Splendori[103], M. Spousta[135], E.J. Staats[35], R. Stamen[63a], E. Stanecka[87], W. Stanek-Maslouska[48], M.V. Stange[50], B. Stanislaus[18a], M.M. Stanitzki[48], E.A. Starchenko[38], G.H. Stark[138], J. Stark[90], P. Staroba[133], P. Starovoitov[84b], R. Staszewski[87], C. Stauch[110], G. Stavropoulos[46], A. Stefl[37], A. Stein[101], P. Steinberg[30], B. Stelzer[147,161a], H.J. Stelzer[131], O. Stelzer[161a], H. Stenzel[58], T.J. Stevenson[151], G.A. Stewart[37], G. Stoicea[28b], M. Stolarski[132a], S. Stonjek[111], A. Straessner[50], J. Strandberg[149], S. Strandberg[47a,47b], M. Stratmann[176], M. Strauss[122], T. Strebler[103], P. Strizenec[29b], R. Ströhmer[171], D.M. Strom[125], R. Stroynowski[45], A. Strubig[47a,47b], S.A. Stucci[30], B. Stugu[17], J. Stupak[122], N.A. Styles[48], D. Su[148], S. Su[62], X. Su[62], D. Suchy[29a], A. D. Sudhakar Ponnu[55], L. Sudit[174], K. Sugizaki[130], V.V. Sulin[38], D.M.S. Sultan[128], L. Sultanaliyeva[25], S. Sultansoy[3b], S. Sun[175], W. Sun[14], S. Sundar Raman[169], N. Sur[99], N. Suri Jr[177], M.R. Sutton[151], M. Svatos[133], P. N. Swallow[33], M. Swiatlowski[161a], A. Swoboda[37], I. Sykora[29a], M. Sykora[135], T. Sykora[135], D. Ta[101], K. Tackmann[48,ag], A. Taffard[164], R. Tafirout[161a], Y. Takubo[83], N. Hod[174], M. Talby[103], A.A. Talyshev[38], N.M. Tamir[156], A. Tanaka[158], J. Tanaka[158], R. Tanaka[66], M. Tanasini[150], Z. Tao[142a], Z. Tao[169], S. Tapia Araya[139g], S. Tapprogge[101], A. Tarek Abouelfadl Mohamed[37], S. Tarem[155], K. Tariq[14], G. Tarna[37], G.F. Tartarelli[71a], M. J. Tartarin[90], P. Tas[135], M. Tasevsky[133],

JHEP05(2026)183

E. Tassi[44b,44a], A.C. Tate[167], Y. Tayalati[36e,aj], G.N. Taylor[106], W. Taylor[161b], R.J. Taylor Vara[168], A.S. Tegetmeier[90], P. Teixeira-Dias[96], J.J. Teoh[160], K. Terashi[158], J. Terron[100], S. Terzo[13], M. Testa[53], R.J. Teuscher[160,n], A. Thaler[79], O. Theiner[56], T. Theveneaux-Pelzer[103], J.P. Thomas[21], E.A. Thompson[18a], P.D. Thompson[21], E. Thomson[130], R. E. Thornberry[45], C. Tian[62], Y. Tian[56], V. Tikhomirov[81], Yu.A. Tikhonov[39], S. Timoshenko[38], D. Timoshyn[135], E.X.L. Ting[1], P. Tipton[177], A. Tishelman-Charny[30], K. Todome[140], S. Todorova-Nova[135], L. Toffolin[69a,69c], M. Togawa[83], J. Tojo[89], S. Tokár[29a], O. Toldaiev[68], G. Tolkachev[103], M. Tomoto[83], L. Tompkins[148], E. Torrence[125], H. Torres[90], D. I. Torres Arza[139g], E. Torró Pastor[168], M. Toscani[31], C. Tosciri[40], M. Tost[11], D.R. Tovey[144], T. Trefzger[171], P.M. Tricarico[13], A. Tricoli[30], I.M. Trigger[161a], S. Trincaz-Duvoid[129], D.A. Trischuk[170], A. Tropina[39], D. Truncali[76a,76b], L. Truong[34c], M. Trzebinski[87], A. Trzupek[87], F. Tsai[150], M. Tsai[107], A. Tsiamis[157], P.V. Tsiareshka[39], S. Tsigaridas[161a], A. Tsirigotis[157,aa], V. Tsiskaridze[154a], E.G. Tskhadadze[154a], Y. Tsujikawa[88], I.I. Tsukerman[38], V. Tsulaia[18a], K. Tsuri[120], D. Tsybychev[150], Y. Tu[64b], A. Tudorache[28b], V. Tudorache[28b], S. B. Tuncay[128], S. Turchikhin[57b,57a], I. Turk Cakir[3a], R. Turra[71a], T. Turtuvshin[39,ak], P.M. Tuts[42], Y. Uematsu[83], F. Ukegawa[162], P.A. Ulloa Poblete[139c,139b], G. Unal[37], A. Undrus[30], J. Urban[29b], P. Urrejola[139e], G. Usai[8], R. Ushioda[159], M. Usman[109], F. Ustuner[52], Z. Uysal[81], V. Vacek[134], B. Vachon[105], T. Vafeiadis[37], A. Vaitkus[97], C. Valderanis[110], E. Valdes Santurio[47a,47b], M. Valente[37], S. Valentinetti[24b,24a], A. Valero[168], E. Valiente Moreno[168], A. Vallier[90], J.A. Valls Ferrer[168], D. R. Van Arneman[116], E.R. Vandewall[148], R. Van Den Broucke[129], A. Van Der Graaf[49], H. Z. Van Der Schyf[34j], P. Van Gemmeren[6], M. Van Rijnbach[37], S. Van Stroud[97], I. Van Vulpen[116], P. Vana[135], M. Vanadia[76a,76b], U. M. Vande Voorde[149], W. Vandelli[37], D. Vannicola[156], L. Vannoli[53], R. Vari[75a], M. Varma[177], E.W. Varnes[7], C. Varni[79], D. Varouchas[66], L. Varriale[168], K.E. Varvell[152], M.E. Vasile[28b], L. Vaslin[83], M. D. Vassilev[148], A. Vasyukov[39], L. M. Vaughan[123], R. Vavricka[135], T. Vazquez Schroeder[13], J. Veatch[32], V. Vecchio[102], M.J. Veen[104], I. Veliscek[30], I. Velkovska[94], L.M. Veloce[160], F. Veloso[132a,132c], A.G. Veltman[52], S. Veneziano[75a], A. Ventura[70a,70b], A. Verbytskyi[111], M. Verducci[74a,74b], C. Vergis[95], M. Verissimo De Araujo[82b], W. Verkerke[116], J.C. Vermeulen[116], C. Vernieri[148], M. Vessella[164], M.C. Vetterli[147,t], A. Vgenopoulos[101], N. Viaux Maira[139g,al], T. Vickey[144], O.E. Vickey Boeriu[144], G.H.A. Viehhauser[128], L. Vigani[63b], M. Vigl[111], M. Villa[24b,24a], M. Villaplana Perez[168], E.M. Villhauer[40], E. Vilucchi[53], M. Vincent[168], M.G. Vincter[35], A. Visibile[116], A. Visive[116], C. Vittori[37], I. Vivarelli[24b,24a], M.I. Vivas Albornoz[48], E. Voevodina[111], F. Vogel[110], J.C. Voigt[50], P. Vokac[134], Yu. Volkotrub[86b], L. Vomberg[25], E. Von Toerne[25], B. Vormwald[37], K. Vorobev[51], M. Vos[168], K. Voss[146], M. Vozak[37], L. Vozdecky[122], N. Vranjes[16], M. Vranjes Milosavljevic[16], M. Vreeswijk[116], N.K. Vu[143b,143a], R. Vuillermet[37], O. Vujinovic[101], I. Vukotic[40], I. K. Vyas[35], J.F. Wack[33], A. Wada[112], S. Wada[162], C. Wagner[148], J.M. Wagner[18a], W. Wagner[176], S. Wahdan[176], H. Wahlberg[91], C. H. Waits[122], J. Walder[136], R. Walker[110], K. Walkingshaw Pass[59], W. Walkowiak[146], A. Wall[130], E.J. Wallin[99], T. Wamorkar[148], K. Wandall-Christensen[168], A. Wang[62], A.Z. Wang[138], C. Wang[48], C. Wang[11], H. Wang[18a], J. Wang[64c], P. Wang[102], P. Wang[97], R. Wang[61], R. Wang[107], R. Wang[6],

JHEP05(2026)183

S.M. Wang[153], S. Wang[14], T. Wang[115], T. Wang[62], W.T. Wang[128], X. Wang[167], X. Wang[143a], X. Wang[48], Y. Wang[150], Y. Wang[114], Z. Wang[107], Z. Wang[143b], Z. Wang[107], C. Wanotayaroj[83], A. Warburton[105], A.L. Warnerbring[146], S. Waterhouse[96], A.T. Watson[21], H. Watson[52], M.F. Watson[21], E. Watton[37], G. Watts[141], B.M. Waugh[97], J. M. Webb[54], C. Weber[30], M.S. Weber[20], C. Wei[62], Y. Wei[54], A.R. Weidberg[128], E.J. Weik[119], J. Weingarten[49], C. Weiser[54], C.J. Wells[48], T. Wenaus[30], T. Wengler[37], N.S. Wenke[111], N. Wermes[25], M. Wessels[63a], A.M. Wharton[92], A.S. White[37], A. White[8], M.J. White[1], D. Whiteson[164], L. Wickremasinghe[126], W. Wiedenmann[175], M. Wielers[136], R. Wierda[149], C. Wiglesworth[43], H.G. Wilkens[37], J. J. H. Wilkinson[33], S. Williams[33], S. Willocq[104], B.J. Wilson[102], D.J. Wilson[102], P.J. Windischhofer[40], F.I. Winkel[31], F. Winklmeier[125], B.T. Winter[54], M. Wittgen[148], M. Wobisch[98], T. Wojtkowski[60], Z. Wolffs[116], J. Wollrath[37], M.W. Wolter[87], H. Wolters[132a,132c], M.C. Wong[138], E.L. Woodward[42], S.D. Worm[48], B.K. Wosiek[87], K.W. Woźniak[87], S. Wozniewski[55], K. Wraight[59], C. Wu[160], C. Wu[21], J. Wu[158], M. Wu[113b], M. Wu[115], S.L. Wu[175], S. Wu[14], X. Wu[62], Y.Q. Wu[160], Y. Wu[62], Z. Wu[4], Z. Wu[113a], J. Wuerzinger[111], T.R. Wyatt[102], B.M. Wynne[52], S. Xella[43], L. Xia[113a], M. Xie[62], A. Xiong[125], D. Xu[14], H. Xu[62], L. Xu[62], R. Xu[130], T. Xu[107], W. Xu[113a], Y. Xu[141], Z. Xu[52], R. Xue[131], B. Yabsley[152], S. Yacoob[11], Y. Yamaguchi[83], E. Yamashita[158], H. Yamauchi[162], T. Yamazaki[18a], Y. Yamazaki[85], S. Yan[59], Z. Yan[104], H.J. Yang[143a,143b], H.T. Yang[62], S. Yang[62], X. Yang[37], X. Yang[14], Y. Yang[158], Y. Yang[62], W-M. Yao[18a], C. L. Yardley[151], J. Ye[14], S. Ye[30], X. Ye[62], Y. Yeh[97], I. Yeletskikh[39], B. Yeo[18b], M.R. Yexley[97], T. P. Yildirim[128], H. Duran Yildiz[3a], K. Yorita[173], C.J.S. Young[37], C. Young[148], I.N.L. Young[59], N.D. Young[125], Y. Yu[62], J. Yuan[14,113c], M. Yuan[107], R. Yuan[143b], L. Yue[97], M. Zaazoua[62], B. Zabinski[87], I. Zahir[36a], A. Zaio[57b,57a], Z.K. Zak[87], T. Zakareishvili[168], S. Zambito[56], J.A. Zamora Saa[139d], J. Zang[158], R. Zanzottera[71a,71b], O. Zaplatilek[134], C. Zeitnitz[176], H. Zeng[14], D.T. Zenger Jr[27], O. Zenin[38], T. Ženiš[29a], S. Zenz[95], D. Zerwas[66], B. Zhang[172], D.F. Zhang[144], G. Zhang[14,am], J. Zhang[142a], J. Zhang[6], L. Zhang[62], L. Zhang[113a], P. Zhang[14,113c], R. Zhang[113a], S. Zhang[90], T. Zhang[158], Y. Zhang[141], Y. Zhang[97], Y. Zhang[62], Y. Zhang[113a], Z. Zhang[18a], Z. Zhang[142a], Z. Zhang[66], H. Zhao[141], T. Zhao[142a], Y. Zhao[35], Z. Zhao[62], Z. Zhao[62], A. Zhemchugov[39], J. Zheng[113a], K. Zheng[167], X. Zheng[62], Z. Zheng[148], D. Zhong[167], B. Zhou[107], B. Zhou[143b], H. Zhou[7], N. Zhou[143a], Y. Zhou[15], Y. Zhou[113a], Y. Zhou[7], J. Zhu[107], X. Zhu[143b], Y. Zhu[143a], X. Zhuang[14], K. Zhukov[68], N.I. Zimine[39], J. Zinsser[63b], M. Ziolkowski[146], L. Živković[16], A. Zoccoli[24b,24a], K. Zoch[61], A. Zografos[37], T.G. Zorbas[144], O. Zormpa[46], L. Zwalinski[37]

[1] *Department of Physics, University of Adelaide, Adelaide, Australia*
[2] *Department of Physics, University of Alberta, Edmonton AB, Canada*
[3a] *Department of Physics, Ankara University, Ankara, Türkiye*
[3b] *Division of Physics, TOBB University of Economics and Technology, Ankara, Türkiye*
[4] *LAPP, Université Savoie Mont Blanc, CNRS/IN2P3, Annecy, France*
[5] *APC, Université Paris Cité, CNRS/IN2P3, Paris, France*
[6] *High Energy Physics Division, Argonne National Laboratory, Argonne IL, United States of America*
[7] *Department of Physics, University of Arizona, Tucson AZ, United States of America*
[8] *Department of Physics, University of Texas at Arlington, Arlington TX, United States of America*

JHEP05(2026)183

[9] Physics Department, National and Kapodistrian University of Athens, Athens, Greece
[10] Physics Department, National Technical University of Athens, Zografou, Greece
[11] Department of Physics, University of Texas at Austin, Austin TX, United States of America
[12] Institute of Physics, Azerbaijan Academy of Sciences, Baku, Azerbaijan
[13] Institut de Física d'Altes Energies (IFAE), Barcelona Institute of Science and Technology, Barcelona, Spain
[14] Institute of High Energy Physics, Chinese Academy of Sciences, Beijing, China
[15] Physics Department, Tsinghua University, Beijing, China
[16] Institute of Physics, University of Belgrade, Belgrade, Serbia
[17] Department for Physics and Technology, University of Bergen, Bergen, Norway
[18a] Physics Division, Lawrence Berkeley National Laboratory, Berkeley CA, United States of America
[18b] University of California, Berkeley CA, United States of America
[19] Institut für Physik, Humboldt Universität zu Berlin, Berlin, Germany
[20] Albert Einstein Center for Fundamental Physics and Laboratory for High Energy Physics, University of Bern, Bern, Switzerland
[21] School of Physics and Astronomy, University of Birmingham, Birmingham, United Kingdom
[22a] Department of Physics, Bogazici University, Istanbul, Türkiye
[22b] Department of Physics Engineering, Gaziantep University, Gaziantep, Türkiye
[22c] Department of Physics, Istanbul University, Istanbul, Türkiye
[23a] Facultad de Ciencias y Centro de Investigaciónes, Universidad Antonio Nariño, Bogotá, Colombia
[23b] Departamento de Física, Universidad Nacional de Colombia, Bogotá, Colombia
[24a] Dipartimento di Fisica e Astronomia A. Righi, Università di Bologna, Bologna, Italy
[24b] INFN Sezione di Bologna, Italy
[25] Physikalisches Institut, Universität Bonn, Bonn, Germany
[26] Department of Physics, Boston University, Boston MA, United States of America
[27] Department of Physics, Brandeis University, Waltham MA, United States of America
[28a] Transilvania University of Brasov, Brasov, Romania
[28b] Horia Hulubei National Institute of Physics and Nuclear Engineering, Bucharest, Romania
[28c] Department of Physics, Alexandru Ioan Cuza University of Iasi, Iasi, Romania
[28d] National Institute for Research and Development of Isotopic and Molecular Technologies, Physics Department, Cluj-Napoca, Romania
[28e] National University of Science and Technology Politechnica, Bucharest, Romania
[28f] West University in Timisoara, Timisoara, Romania
[28g] Faculty of Physics, University of Bucharest, Bucharest, Romania
[29a] Faculty of Mathematics, Physics and Informatics, Comenius University, Bratislava, Slovak Republic
[29b] Department of Subnuclear Physics, Institute of Experimental Physics of the Slovak Academy of Sciences, Kosice, Slovak Republic
[30] Physics Department, Brookhaven National Laboratory, Upton NY, United States of America
[31] Universidad de Buenos Aires, Facultad de Ciencias Exactas y Naturales, Departamento de Física, y CONICET, Instituto de Física de Buenos Aires (IFIBA), Buenos Aires, Argentina
[32] California State University, CA, United States of America
[33] Cavendish Laboratory, University of Cambridge, Cambridge, United Kingdom
[34a] Department of Physics, University of Cape Town, Cape Town, South Africa
[34b] iThemba Labs, Western Cape, South Africa
[34c] Department of Mechanical Engineering Science, University of Johannesburg, Johannesburg, South Africa
[34d] National Institute of Physics, University of the Philippines Diliman (Philippines), Philippines
[34e] Department of Physics, Stellenbosch University, Matieland, South Africa
[34f] University of KwaZulu-Natal, School of Agriculture and Science, Mathematics, Westville, South Africa
[34g] University of South Africa, Department of Physics, Pretoria, South Africa
[34h] University of Pretoria, Department of Mechanical and Aeronautical Engineering, Pretoria, South Africa
[34i] University of Zululand, KwaDlangezwa, South Africa
[34j] School of Physics, University of the Witwatersrand, Johannesburg, South Africa
[35] Department of Physics, Carleton University, Ottawa ON, Canada

JHEP05(2026)183

[36a] Faculté des Sciences Ain Chock, Université Hassan II de Casablanca, Morocco
[36b] Faculté des Sciences, Université Ibn-Tofail, Kénitra, Morocco
[36c] Faculté des Sciences Semlalia, Université Cadi Ayyad, LPHEA-Marrakech, Morocco
[36d] LPMR, Faculté des Sciences, Université Mohamed Premier, Oujda, Morocco
[36e] Faculté des sciences, Université Mohammed V, Rabat, Morocco
[36f] Institute of Applied Physics, Mohammed VI Polytechnic University, Ben Guerir, Morocco
[37] CERN, Geneva, Switzerland
[38] Affiliated with an institute formerly covered by a cooperation agreement with CERN
[39] Affiliated with an international laboratory covered by a cooperation agreement with CERN
[40] Enrico Fermi Institute, University of Chicago, Chicago IL, United States of America
[41] LPC, Université Clermont Auvergne, CNRS/IN2P3, Clermont-Ferrand, France
[42] Nevis Laboratory, Columbia University, Irvington NY, United States of America
[43] Niels Bohr Institute, University of Copenhagen, Copenhagen, Denmark
[44a] Dipartimento di Fisica, Università della Calabria, Rende, Italy
[44b] INFN Gruppo Collegato di Cosenza, Laboratori Nazionali di Frascati, Italy
[45] Physics Department, Southern Methodist University, Dallas TX, United States of America
[46] National Centre for Scientific Research "Demokritos", Agia Paraskevi, Greece
[47a] Department of Physics, Stockholm University, Sweden
[47b] Oskar Klein Centre, Stockholm, Sweden
[48] Deutsches Elektronen-Synchrotron DESY, Hamburg and Zeuthen, Germany
[49] Fakultät Physik, Technische Universität Dortmund, Dortmund, Germany
[50] Institut für Kern- und Teilchenphysik, Technische Universität Dresden, Dresden, Germany
[51] Department of Physics, Duke University, Durham NC, United States of America
[52] SUPA — School of Physics and Astronomy, University of Edinburgh, Edinburgh, United Kingdom
[53] INFN e Laboratori Nazionali di Frascati, Frascati, Italy
[54] Physikalisches Institut, Albert-Ludwigs-Universität Freiburg, Freiburg, Germany
[55] II. Physikalisches Institut, Georg-August-Universität Göttingen, Göttingen, Germany
[56] Département de Physique Nucléaire et Corpusculaire, Université de Genève, Genève, Switzerland
[57a] Dipartimento di Fisica, Università di Genova, Genova, Italy
[57b] INFN Sezione di Genova, Italy
[58] II. Physikalisches Institut, Justus-Liebig-Universität Giessen, Giessen, Germany
[59] SUPA — School of Physics and Astronomy, University of Glasgow, Glasgow, United Kingdom
[60] LPSC, Université Grenoble Alpes, CNRS/IN2P3, Grenoble INP, Grenoble, France
[61] Laboratory for Particle Physics and Cosmology, Harvard University, Cambridge MA, United States of America
[62] Department of Modern Physics and State Key Laboratory of Particle Detection and Electronics, University of Science and Technology of China, Hefei, China
[63a] Kirchhoff-Institut für Physik, Ruprecht-Karls-Universität Heidelberg, Heidelberg, Germany
[63b] Physikalisches Institut, Ruprecht-Karls-Universität Heidelberg, Heidelberg, Germany
[64a] Department of Physics, Chinese University of Hong Kong, Shatin, N.T., Hong Kong, China
[64b] Department of Physics, University of Hong Kong, Hong Kong, China
[64c] Department of Physics and Institute for Advanced Study, Hong Kong University of Science and Technology, Clear Water Bay, Kowloon, Hong Kong, China
[65] Department of Physics, National Tsing Hua University, Hsinchu, Taiwan
[66] IJCLab, Université Paris-Saclay, CNRS/IN2P3, 91405, Orsay, France
[67] Centro Nacional de Microelectrónica (IMB-CNM-CSIC), Barcelona, Spain
[68] Department of Physics, Indiana University, Bloomington IN, United States of America
[69a] INFN Gruppo Collegato di Udine, Sezione di Trieste, Udine, Italy
[69b] ICTP, Trieste, Italy
[69c] Dipartimento Politecnico di Ingegneria e Architettura, Università di Udine, Udine, Italy
[70a] INFN Sezione di Lecce, Italy
[70b] Dipartimento di Matematica e Fisica, Università del Salento, Lecce, Italy
[71a] INFN Sezione di Milano, Italy

JHEP05(2026)183

[71b] *Dipartimento di Fisica, Università di Milano, Milano, Italy*
[72a] *INFN Sezione di Napoli, Italy*
[72b] *Dipartimento di Fisica, Università di Napoli, Napoli, Italy*
[73a] *INFN Sezione di Pavia, Italy*
[73b] *Dipartimento di Fisica, Università di Pavia, Pavia, Italy*
[74a] *INFN Sezione di Pisa, Italy*
[74b] *Dipartimento di Fisica E. Fermi, Università di Pisa, Pisa, Italy*
[75a] *INFN Sezione di Roma, Italy*
[75b] *Dipartimento di Fisica, Sapienza Università di Roma, Roma, Italy*
[76a] *INFN Sezione di Roma Tor Vergata, Italy*
[76b] *Dipartimento di Fisica, Università di Roma Tor Vergata, Roma, Italy*
[77a] *INFN Sezione di Roma Tre, Italy*
[77b] *Dipartimento di Matematica e Fisica, Università Roma Tre, Roma, Italy*
[78a] *INFN-TIFPA, Italy*
[78b] *Università degli Studi di Trento, Trento, Italy*
[79] *Universität Innsbruck, Department of Astro and Particle Physics, Innsbruck, Austria*
[80] *Department of Physics and Astronomy, Iowa State University, Ames IA, United States of America*
[81] *Istinye University, Sariyer, Istanbul, Türkiye*
[82a] *Departamento de Engenharia Elétrica, Universidade Federal de Juiz de Fora (UFJF), Juiz de Fora, Brazil*
[82b] *Universidade Federal do Rio De Janeiro COPPE/EE/IF, Rio de Janeiro, Brazil*
[82c] *Instituto de Física, Universidade de São Paulo, São Paulo, Brazil*
[82d] *Rio de Janeiro State University, Rio de Janeiro, Brazil*
[82e] *Federal University of Bahia, Bahia, Brazil*
[83] *KEK, High Energy Accelerator Research Organization, Tsukuba, Japan*
[84a] *Khalifa University of Science and Technology, Abu Dhabi, United Arab Emirates*
[84b] *University of Sharjah, Sharjah, United Arab Emirates*
[85] *Graduate School of Science, Kobe University, Kobe, Japan*
[86a] *AGH University of Krakow, Faculty of Physics and Applied Computer Science, Krakow, Poland*
[86b] *Marian Smoluchowski Institute of Physics, Jagiellonian University, Krakow, Poland*
[87] *Institute of Nuclear Physics Polish Academy of Sciences, Krakow, Poland*
[88] *Faculty of Science, Kyoto University, Kyoto, Japan*
[89] *Research Center for Advanced Particle Physics and Department of Physics, Kyushu University, Fukuoka, Japan*
[90] *L2IT, Université de Toulouse, CNRS/IN2P3, UPS, Toulouse, France*
[91] *Instituto de Física La Plata, Universidad Nacional de La Plata and CONICET, La Plata, Argentina*
[92] *Physics Department, Lancaster University, Lancaster, United Kingdom*
[93] *Oliver Lodge Laboratory, University of Liverpool, Liverpool, United Kingdom*
[94] *Department of Experimental Particle Physics, Jožef Stefan Institute and Department of Physics, University of Ljubljana, Ljubljana, Slovenia*
[95] *Department of Physics and Astronomy, Queen Mary University of London, London, United Kingdom*
[96] *Department of Physics, Royal Holloway University of London, Egham, United Kingdom*
[97] *Department of Physics and Astronomy, University College London, London, United Kingdom*
[98] *Louisiana Tech University, Ruston LA, United States of America*
[99] *Fysiska institutionen, Lunds universitet, Lund, Sweden*
[100] *Departamento de Física Teorica C-15 and CIAFF, Universidad Autónoma de Madrid, Madrid, Spain*
[101] *Institut für Physik, Universität Mainz, Mainz, Germany*
[102] *School of Physics and Astronomy, University of Manchester, Manchester, United Kingdom*
[103] *CPPM, Aix-Marseille Université, CNRS/IN2P3, Marseille, France*
[104] *Department of Physics, University of Massachusetts, Amherst MA, United States of America*
[105] *Department of Physics, McGill University, Montreal QC, Canada*
[106] *School of Physics, University of Melbourne, Victoria, Australia*
[107] *Department of Physics, University of Michigan, Ann Arbor MI, United States of America*

JHEP05(2026)183

[108] Department of Physics and Astronomy, Michigan State University, East Lansing MI, United States of America
[109] Group of Particle Physics, University of Montreal, Montreal QC, Canada
[110] Fakultät für Physik, Ludwig-Maximilians-Universität München, München, Germany
[111] Max-Planck-Institut für Physik (Werner-Heisenberg-Institut), München, Germany
[112] Graduate School of Science and Kobayashi-Maskawa Institute, Nagoya University, Nagoya, Japan
[113a] Department of Physics, Nanjing University, Nanjing, China
[113b] School of Science, Shenzhen Campus of Sun Yat-sen University, China
[113c] University of Chinese Academy of Science (UCAS), Beijing, China
[114] Department of Physics and Astronomy, University of New Mexico, Albuquerque NM, United States of America
[115] Institute for Mathematics, Astrophysics and Particle Physics, Radboud University/Nikhef, Nijmegen, Netherlands
[116] Nikhef National Institute for Subatomic Physics and University of Amsterdam, Amsterdam, Netherlands
[117] Department of Physics, Northern Illinois University, DeKalb IL, United States of America
[118a] New York University Abu Dhabi, Abu Dhabi, United Arab Emirates
[118b] United Arab Emirates University, Al Ain, United Arab Emirates
[119] Department of Physics, New York University, New York NY, United States of America
[120] Ochanomizu University, Otsuka, Bunkyo-ku, Tokyo, Japan
[121] Ohio State University, Columbus OH, United States of America
[122] Homer L. Dodge Department of Physics and Astronomy, University of Oklahoma, Norman OK, United States of America
[123] Department of Physics, Oklahoma State University, Stillwater OK, United States of America
[124] Palacký University, Joint Laboratory of Optics, Olomouc, Czech Republic
[125] Institute for Fundamental Science, University of Oregon, Eugene, OR, United States of America
[126] Graduate School of Science, University of Osaka, Osaka, Japan
[127] Department of Physics, University of Oslo, Oslo, Norway
[128] Department of Physics, Oxford University, Oxford, United Kingdom
[129] LPNHE, Sorbonne Université, Université Paris Cité, CNRS/IN2P3, Paris, France
[130] Department of Physics, University of Pennsylvania, Philadelphia PA, United States of America
[131] Department of Physics and Astronomy, University of Pittsburgh, Pittsburgh PA, United States of America
[132a] Laboratório de Instrumentação e Física Experimental de Partículas — LIP, Lisboa, Portugal
[132b] Departamento de Física, Faculdade de Ciências, Universidade de Lisboa, Lisboa, Portugal
[132c] Departamento de Física, Universidade de Coimbra, Coimbra, Portugal
[132d] Centro de Física Nuclear da Universidade de Lisboa, Lisboa, Portugal
[132e] Departamento de Física, Escola de Ciências, Universidade do Minho, Braga, Portugal
[132f] Departamento de Física Teórica y del Cosmos, Universidad de Granada, Granada (Spain), Spain
[132g] Departamento de Física, Instituto Superior Técnico, Universidade de Lisboa, Lisboa, Portugal
[133] Institute of Physics of the Czech Academy of Sciences, Prague, Czech Republic
[134] Czech Technical University in Prague, Prague, Czech Republic
[135] Charles University, Faculty of Mathematics and Physics, Prague, Czech Republic
[136] Particle Physics Department, Rutherford Appleton Laboratory, Didcot, United Kingdom
[137] IRFU, CEA, Université Paris-Saclay, Gif-sur-Yvette, France
[138] Santa Cruz Institute for Particle Physics, University of California Santa Cruz, Santa Cruz CA, United States of America
[139a] Departamento de Física, Pontificia Universidad Católica de Chile, Santiago, Chile
[139b] Millennium Institute for Subatomic physics at high energy frontier (SAPHIR), Santiago, Chile
[139c] Instituto de Investigación Multidisciplinario en Ciencia y Tecnología, y Departamento de Física, Universidad de La Serena, Chile
[139d] Universidad Andres Bello, Department of Physics, Santiago, Chile
[139e] Universidad San Sebastian, Recoleta, Chile
[139f] Instituto de Alta Investigación, Universidad de Tarapacá, Arica, Chile
[139g] Departamento de Física, Universidad Técnica Federico Santa María, Valparaíso, Chile

JHEP05(2026)183

[140] Department of Physics, Institute of Science, Tokyo, Japan
[141] Department of Physics, University of Washington, Seattle WA, United States of America
[142a] Institute of Frontier and Interdisciplinary Science and Key Laboratory of Particle Physics and Particle Irradiation (MOE), Shandong University, Qingdao, China
[142b] School of Physics, Zhengzhou University, China
[143a] State Key Laboratory of Dark Matter Physics, School of Physics and Astronomy, Shanghai Jiao Tong University, Key Laboratory for Particle Astrophysics and Cosmology (MOE), SKLPPC, Shanghai, China
[143b] State Key Laboratory of Dark Matter Physics, Tsung-Dao Lee Institute, Shanghai Jiao Tong University, Shanghai, China
[144] Department of Physics and Astronomy, University of Sheffield, Sheffield, United Kingdom
[145] Department of Physics, Shinshu University, Nagano, Japan
[146] Department Physik, Universität Siegen, Siegen, Germany
[147] Department of Physics, Simon Fraser University, Burnaby BC, Canada
[148] SLAC National Accelerator Laboratory, Stanford CA, United States of America
[149] Department of Physics, Royal Institute of Technology, Stockholm, Sweden
[150] Departments of Physics and Astronomy, Stony Brook University, Stony Brook NY, United States of America
[151] Department of Physics and Astronomy, University of Sussex, Brighton, United Kingdom
[152] School of Physics, University of Sydney, Sydney, Australia
[153] Institute of Physics, Academia Sinica, Taipei, Taiwan
[154a] E. Andronikashvili Institute of Physics, Iv. Javakhishvili Tbilisi State University, Tbilisi, Georgia
[154b] High Energy Physics Institute, Tbilisi State University, Tbilisi, Georgia
[154c] University of Georgia, Tbilisi, Georgia
[155] Department of Physics, Technion, Israel Institute of Technology, Haifa, Israel
[156] Raymond and Beverly Sackler School of Physics and Astronomy, Tel Aviv University, Tel Aviv, Israel
[157] Department of Physics, Aristotle University of Thessaloniki, Thessaloniki, Greece
[158] International Center for Elementary Particle Physics and Department of Physics, University of Tokyo, Tokyo, Japan
[159] Graduate School of Science and Technology, Tokyo Metropolitan University, Tokyo, Japan
[160] Department of Physics, University of Toronto, Toronto ON, Canada
[161a] TRIUMF, Vancouver BC, Canada
[161b] Department of Physics and Astronomy, York University, Toronto ON, Canada
[162] Division of Physics and Tomonaga Center for the History of the Universe, Faculty of Pure and Applied Sciences, University of Tsukuba, Tsukuba, Japan
[163] Department of Physics and Astronomy, Tufts University, Medford MA, United States of America
[164] Department of Physics and Astronomy, University of California Irvine, Irvine CA, United States of America
[165] University of West Attica, Athens, Greece
[166] Department of Physics and Astronomy, University of Uppsala, Uppsala, Sweden
[167] Department of Physics, University of Illinois, Urbana IL, United States of America
[168] Instituto de Física Corpuscular (IFIC), Centro Mixto Universidad de Valencia — CSIC, Valencia, Spain
[169] Department of Physics, University of British Columbia, Vancouver BC, Canada
[170] Department of Physics and Astronomy, University of Victoria, Victoria BC, Canada
[171] Fakultät für Physik und Astronomie, Julius-Maximilians-Universität Würzburg, Würzburg, Germany
[172] Department of Physics, University of Warwick, Coventry, United Kingdom
[173] Waseda University, Tokyo, Japan
[174] Department of Particle Physics and Astrophysics, Weizmann Institute of Science, Rehovot, Israel
[175] Department of Physics, University of Wisconsin, Madison WI, United States of America
[176] Fakultät für Mathematik und Naturwissenschaften, Fachgruppe Physik, Bergische Universität Wuppertal, Wuppertal, Germany
[177] Department of Physics, Yale University, New Haven CT, United States of America
[178] Yerevan Physics Institute, Yerevan, Armenia

JHEP05(2026)183

[a] Also at Department of Physics, King's College London, London, United Kingdom
[b] Also at Institute of Physics, Azerbaijan Academy of Sciences, Baku, Azerbaijan
[c] Also at Imam Mohammad Ibn Saud Islamic University, Saudi Arabia
[d] Also at Department of Physics, University of Thessaly, Greece
[e] Also at An-Najah National University, Nablus, Palestine
[f] Also at Department of Physics, University of Fribourg, Fribourg, Switzerland
[g] Also at Department of Physics, Westmont College, Santa Barbara, United States of America
[h] Also at Departament de Fisica de la Universitat Autonoma de Barcelona, Barcelona, Spain
[i] Also at Borough of Manhattan Community College, City University of New York, New York NY, United States of America
[j] Also at University of Sienna, Italy
[k] Also at The Collaborative Innovation Center of Quantum Matter (CICQM), Beijing, China
[l] Also at Faculty of Physics, Sofia University, 'St. Kliment Ohridski', Sofia, Bulgaria
[m] Also at Università di Napoli Parthenope, Napoli, Italy
[n] Also at Institute of Particle Physics (IPP), Canada
[o] Also at Department of Physics, Bolu Abant Izzet Baysal University, Bolu, Türkiye
[p] Also at Affiliated with an institute formerly covered by a cooperation agreement with CERN
[q] Also at Faculty of Physics, University of Bucharest, Romania
[r] Also at National Institute of Physics, University of the Philippines Diliman (Philippines), Philippines
[s] Also at Department of Financial and Management Engineering, University of the Aegean, Chios, Greece
[t] Also at TRIUMF, Vancouver BC, Canada
[u] Also at Institucio Catalana de Recerca i Estudis Avancats, ICREA, Barcelona, Spain
[v] Also at Henan University, China
[w] Also at Yeditepe University, Physics Department, Istanbul, Türkiye
[x] Also at Institute of Theoretical Physics, Ilia State University, Tbilisi, Georgia
[y] Also at CERN, Geneva, Switzerland
[z] Also at Center for Interdisciplinary Research and Innovation (CIRI-AUTH), Thessaloniki, Greece
[aa] Also at Hellenic Open University, Patras, Greece
[ab] Also at Department of Modern Physics and State Key Laboratory of Particle Detection and Electronics, University of Science and Technology of China, Hefei, China
[ac] Also at Department of Physics, Stellenbosch University, South Africa
[ad] Also at University of Colorado Boulder, Department of Physics, Colorado, United States of America
[ae] Also at Département de Physique Nucléaire et Corpusculaire, Université de Genève, Genève, Switzerland
[af] Also at Centre of Physics of the Universities of Minho and Porto (CF-UM-UP), Portugal
[ag] Also at Institut für Experimentalphysik, Universität Hamburg, Hamburg, Germany
[ah] Also at Institute for Nuclear Research and Nuclear Energy (INRNE) of the Bulgarian Academy of Sciences, Sofia, Bulgaria
[ai] Also at Washington College, Chestertown, MD, United States of America
[aj] Also at Institute of Applied Physics, Mohammed VI Polytechnic University, Ben Guerir, Morocco
[ak] Also at Institute of Physics and Technology, Mongolian Academy of Sciences, Ulaanbaatar, Mongolia
[al] Also at Millennium Institute for Subatomic physics at high energy frontier (SAPHIR), Santiago, Chile
[am] Also at University of Chinese Academy of Sciences (UCAS), Beijing, China
[†] Deceased

JHEP05(2026)183